PREFACE

This thesis is divided into three parts.

Part I of the thesis deals with a discussion of the processes involved in the thermal and photolytic decompositions of ozone. The reaction is described in terms of potential-energy surfaces, the object being to resolve the question as to the correct mechanism for the decomposition. Previously, the reaction had been described by schemes which differed mainly with regard to the role played by excited oxygen molecules formed from ozone. Consideration of potential-energy surfaces offered a means of arriving at a satisfactory solution to the problem.

Parts II and III deal with experimental studies of the thermal decomposition of organic compounds - dimethyl and diethyl ether. The mechanism by which these materials break down to more stable products has been the object of considerable controversy for the past three decades. Early workers considered the reactions to be of a simple molecular nature - the molecules acquiring enough energy by collisions to reorganise their atoms and then fall apart spontaneously. The fragments from such a split were themselves stable molecular products. This view was based largely on the fact that many organic decompositions obey simple kinetic laws. This explanation had to be discarded when F.O. Rice and coworkers

showed by the Paneth mirror technique that free radicals are present when organic substances decompose in the gaseous phase. Mechanisms were proposed in 1934 involving elementary free radical reactions by Rice and Herzfeld. It was shown that most of the experimental observations including the simple orders could be explained by a complex mechanism. Later work has shown that the principles postulated by Rice and Herzfeld were largely correct for the over-all processes, but that important modifications regarding individual elementary steps had to be made. This became one area of intensive theoretical and experimental research. Today there are still many questions of fundamental importance to be answered. This research on the uninhibited decompositions of dimethyl and diethyl ether was concerned with the elucidation of some of the elementary free radical processes in order to arrive at more satisfactory over-all mechanisms.

The view that part of the decomposition of organic compounds was molecular was raised by Sir Cyril Hinshelwood and his students. Nitric oxide added in very small quantities decreased the rate of the pyrolyses to a fraction of the rate in the absence of NO. The residual reaction was thought to be purely molecular. This view has been maintained over the past twenty years in spite of the accumulation of evidence indicating that the inhibited decompositions are also mainly

governed by free radical processes. The obstacle to the acceptance of free radical mechanisms for the inhibited reactions was probably because until very recently no one was successful in devising general free radical schemes which could explain the experimental observations satisfactorily. Wojciechowski and Laidler, however, in 1960 proposed a new mechanism in which the nitric oxide could initiate free radical chains by abstraction of a hydrogen atom, and also take part in termination reactions. These proposals were tested and found to be successful in explaining decompositions of a number of hydrocarbons, although some modifications have had to be made. As a further test as to the generality of these schemes, the inhibited decompositions of dimethyl and diethyl ether were studied.

Part I of this thesis has been published in the Canadian Journal of Chemistry, 40, 539 (1961). Part II has been submitted as a three-part paper for publication in the Canadian Journal of Chemistry, and Part III has been submitted in two parts for the Proceedings of the Royal Society.

ACKNOWLEDGMENTS

This research was conducted under the direction of Professor K.J. Laidler, whose vigilant attention, patience, and encouragement are most gratefully appreciated. With

gratitude the author wishes to remember Dr. B.W. Wojciechowski and Dr. Margaret Back for useful and constructive criticism and Dr. F.P. Lossing of the National Research Council, for the mass-spectrometry analyses. Suggestions offered by Dr. W.A. Bryce, and by Dr. S.W. Benson on theinterpretation of certain reactions are also gratefully acknowledged. Thanks are due as well to Dr. G.R. Freeman for the use of his Oxford D. Phil. Thesis. Finally, it is the author's special pleasure to record the important contribution made by his wife who assisted in many ways throughout the course of this research.

TABLE OF CONTENTS

LIST OF TABLES

LIST OF FIGURES

LIST OF PLATES

ABSTRACTS

Elementary Processes in the Decomposition of Ozone

Potential-energy surfaces are considered for the O_4 complex, treated as the three-body complex O ... O ... O_2. By means of these it is shown that $O(^3P)$ reacting with O_3 may give rise to a molecule of O_2 in its ground state and one in any of the states $^3\Sigma_g^-$ (ground), $^1\Delta g$ and $^1\Sigma_g^+$; $^3\Sigma_u^+$ cannot be produced. Most of the oxygen molecules produced are expected to be in the ground electronic state, but will be vibrationally excited. Such molecules are readily deactivated and unlikely to lead to energy chains by the reaction

$$O_2^{\circ} + O_3 \rightarrow 2\,O_2 + O$$

Such chains are therefore unlikely in the thermal decomposition and in that initiated by visible radiation. In ultraviolet light $O(^1D)$ atoms are produced and the potential-energy surfaces show that these give rise very efficiently to $O(^1D) + O_3 \rightarrow O_2 + O_2\,(^3\Sigma_u^-)$; the latter have 1l4 kcal in excess of the ground state. It is suggested that the subsequent radiative process

$$O_2(^3\Sigma_u^-) \rightarrow O_2(^3\Sigma_g^-) + h\nu$$

is responsible for sustaining the population of vibrationally excited oxygen molecules in the ground state and that these

propagate energy chains as postulated by McGrath and Norrish. The significance of these conclusions is discussed with reference to the experimental evidence.

Kinetics and Mechanisms of the Pyrolysis of Dimethyl Ether

A. The Uninhibited Reaction

An experimental study has been made of the thermal decomposition of dimethyl ether, the temperature range being 500 to 550°C and the pressure range 100 to 700 mm Hg. A considerable surface effect was noted, and the results were not very reproducible. The reaction was of the three-halves order and the rate constant could be expressed as $2.98 \times 10^{14} e^{-54,900/RT}$ $cc^{1/2}$ $mole^{-1/2}$ sec^{-1}. On the basis of the results obtained in the presence of hydrogen sulphide (Part II C) it is concluded that the initiating step, the dissociation of CH_3OCH_3 into CH_3O and CH_3, is in its second-order region. In order for the over-all order to be three-halves the main terminating step must be either of the type $\beta\beta M$ or $\beta\mu$. The concentrations of the various radicals, and the rates of the various chain-ending steps, are calculated from known or estimated kinetic parameters for the elementary processes. It is concluded that the predominant chain-ending step is probably $CH_3 + CH_3 + H \rightarrow C_2H_6 + H$, but that there may be a significant contribution from $CH_3 + CHO + H \rightarrow CH_3CHO + H$, and from $CH_3 + CH_2OCH_3 + H \rightarrow C_2H_5OCH_3 + H$.

B. The Reaction Inhibited by Nitric Oxide and Propylene

The thermal decomposition of dimethyl ether, inhibited by nitric oxide and by propylene, was studied in the temperature range of 500 to 600°C. About 1.5 mm of nitric oxide gave maximal inhibition, the rate then being approximately 8% of the uninhibited rate. With propylene approximately 70 mm gave maximal inhibition, the rate being slightly higher than that using nitric oxide (~12.5% of the uninhibited rate). In both cases the degree of inhibition was independent of the ether pressure. In the maximally inhibited regions both reactions are three-halves order with respect to ether pressure. As the pressure of nitric oxide was increased beyond 10 - 15 mm, the overall rate increased, and in this region the reaction is first order with respect to both nitric oxide and ether. A fifty-fifty mixture of CH_3OCH_3 and CD_3OCD_3, with enough NO to ensure maximum inhibition, was pyrolyzed. Even at very low percentage decomposition the CD_3H/CD_4 ratio was approximately the same as in the uninhibited decomposition, proving that the inhibited reaction is largely a chain process. Detailed inhibition mechanisms are proposed in which the inhibitor is involved both in initiation and termination reactions.

C. The Reaction Accelerated by Hydrogen Sulphide

The thermal decomposition of dimethyl ether in the

presence of hydrogen sulphide was studied in the temperature range of 480 to 530°C, and over the pressure range of 5 to 500 mm. of Hg. For a given pressure of dimethyl ether the rate of decomposition increased with the addition of increasing quantities of hydrogen sulphide, reaching a plateau after approximately 30% H_2S had been added. The relative rate of decomposition then remained constant until more than 50% H_2S had been added. Further increase in the hydrogen sulphide concentration produced a linear increase in the relative rate. In the region between 30 and 50% added H_2S, the decomposition of dimethyl ether was three-halves order with respect to ether pressure, and zero order with respect to hydrogen sulphide pressure. In this region the three-halves-order rate constant can be expressed by $k = 1.06 \times 10^{14} e^{-53,200/RT}$ $cc^{1/2}$ $mole^{-1/2}$ sec^{-1}. In the region beyond 50% added H_2S, the reaction was first-order with respect to dimethyl ether, and one-half order with respect to hydrogen sulphide. In this region the three-halves-order rate constant is given by $k = 4.90 \times 10^{14} e^{-52,500/RT}$ $cc^{1/2}$ $mole^{-1/2}$ sec^{-1}. The experimental facts are shown to be consistent with a mechanism involving hydrosulphide radicals as the principal chain carriers. These HS radicals are produced mainly from the reaction of methyl radicals with hydrogen sulphide. The work leads to a value of 85.6 kcal. for the dissociation energy of H_2S into H + SH.

presence of hydrogen sulphide was studied in the temperature range of 480 to 530°C, and over the pressure range of 5 to 500 mm. of Hg. For a given pressure of dimethyl ether the rate of decomposition increased with the addition of increasing quantities of hydrogen sulphide, reaching a plateau after approximately 30% H_2S had been added. The relative rate of decomposition then remained constant until more than 50% H_2S had been added. Further increase in the hydrogen sulphide concentration produced a linear increase in the relative rate. In the region between 30 and 50% added H_2S, the decomposition of dimethyl ether was three-halves order with respect to ether pressure, and zero order with respect to hydrogen sulphide pressure. In this region the three-halves-order rate constant can be expressed by $k = 1.06 \times 10^{14} e^{-53,200/RT}$ $cc^{1/2}$ $mole^{-1/2}$ sec^{-1}. In the region beyond 50% added H_2S, the reaction was first-order with respect to dimethyl ether, and one-half order with respect to hydrogen sulphide. In this region the three-halves-order rate constant is given by $k = 4.98 \times 10^{14} e^{-52,500/RT}$ $cc^{1/2}$ $mole^{-1/2}$ sec^{-1}. The experimental facts are shown to be consistent with a mechanism involving hydrosulphide radicals as the principal chain carriers. These HS radicals are produced mainly from the reaction of methyl radicals with hydrogen sulphide. The work leads to a value of 85.6 kcal. for the dissociation energy of H_2S into H + SH.

Kinetics and Mechanisms of the Pyrolysis of Diethyl Ether

A. The Uninhibited Reaction

The uninhibited thermal decomposition of diethyl ether was studied from 560 to 620°C and at pressures ranging from 15 to 370 mm. Hg. The order of the over-all reaction was between 1 and 3/2, the order being greater the higher the pressure. Analytical and kinetic data provide strong evidence that there is a molecular split of diethyl ether into ethanol and ethylene. The reaction leading to acetaldehyde and ethane, on the other hand, is concluded to be almost entirely a free radical chain process. A detailed chain mechanism is postulated, involving first order initiation and the reaction between C_2H_5 and $CH_2CH_2OC_2H_5$ as the chain ending step. This mechanism is shown to lead to a steady-state rate equation which leads to first-order kinetics at lower ether pressures and three-halves-order kinetics at higher ones. The kinetic results lead to activation energies which are in satisfactory agreement with values calculated on the basis of the elementary reactions.

B. The Reaction Inhibited by Nitric Oxide

The pyrolysis of diethyl ether, inhibited by nitric oxide, was studied in the temperature range of 560 to 640°C,

and at pressures between 10 and 360 mm. Hg. About 7 mm. of nitric oxide gave maximal inhibition. The degree of maximal inhibition varied with the temperature but was independent of the other pressure. As the nitric oxide pressure was increased beyond 35 - 40 mm. the rate increased linearly. In the maximally inhibited region the order with respect to ether varied between 1 at high temperatures and low pressures to 3/2 at low temperature and high pressures. A mechanism is proposed, in which nitric oxide is involved in both initiation and termination, and leads to a rate expression showing both first-order and three-halves-order dependence on ether pressure. The first-order component of the reaction is concluded to consist of both a molecular split into ethanol and ethylene and a free-radical part. The mechanism proposed is shown to be consistent with the experimental results.

Part I

ELEMENTARY PROCESSES IN THE DECOMPOSITION OF OZONE

INTRODUCTION

Recent papers (1,2) have been concerned with the evidence for and against the existence of energy chains in the thermal and photochemical decomposition of ozone. There is general agreement that, in the thermal reaction and that brought about by visible (red) radiation, there is production of oxygen atoms in their ground (^3P) states, and that in ultraviolet light, excited (^1D) atoms are produced. An important question is whether these two types of atoms can give rise to energy chains by reacting with O_3 and producing excited oxygen molecules which can regenerate oxygen atoms by reaction with O_3. Benson (2) and McGrath and Norrish (3) have argued that the experimental evidence supports the conclusion that $O(^3P)$ atoms cannot give rise to chains, but that $O(^1D)$ atoms do; in other words, there are energy chains in the ultraviolet reaction, but not in the thermal reaction or in the reaction brought about by red light. These authors, however, have postulated quite different mechanisms for the reaction in the ultraviolet.

The question is here examined from the standpoint of potential-energy surfaces, and the conclusions are essentially the same as Benson's. It is suggested, however, that a modified McGrath and Norrish mechanism is probably

correct for the ultraviolet reaction.

POTENTIAL-ENERGY SURFACES

The course of a reaction between oxygen atoms and ozone molecules may be considered with reference to the potential-energy surfaces for the O_4 system. Figure 1 shows that this requires six parameters for its complete description, but for convenience it may be considered as the three-body system O ... O ... O_2, and energy plotted as a function of the two distances r_1 and r_2. Such a potential surface, shown as Fig. 2, may be regarded as a section through the complete seven-dimensional diagram required for a tetratomic complex, this section relating to a particular interatomic distance r' and to particular values for θ_1 and θ_2 and for the torsional angle ϕ.

Figure 2 shows two sets of curves, one for r_1 very large (i.e. for $O + O_3$) and the other for r_2 very large (for $O_2 + O_2$). These curves are connected by surfaces within the diagram, and reactions must involve motion along a potential-energy surface, possibly with a jump at a suitable crossing point.

The initial state of the reaction $O(^3P) + O_3$ is represented by point A in the diagram, and points B, C, and D represent the possible final states; experimentally (4) the

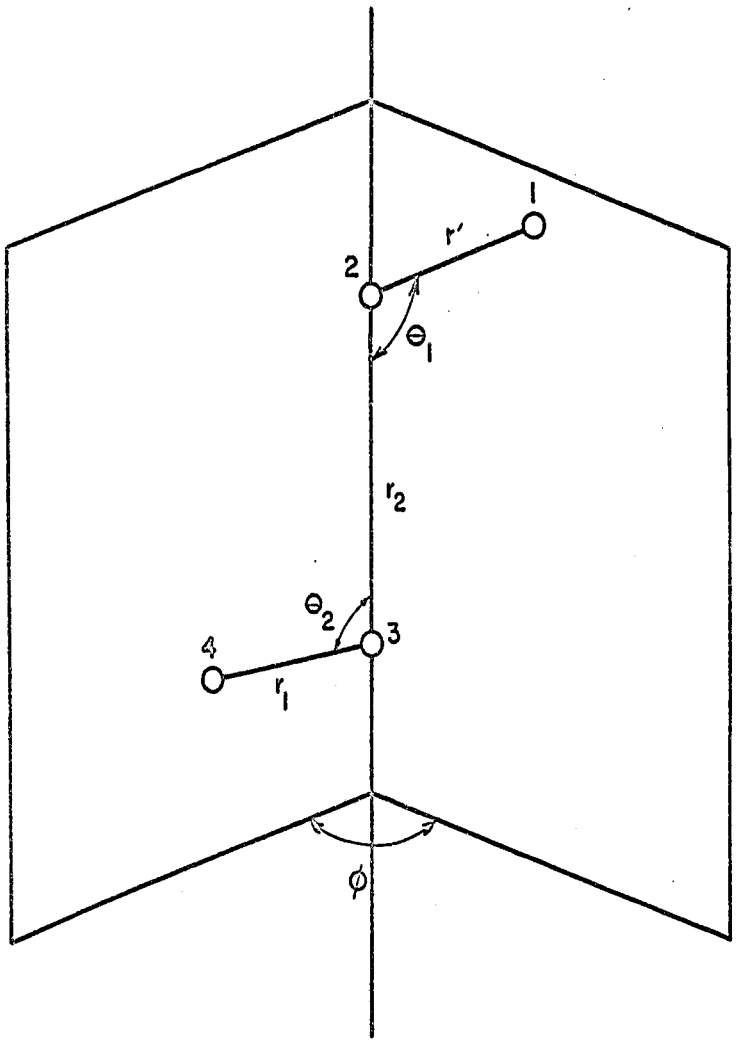

Figure 1. The O_4 species.

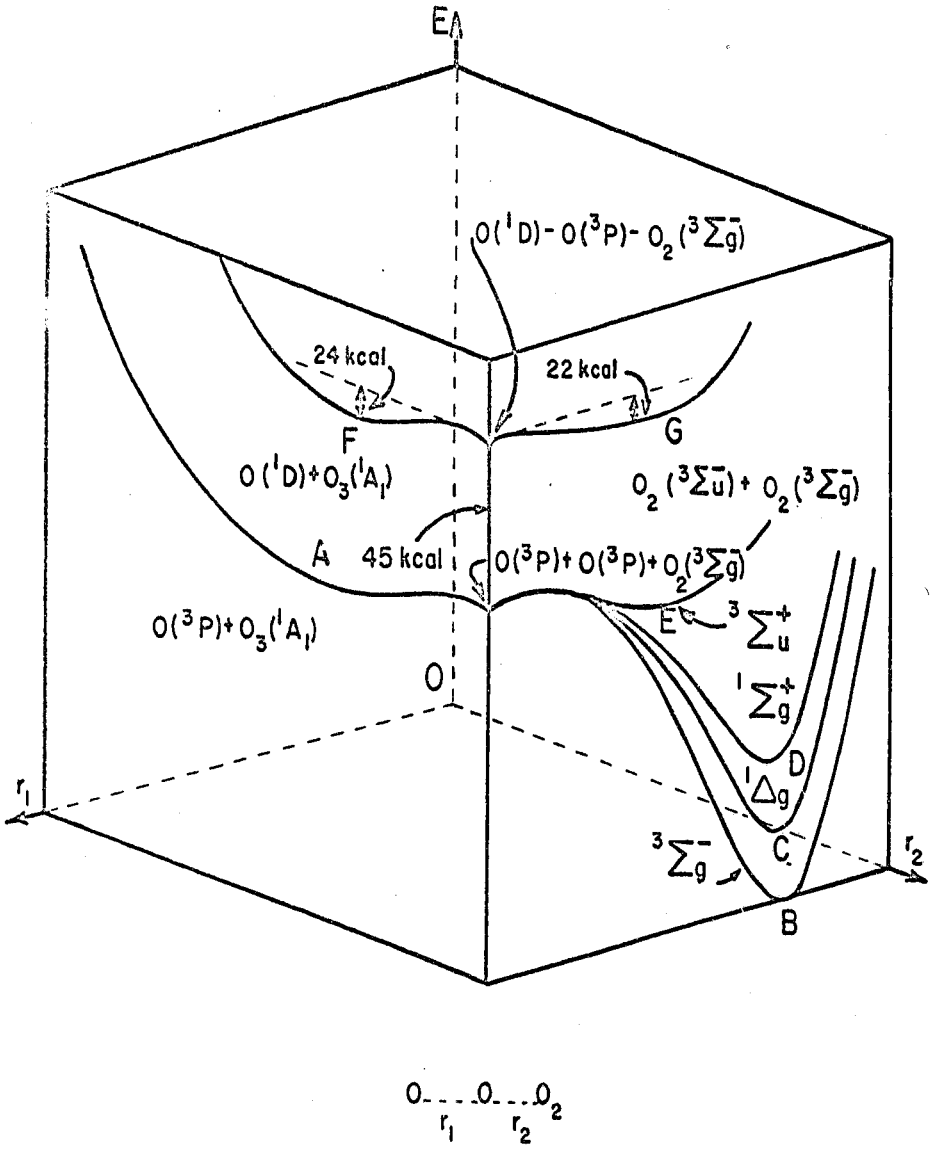

Figure 2. Potential-energy surfaces for O_4, treated as the three-body system O ... O ... O_2.

activation energy is 6 kcal, so that the production of $O_2(^3\Sigma_g^-) + O_2(^3\Sigma_u^+)$ is excluded on energetic grounds since the final state E lies 8 kcal higher than the initial state. The reaction paths connecting A with B, C, and D are represented schematically in Fig. 3. If the splitting of the surfaces occurs after the activated state the probabilities of forming the $^3\Sigma_g^-$, $^1\Delta_g$, and $^1\Sigma_g^+$ states will be respectively 1/2, 1/3, and 1/6, corresponding to the multiplicities. (The $^1\Delta_g$ state is doubly degenerate.) It is also possible for the activated complex for the formation of $^1\Sigma_g^+$ to be higher than that for $^1\Delta_g$, which may be higher than that for $^3\Sigma_g^-$; in this case the probability of forming $O_2(^3\Sigma_g^-)$ is greater than 1/2. Most of the energy released in the reaction will therefore pass into non-electronic forms, and will be readily dissipated on collisions.

For energy chains to be set up the reaction

$$(1) \qquad O_2^* + O_3 \longrightarrow 2O_2 + O$$

must occur. The ΔH for this reaction (5) is $25.7 - E_0$, where E_0 is the excitation energy for the O_2 molecule, so that for the reaction to be exothermic E_0 must be at least 25.7 kcal. This condition is only satisfied by the $^1\Sigma_g^+$ state or by the lower ($^1\Delta_g$ and $^3\Sigma_g^-$) states if they have sufficient vibrational energy. Since, however, the $^1\Sigma_g^+$ state is formed with, at

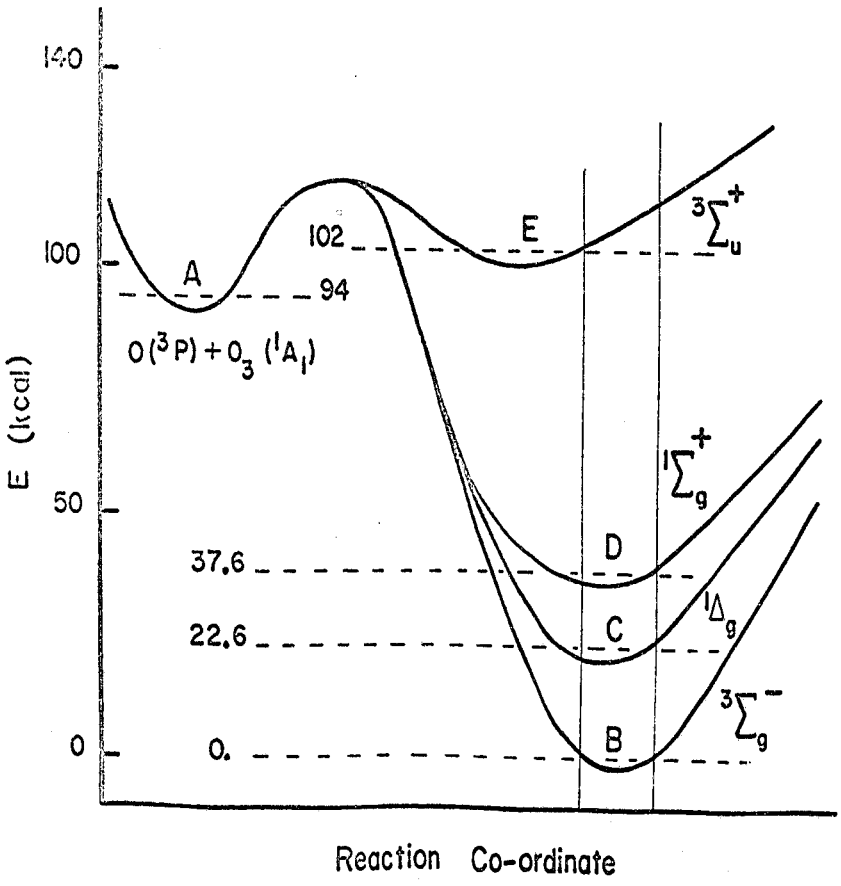

Figure 3. Section through Fig. 2 showing the possible reaction paths.

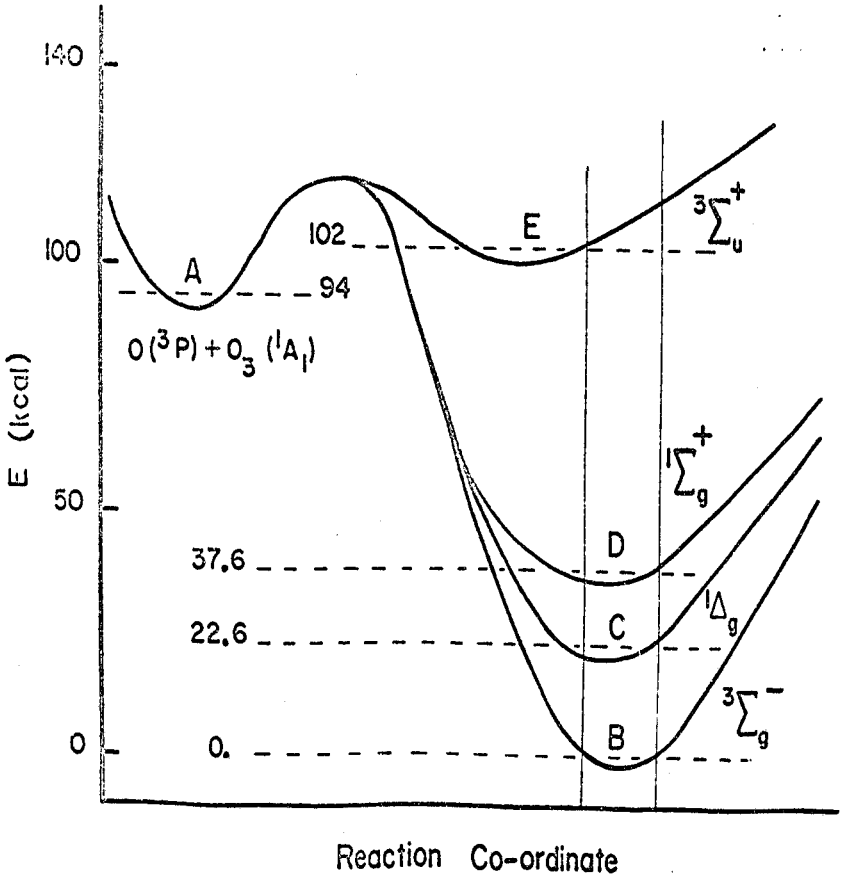

Figure 3. Section through Fig. 2 showing the possible reaction paths.

the most, a probability of 1/6, and vibrational energy is readily dissipated, it is clear that the formation of oxygen atoms by reaction (1) will occur only with low efficiency. Energy chains cannot, therefore, be of any importance when $O(^3P)$ atoms are involved, i.e. in the thermal decomposition and in the photochemical decomposition induced by visible radiation.

Point P in Fig. 2 represents the system $O(^1D) + O_3$; it is connected by a surface to the curve through 0 and corresponding to the formation of $O_2(^3\Sigma_g^-) + O_2^*(^3\Sigma_u^-)$. The latter species has an energy of 141 kcal in excess of the ground state. Schumacher (1) has pointed out, as evident from Fig. 2 also, that this reaction is endothermic, the difference in energy between the initial and the final state being 2 kcal. One would expect, therefore, that this reaction should have an appreciable activation energy. Benson (2) has answered this objection by taking into account the fact that the O atoms can have excess translational energies, which are dissipated relatively slowly, and hence the production of $O_2^*(^3\Sigma_u^-)$ molecules can be quite fast at high O_3 concentrations. The nature of the surface does not permit the formation of the second molecule of oxygen in any lower excited state, except with very low probability. The highly excited $^3\Sigma_u^-$ molecules have a short life of 2.5×10^{-9} second (6) due to

the radiative process $O_2(^3\Sigma_u^-) \rightarrow O_2(^3\Sigma_g^-) + h\nu$, which gives rise to the Schumann-Runge emission bands of O_2. The ground-state oxygen molecules produced by this process will, according to the Frank-Condon principle, give vibrationally excited O_2 molecules in exactly those levels observed in the ozone photolysis by McGrath and Norrish. This can be readily seen by reference to Fig. 4.

It is perhaps significant that these workers (8) observed a maximum value around $v'' = 13$ (53.5 kcal/mole) in the vibrational energy distribution. There is no explanation for this maximum given in their paper, and one would expect that if vibrationally excited O_2 molecules were produced solely by the endothermic process

$$O(^1D) + O_3(^1A) \rightarrow O_2^*(^3\Sigma_g^-) + O_2(^3\Sigma_g^-),$$

the population of those vibrational levels should be a maximum at the lower energy levels. The fact that there is a maximum at $v'' = 13$, however, strongly suggests that the population of these vibrational energy levels is a result of the process

$$O_2(^3\Sigma_u^-) \rightarrow O_2^*(^3\Sigma_g^-) + h\nu.$$

As can be seen from Fig. 4, the transition from the minimum of the $^3\Sigma_u^-$ state would produce O_2 molecules in the ground state ($^3\Sigma_g^-$) in roughly the 12th or 13th vibrational level.

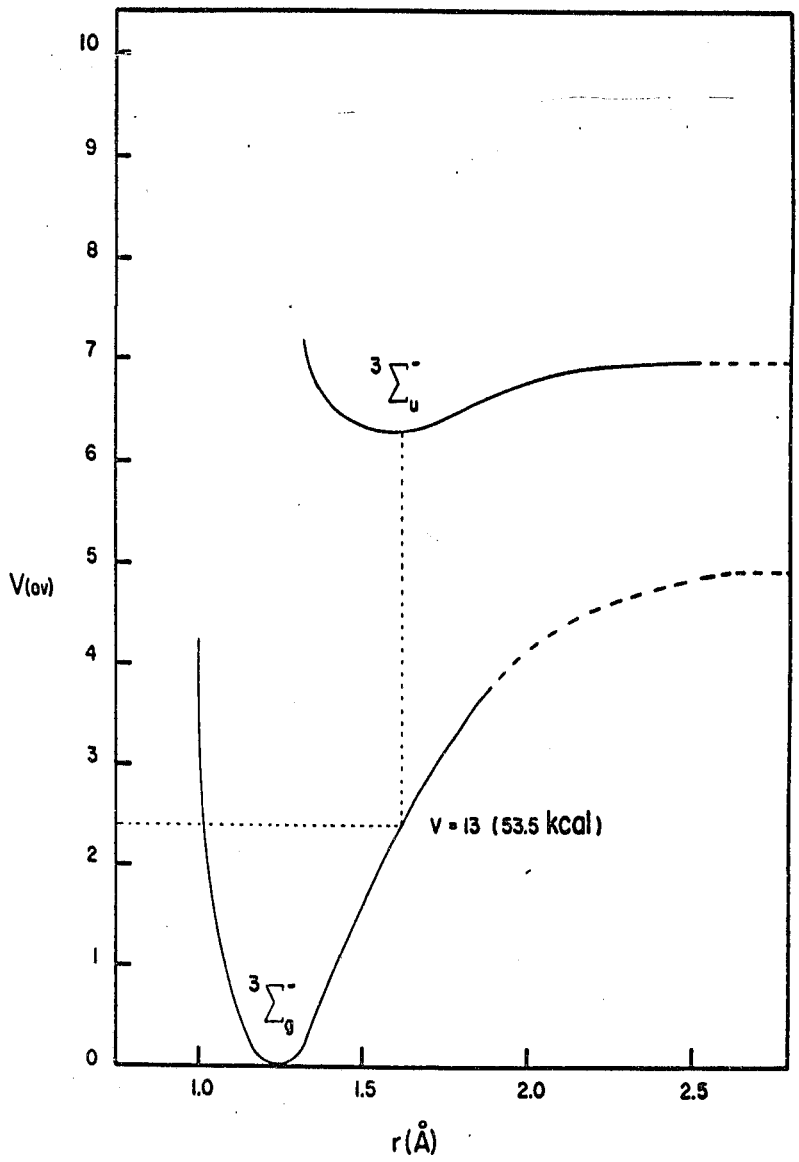

Figure 4. Potential energy curves (7) for the O_2 molecule, showing that a maximum in the vibrational energy distribution is expected for v = 13 for

$$^3\sum_u^- \longrightarrow {}^3\sum_g^-$$

This should then be a maximum, as is the case. The radiation given off in the process is of very short wavelength (2000 Å) (1) and consequently would be absorbed by undecomposed ozone.

DISCUSSION

The above conclusions are consistent with the experimental results of the aforementioned authors. Some specific remarks about the decomposition mechanism may now be made.

McGrath and Norrish (2,8) flash photolysed, using ultraviolet radiation, a mixture of O_3, H_2O, and H_2 in the ratio 1:3:100, and obtained strong OH absorption. This is attributed to the occurrence of the exothermic reaction

$$O(^1D) + H_2O \longrightarrow 2\ OH + 29.2\ kcal.$$

Hydroxyl radicals could not be obtained with $O(^3P)$ atoms, owing to the endothermicity of the reaction

$$O(^3P) + H_2O \longrightarrow 2\ OH - 16.8\ kcal.$$

In agreement with this the addition of water has little or no effect on the thermal decomposition of ozone (2,9).

The most likely mechanism for the thermal decomposition of ozone (where only $O(^3P)$ atoms can be produced) is that of Benson and Axworthy (10), which is

(2) $O_3 + M \rightleftharpoons O + O_2 + M$

(3) $O + O_3 \rightarrow 2\,O_2$.

At the ordinary pressures the first reaction will be in its second-order region (11). The probability of forming electronically excited $O_2(^1\Sigma_g^+)$ is very low, as was pointed out above, and therefore the possibility of energy chains in the thermal reaction is excluded. If, however, energy chains were involved, the following reactions would have to be added:

(4) $O + O_3 \rightarrow O_2 + O_2^*$

(5) $O_2^* + O_3 \rightarrow 2\,O_2 + O$,

but Benson and Axworthy (4,10) showed that this led to a kinetic scheme which is inconsistent with experiment.

Similar comments apply to the work with visible radiation, which produces $O(^3P)$ atoms. The quantum yields are probably (2) always less than 2, so that there is no evidence for energy chains.

The most probable mechanism in ultraviolet light involves as the initiating step

(6) $O_3 + h\nu \rightarrow O_2(\text{singlet}) + O(^1D)$.

The oxygen molecules must be in a singlet state for spin conservation; it may be the $^1\Sigma_g^+$ state, which requires that

the wavelength be less than 3100 Å. Reaction (6) will be followed by

$$(7) \qquad O(^1D) + O_3 \rightarrow O_2(^3\Sigma_g^-) + O_2(^3\Sigma_u^-)$$

as discussed above, and this is followed by the rapid transition

$$(8) \qquad O_2(^3\Sigma_u^-) \rightarrow O_2^*(^3\Sigma_g^-) + h\nu$$

The propagation of the chain then takes place by the vibrationally excited $O_2^*(^3\Sigma_g^-)$ molecules of excitation energy > 69 kcal reacting with ozone, i.e.

$$(9) \qquad O_2^*(^3\Sigma_g^-) + O_3(^1A) \rightarrow 2\,O_2(^3\Sigma_g^-) + O(^1D).$$

The latter reaction is the essential feature in the McGrath and Norrish mechanism. The termination steps are probably

$$(10) \qquad O + O + M \rightarrow O_2 + M$$

$$O + O_2 + M \rightarrow O_3 + M$$

$$O_2^* + M \rightarrow O_2 + M,$$

where M represents a molecule of oxygen, ozone, or an inert gas.

Very recently the photochemical decomposition of ozone in yellow-red light (5800-6200 Å) was investigated (12).

The highest quantum efficiency observed was 2.0 Mol/hv. On the basis of these experiments Schumacher now agrees that there are no energy chains in the thermal, nonexplosive ozone decomposition.

Part II

KINETICS AND MECHANISMS OF THE PYROLYSIS OF DIMETHYL ETHER

A. The Uninhibited Reaction

INTRODUCTION

During recent years determinations have been made of the kinetic parameters for a large number of the elementary processes that occur in organic pyrolyses. As a result there has been a revival of interest in the problem of establishing the over-all mechanisms for such reactions, and in confirming them quantitatively. Recent work of this kind in these laboratories has been concerned with the thermal decompositions of propylene (13), ethane (14), propane (15) and butane (16). In all cases it has been found that the reactions occur predominantly by free-radical mechanisms, the molecular mechanisms being of minor importance. In the cases of the ethane and propane it was concluded that under the experimental conditions the initiating unimolecular dissociation of the reactant molecule was in its low-pressure second-order region; with the larger butane molecule, on the other hand, the initial reaction is first-order. It is of considerable interest to come to a conclusion about this matter for other decomposing substances, and the present

investigation is concerned with the pyrolysis of dimethyl ether. For this substance the evidence as to the order of the initiating step comes from an investigation of the reaction in the presence of hydrogen sulphide, and is discussed in Part II, C. This part describes an experimental study of the uninhibited dimethyl ether decomposition, and considers in some detail the nature of the chain-ending steps.

A number of previous investigations have been made of the dimethyl ether pyrolysis, and the results may be referred to briefly. The reaction was first studied by Askey and Hinshelwood (17), who concluded it to be first-order with respect to the ether. The formation of products could be represented by the equation

$$CH_3OCH_3 \rightarrow CH_4 + CH_2O \rightarrow CH_4 + CO + H_2.$$

The formaldehyde builds up in the system and its concentration goes through a maximum when the reaction is about half complete. Later workers (18-23) found a great deal of evidence indicating that the decomposition was a chain reaction and could be described by a mechanism of the Rice-Herzfeld (24) type.

Benson (25) analysed existing data and found that the reaction was three-halves order with respect to ether.

Benson and Jain (26) confirmed the three-halves order relative to ether and obtained a rate constant of $k = 1.3 \times 10^{15} e^{-55,600/RT}$ $cc^{1/2}$ $mole^{-1/2}$ sec^{-1}. They found very little effect of added inert gas. The decomposition mechanism postulated by these authors involved first-order initiation, and termination involving two β radicals. They assumed that the CH_3OCH_2 radical is an important chain breaker and that the reaction

$$CH_3OCH_2 \rightarrow CH_2O + CH_3$$

is in its second order region. Anderson and Benson (27) confirmed the presence of $CH_3OC_2H_5$ and $CH_3OCH_2CH_2OCH_3$ in the products of the pyrolysis. Their results also indicate that the reaction

$$CH_3 + CH_3OCH_2 \rightarrow CH_3OCH_2CH_3$$

is an important termination step.

Imai and Toyama (28) recently decomposed dimethyl ether in the temperature range of 360 to 440°C, and found that the rate constant could be represented as

$$k = 1.45 \times 10^{15} e^{-54,500/RT}\ cc^{1/2}\ mole^{-1/2}\ sec^{-1}.$$

This is in good agreement with that obtained by Benson and Jain (26).

EXPERIMENTAL

Since the apparatus was the same and the procedure was very similar for the study of the uninhibited, inhibited and accelerated decompositions, a general experimental description is given here, which also applies to section B and C.

Apparatus

A usual vacuum static system was employed, the only unique feature being the pressure measurement and recording arrangement. Plate 1 is a photograph of the apparatus, which is drawn schematically in Fig. 5.

The entire system could be evacuated to less than 10^{-5} mm. Hg. by means of an Edwards 'Speedivac' model 203 oil vapour diffusion pump (P_1) which was backed by a single stage Welch rotary pump (P_2). A single manifold connected all parts of the apparatus. Gases used in the experiments were stored in bulbs V_1, V_2 and V_3, each having freezing nipples for purification of the gases. Storage bulbs V_1 and V_2 were used to store purified ether and nitric oxide, propylene or hydrogen sulphide respectively. These were approximately of 2-liter capacity. V_3 was used for storage of fully deuterated dimethyl ether or deuterated methane, and was approximately of 1 liter capacity. Pressures in these

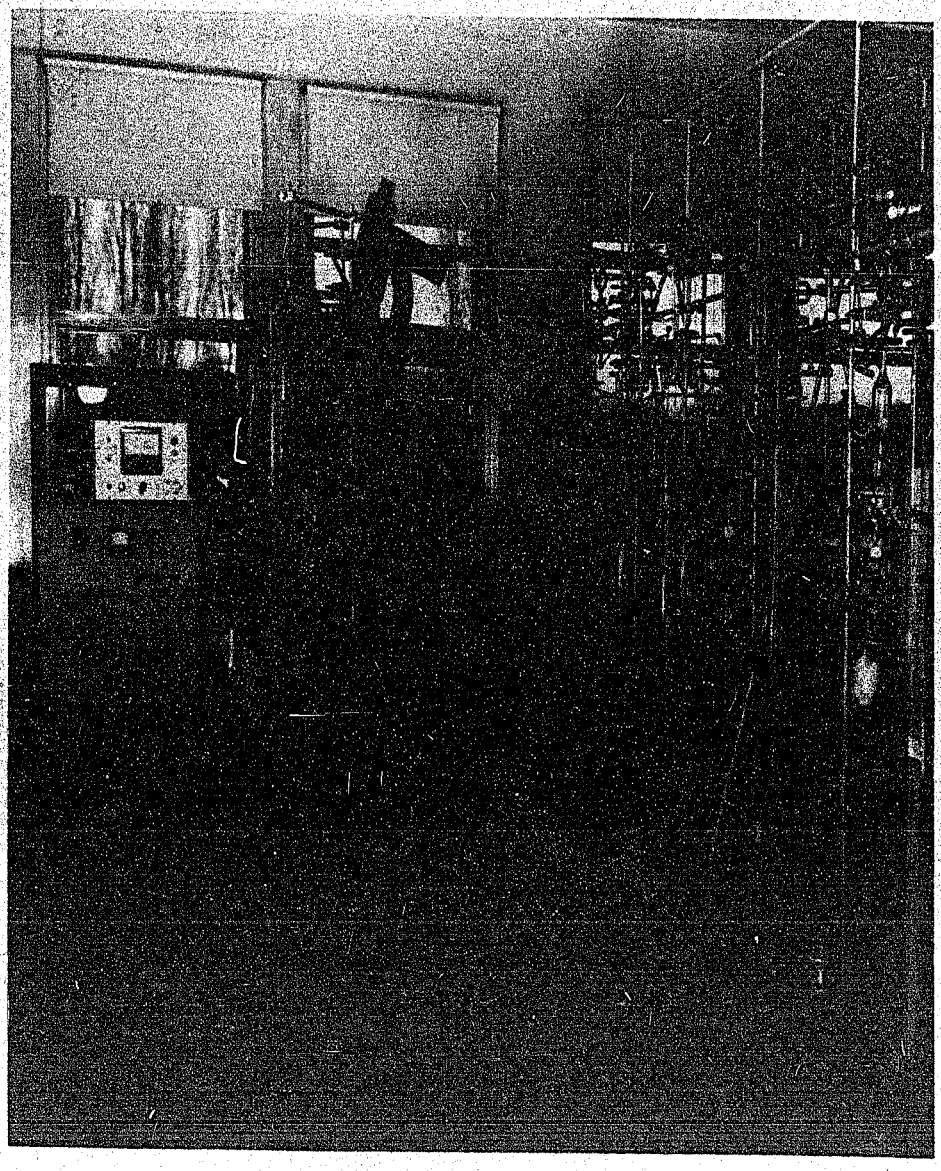

Plate 1. View of the Apparatus.

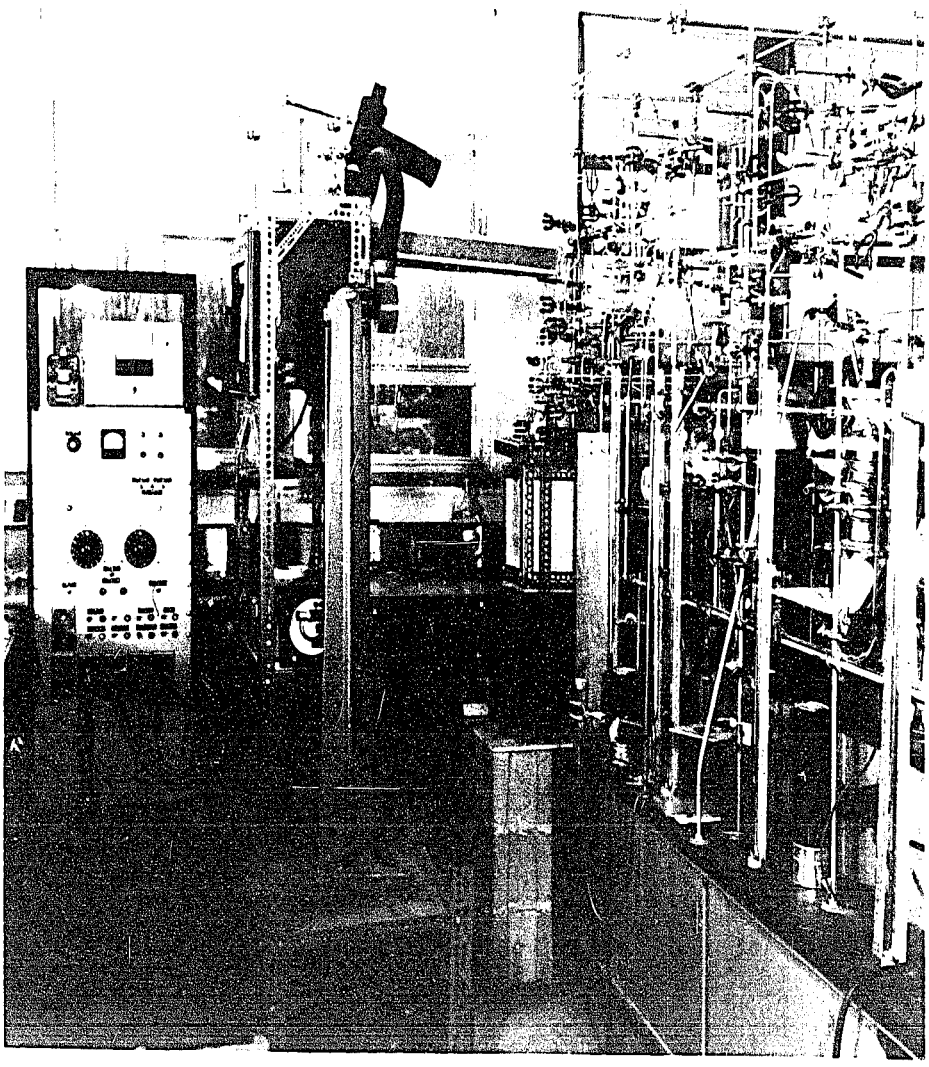

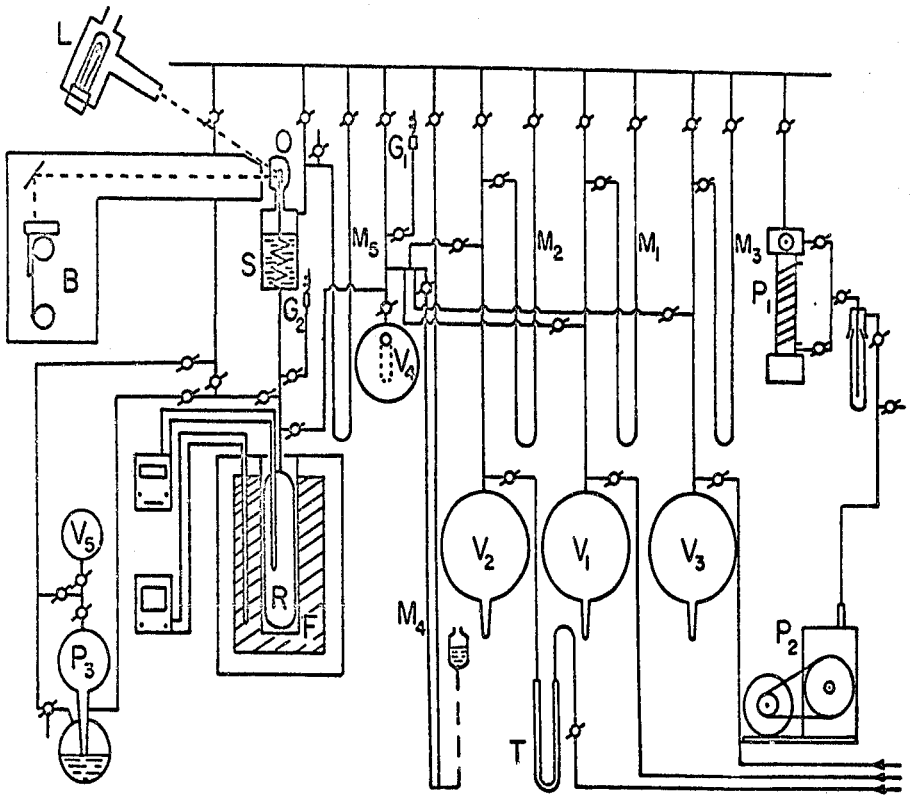

Figure 5. Schematic diagram of the apparatus.

bulbs were measured on the corresponding mercury manometers M_1, M_2 and M_3. The inlet to each bulb was attached to the cylinders of the research grade gases. A u-trap (T) of approximately 1 meter length and 1 cm. diameter containing high activity silica gel for the purification of nitric oxide was connected to the inlet side of V_2. Trap T could be readily removed when other gases were to be stored in V_2. Each of the storage vessels was attached to the mixing bulb V_4. This was a 1-liter spherical flask having a small cold finger of approximately 2.5 cm. diameter and 10 cm. depth. Pressures in the mixing vessel could be measured on the attached constant-volume mercury manometer M_4 or if the pressures were very low, on a Pirani Autovac Gauge (type 3294 B). The gauge heads are shown on the diagram as G_1 and G_2.

The reaction vessel (R) was attached to the outlet of V_4. The reaction vessel was a cylindrical quartz tube of about 250 ml. volume. Pressure changes in R were followed by means of a quartz spiral Bourdon gauge (S). Connecting tubing from the reaction vessel to the spiral gauge, and to the attached stopcocks, was all capillary tubing and hence the dead space was only about 4 ml. The second Pirani gauge head (G_2) was attached to the reaction vessel as shown.

The outlet side of R was attached to a Toepler pump (P_3)

as well as to the manifold. Reaction products could therefore be collected for analysis or be simply pumped out of the system. If analyses were to be made the products could be pushed into a removable sampling bulb (V_5).

Details of the gauge and the pressure recording arrangement have been described previously (13). Light from a 500 watt projection lamp (L) was reflected off a small mirror (O) which was glued to the rotating vertical axial arm of the spiral gauge (S). The reflected light then passed through a light shield to a Beckman photopen recorder (R). The pen of the recorder was attached to a carriage on which were mounted two photocells. When the carriage was moved into the light path it would 'lock' on the beam, and follow it as it moved horizontally, owing to the rotation of the mirror (O) as the pressure changed in the reaction vessel. The circuits of the recorder were arranged so that equal outputs from the two photocells were maintained. Thus the carriage would move with the light beam centered on the two photocells. A pressure change of 18.6 m. Hg. in the reaction vessel (R) resulted in a deflection of 1 inch on the recorder. The total span of the recorder thus represented a pressure change of 186 m. Hg. Pressure measured by means of the spiral gauge arrangement could be measured to $\pm$ 0.6 m. Hg.

In order to damp out spurious oscillations, the spiral gauge was immersed in silicone oil. Pressure changes between zero and slightly above one atmosphere could be studied by changing the pressure of dry air above the silicone oil. This pressure was measured by means of the mercury manometer (M_5). The range of rates over which measurements could be made could be extended by interchanging gears in the gear train of the chart drive. Thus rates as slow as approximately 2×10^{-3} cm. sec.$^{-1}$ or as fast as 4 cm. sec.$^{-1}$ could be measured.

The furnace was made from a four-inch copper cylindrical block (F), one foot long, with a hole bored into it axially to accommodate the reaction vessel. Two windings of nichrome wire around the copper block were used for temperature control. An asbestos box containing powdered asbestos encased the whole assembly. The furnace could be raised or lowered by means of a jack, so that the reaction vessel could be removed and cleaned. The temperature of the furnace was controlled to slightly below the desired temperature by manual adjustment of a Variac on one winding, and then brought up to the desired set point and controlled by means of a thermocouple-activated Thermo Electronic controller which was operating on the second winding. The voltage on the second winding could be adjusted to minimize

surges due to the off-on control. The thermocouple of the controller was placed in a small diameter but deep hole in the copper furnace block. A second calibrated thermocouple, placed in a well in the reaction vessel, was used for temperature measurement of the reaction in conjunction with a Thermo Electric Mini-Mite self compensating potentiometer. Temperature variation was of the order of $\pm$ 0.2°C.

Procedure

After evacuation of the apparatus the gases were admitted to the storage vessels. The dimethyl ether, nitric oxide and hydrogen sulphide were obtained from Matheson Co. of Canada Ltd., and their stated purities were 99.5%, 99.0% and 99.5% respectively. Propylene was Phillips research grade, stated to be 99.9% pure. The nitric oxide was passed through a silica gel trap as it was admitted to the system. This removed most of the impurities, with the exception of nitrogen. All the gases were purified further by freeze-thawing (to remove low boiling gases) and then by repeated low temperature fractional distillations. A minimum of three trap-to-trap distillations were carried out. The fully deuterated dimethyl ether and methane were supplied by Merck, Sharp and Dohme of Montreal and were both stated to be of 99% purity. Both of these gases were purified further as above, although the number of distillations of

d_4-methane was kept to a minimum owing to its high vapour pressure at liquid nitrogen temperature.

The gases were then admitted as desired to the mixing vessel (V_4). In order to ensure complete mixing of the ether and additive (i.e. nitric oxide, propylene, hydrogen sulphide, d_{10}-dimethyl ether, or d_4-methane) and hence eliminate any errors due to variation in reactant composition, the experimental procedure was as follows: A measured quantity of purified dimethyl ether was condensed on the cold finger in the one-liter spherical flask (V_4). Only one stopcock was attached to this mixing volume and the connecting tubing was kept to a minimum. A known quantity of the additive was then admitted to the mixing volume which contained the frozen ether. After all the additive was condensed, the stopcock was closed and the cold finger allowed to warm to room temperature. The warm gases were allowed to mix for about 15 minutes before being admitted to the reaction vessel.

Prior to a run the reaction vessel (R) was pumped down to approximately 10μ. It was established early in the investigation that this small residual pressure had no detectable effect on the rates. The reaction vessel was then isolated from the system by closing the connecting stopcocks. The pressure above the silicone oil was adjusted

to approximately the same pressure as the pressure of the reactant mixture. The stopcock connecting the reaction vessel to the mixing vessel was now opened for a few seconds to admit the mixture, then closed quickly. The pressure change was immediately recorded on the chart of the recorder as described above. After following the pressure change for the desired length of time (which varied from less than a minute to more than three hours), the vessel was pumped out. When this was desired, products were collected for analysis by the Toepler pump as described above. The whole procedure was repeated so that the reactions could be studied over a wide range of pressure and temperature.

Rates were calculated from the slopes of the pressure-time curves at the initial point or at the inflexion point. The data obtained were fully reproducible except in the case of the uninhibited decomposition of dimethyl ether, which is discussed below.

The isotopic mixing experiments were carried out using equal amounts of CH_3OCH_3 and CD_3OCD_3. For the inhibited decomposition sufficient nitric oxide was added to ensure maximum inhibition. The reaction temperature was 550°, and the extent of the reaction varied from approximately 1 to 20%. The CD_3H/CD_4 ratio was determined by means of a mass spectrometer using samples from liquid-nitrogen non-condensible

to approximately the same pressure as the pressure of the reactant mixture. The stopcock connecting the reaction vessel to the mixing vessel was now opened for a few seconds to admit the mixture, then closed quickly. The pressure change was immediately recorded on the chart of the recorder as described above. After following the pressure change for the desired length of time (which varied from less than a minute to more than three hours), the vessel was pumped out. When this was desired, products were collected for analysis by the Toepler pump as described above. The whole procedure was repeated so that the reactions could be studied over a wide range of pressure and temperature.

Rates were calculated from the slopes of the pressure-time curves at the initial point or at the inflexion point. The data obtained were fully reproducible except in the case of the uninhibited decomposition of dimethyl ether, which is discussed below.

The isotopic mixing experiments were carried out using equal amounts of CH_3OCH_3 and CD_3OCD_3. For the inhibited decomposition sufficient nitric oxide was added to ensure maximum inhibition. The reaction temperature was 550°, and the extent of the reaction varied from approximately 1 to 20%. The CD_3H/CD_4 ratio was determined by means of a mass spectrometer using samples from liquid-nitrogen non-condensible

fractions of the reacted mixture.

Some runs were carried at 500°C out using mixtures containing approximately 10% CD_4, 90% dimethyl ether and 0-1% nitric oxide (enough for maximum inhibition).

RESULTS

The decomposition of dimethyl ether was studied in the temperature range of 500 to 550°C, and over a pressure range of approximately 100 to 700 mm. Hg. A typical pressure-time curve for the reaction is shown as Curve A of Fig. 6. Rates were calculated from the slopes of the pressure-time curves at the inflexion point. The reaction was found to be three-halves order with respect to dimethyl ether over the complete range of pressure and temperature. It proved very difficult to obtain reproducible results, since the uninhibited reaction appeared to be influenced to a great extent by the condition of the surface of the reaction vessel. Greater reproducibility could be obtained after the surface had been exposed to nitric oxide either alone or mixed with other. Enough reproducible data were accumulated by first treating the surface in this way, in order to verify the results of previous workers (26,28). An Arrhenius plot of the data is shown in Fig. 7. Most of the points shown are the average of many and the approximate deviations are

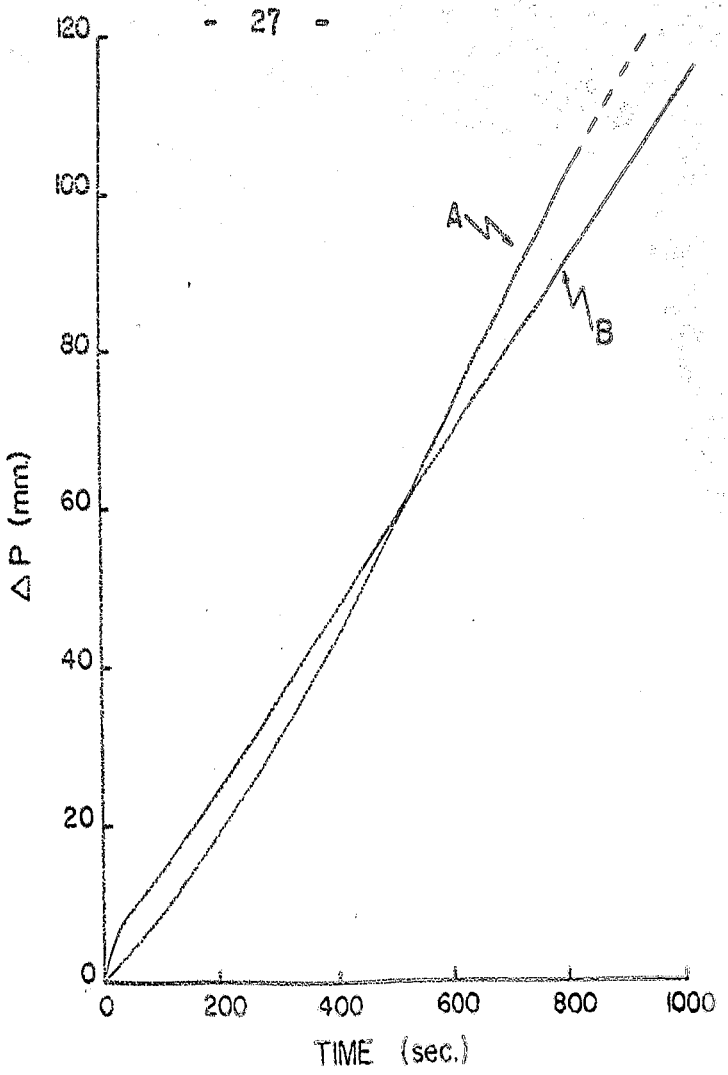

Figure 6. Curve A: A typical pressure-time curve for the uninhibited pyrolysis of dimethyl ether; this is a tracing of an actual record obtained at 520°C and at an initial pressure of 197 mm Hg.
Curve B: A pressure-time curve showing the effect of 0.4 mm of oxygen on the uninhibited pyrolysis of dimethyl ether. All other conditions are the same as for curve A.

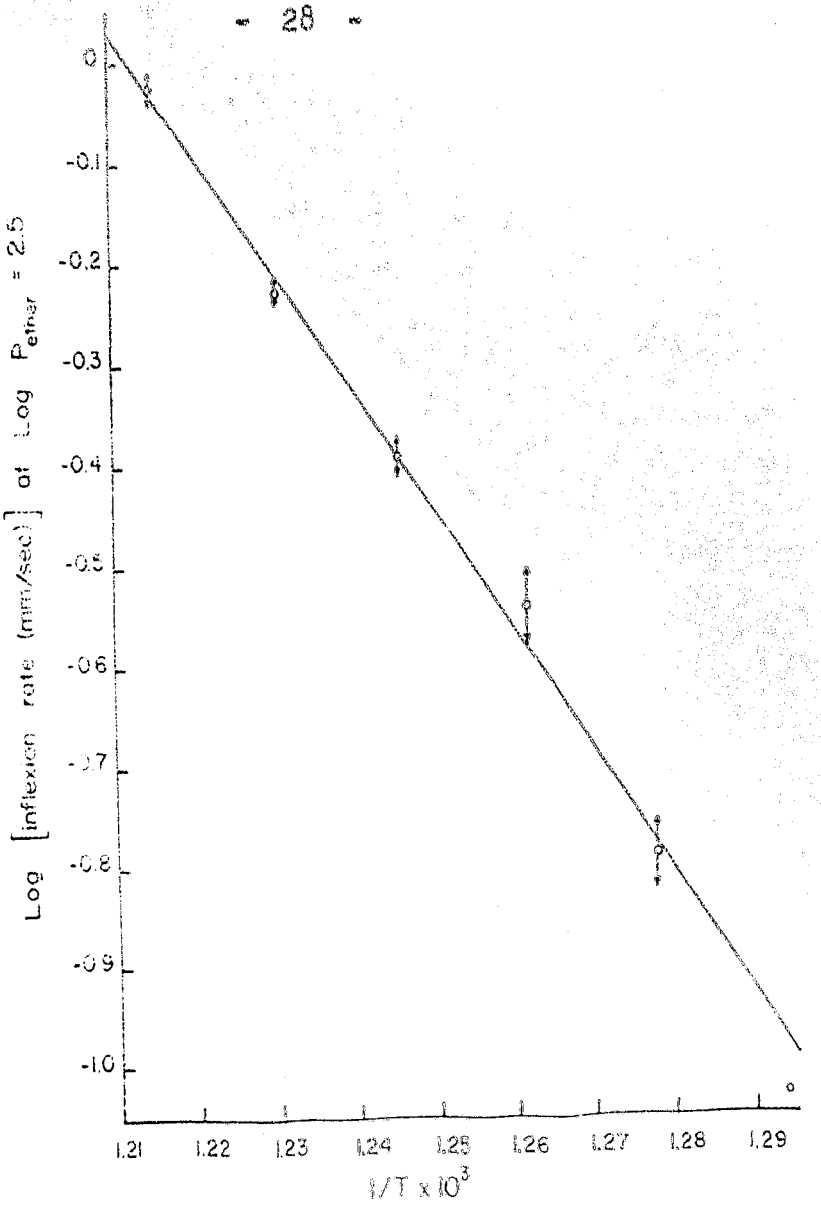

Figure 7. Arrhenius plot for the pyrolysis of dimethyl ether.

indicated (for the point at 500°C ($\frac{1}{T} \times 10^3 = 1.294$) only a single value was obtained). The activation energy was 54.9 kcal. mole^{-1}.

Because inflexion-point rates were used rather than initial rates (rates at the inflexion point were more reproducible), it was necessary to correlate the pressure change with the rate of disappearance of ether at decompositions of 20 to 30%. The data of Benson and Jain (26) were utilised for this purpose. Figure 1 of their paper is a plot of $\Delta CH_2O/\Delta CH_3OCH_3$ as a function of percentage decomposition. The over-all reaction is represented by

$$\underset{(1-x)}{CH_3OCH_3} \rightarrow \underset{(x-y)}{CH_2O} + \underset{x}{CH_4} + \underset{(y)}{H_2} + \underset{(y)}{CO}$$

Benson and Jain have plotted $1-y/x$ against x. The change in pressure Δp, i.e. $x + y$, can thus be calculated from their data, and this can now be plotted against x. One can therefore obtain a plot of $\Delta p/p$ versus $\Delta Z/p$, where ΔZ is the change in partial pressure of ether. The experimental Δp can be calculated from the pressure-time curves obtained in the present work, and the corresponding value of ΔZ can be estimated graphically. In all cases $\Delta Z/\Delta p = 0.70 \pm$

0.02. The three-halves-order rate constant was therefore multiplied by 0.70, yielding

$$k = 2.98 \times 10^{14} e^{-54900/RT} \text{ cc}^{1/2} \text{ mole}^{-1/2} \text{ sec}^{-1}$$

The activation energy is in good agreement with the values obtained by previous workers, and quoted above. The frequency factor and rates are, however, significantly lower than those obtained previously. This may be because our technique has minimized the surface-catalysed reaction.

The shape of the pressure-time curve was found to be altered considerably by the addition of a small quantity (~0.2%) of oxygen. The initial rate of decomposition appeared to be greatly enhanced by the presence of oxygen, which in turn seems to be used up rapidly as suggested by the pressure-time curve shown in Fig. 6, Curve B. These effects differ somewhat from those reported by Benson and Jain (26) who state that the reaction is relatively insensitive to surface effects and to small amounts of added oxygen. Professor Benson has, however, informed us that he and Jain did observe an initial effect of oxygen, which was rapidly consumed; there therefore seems to be agreement on this point.

The uninhibited decomposition of dimethyl ether exhibits a well-defined induction period, which is particular-

0.02. The three-halves-order rate constant was therefore multiplied by 0.70, yielding

$$k = 2.98 \times 10^{14} e^{-54900/RT} \text{ cc}^{1/2} \text{ mole}^{-1/2} \text{ sec}^{-1}$$

The activation energy is in good agreement with the values obtained by previous workers, and quoted above. The frequency factor and rates are, however, significantly lower than those obtained previously. This may be because our technique has minimized the surface-catalyzed reaction.

The shape of the pressure-time curve was found to be altered considerably by the addition of a small quantity (~0.2%) of oxygen. The initial rate of decomposition appeared to be greatly enhanced by the presence of oxygen, which in turn seems to be used up rapidly as suggested by the pressure-time curve shown in Fig. 6, Curve B. These effects differ somewhat from those reported by Benson and Jain (26) who state that the reaction is relatively insensitive to surface effects and to small amounts of added oxygen. Professor Benson has, however, informed us that he and Jain did observe an initial effect of oxygen, which was rapidly consumed; there therefore seems to be agreement on this point.

The uninhibited decomposition of dimethyl ether exhibits a well-defined induction period, which is particular-

ly evident at lower pressures. Figure 8 shows that this induction period can be considerably shortened, and probably eliminated completely, by the addition of suitable amounts of formaldehyde. The formaldehyde also considerably increases the rate of the decomposition. An increase in rate on the addition of formaldehyde was also reported by Benson and Jain (26).

DISCUSSION

It is convenient to base a discussion of the mechanism of the dimethyl ether pyrolysis on that proposed by Benson and Jain (26)*;

[11]	CH_3OCH_3	→	$CH_3 + CH_3O$
[12]	$CH_3 + CH_3OCH_3$	→	$CH_4 + CH_2OCH_3$
[13a]	$H + CH_2OCH_3$	→	$CH_2O + CH_3 + H$
[14]	CH_3O	→	$CH_2O + H$
[15]	$H + CH_3OCH_3$	→	$H_2 + CH_2OCH_3$
[16]	$CH_3 + CH_2OCH_3$	→	$CH_3CH_2OCH_3$

The main features of this scheme are that the initiation reaction [11] is first-order, that the decomposition of the radical (reaction [13a]) is in its second-order region, and

---

* The letter a in an equation number (e.g. [13a]) is used to emphasize the fact that the reaction is in its low-pressure region.

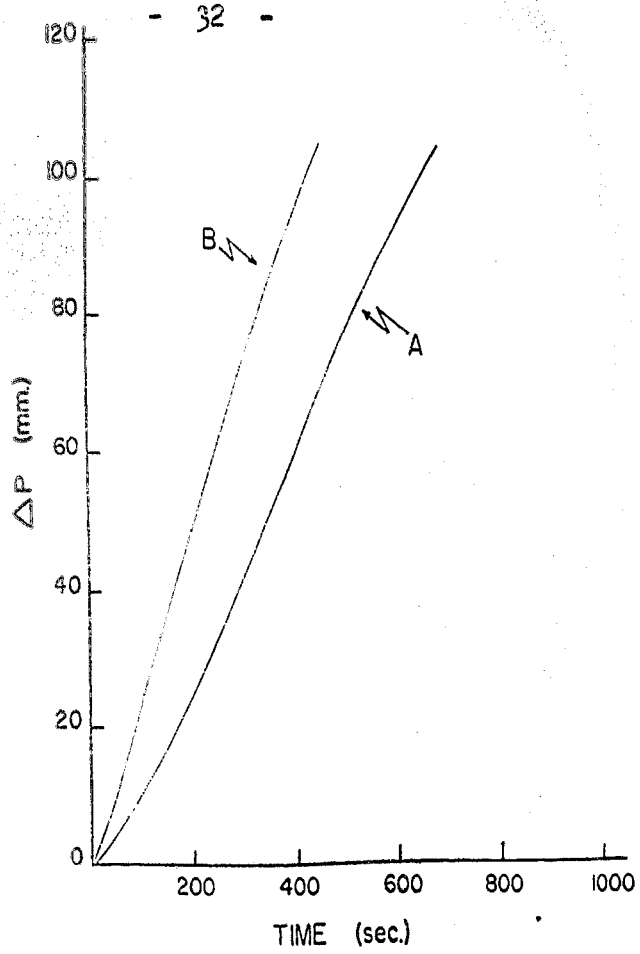

Figure 8. Pressure-time curves for the ether decomposition at 540°C and an initial pressure of 122 mm. Curve A is for the reaction in the absence of formaldehyde; curve B for the reaction in the presence of 24 mm. of formaldehyde.

that the main termination process involves CH_3 and CH_3OCH_2. If reaction [13a] is second-order the radical CH_3OCH_2 is a β radical, as is CH_3. The termination is thus of the $\beta\beta$ type, and this together with first-order initiation gives rise to three-halves order kinetics. Following the terminology of Laidler, Sagert and Wojciechowski (15) this mechanism may be denoted by $^1\beta\beta_{3/2}$, the initial superscript indicating the order of the initiation process, and the subscript 3/2 denoting the over-all order.

It may be noted that three-halves order over-all kinetics are also obtained if the orders of reactions [11] and [13a] are reversed; i.e. if the reactions are

[11a] $H + CH_3OCH_3 \rightarrow CH_3 + CH_3O + M$

[13] $CH_2OCH_3 \rightarrow CH_2O + CH_3$

Initiation is now second-order and CH_2OCH_3 is a μ radical; this again gives rise to three-halves order kinetics ($^2\beta\mu_{3/2}$).

Benson and Jain's main reason for preferring the $^1\beta\beta_{3/2}$ scheme is that the apparent first-order frequency factor for reaction [13], as calculated by Trotman-Dickenson (29) from the results of Marcus, Darwent and Steacie (30) is $\sim 10^{10}$ sec^{-1}; this is much too low to be a true frequency factor for a unimolecular dissociation involving no change of multiplicity. An apparent way out of the difficulty is

to suggest that the reaction is really in its second-order region. It might also be urged in favour of the Benson-Jain scheme that if the dissociation of CH_3OCH_3 were second-order that of CH_2OCH_3 would be second-order *a fortiori*, in view of its lower activation energy and smaller number of degrees of freedom.

Further consideration, however, reveals that these arguments are not as convincing as they appear at first sight. Thus the analytical methods on which the experimental results of Marcus *et al.* are based are not very reliable, and involved measuring amounts of CH_2O, CO and 'dimer' ($CH_3OCH_2CH_2OCH_3$) produced from the radical CH_2OCH_3. It seems very possible that some of what was reported as 'dimer' was actually polymerised formaldehyde, since formaldehyde is known to polymerise readily under similar analytical conditions (31). This would have a very serious effect on the experimental results, and the frequency factor and activation energy for reaction [13] therefore cannot be relied upon.

Secondly, there is a precedent for suggesting that reaction [13] is second-order and reaction [11] first-order, since a similar situation exists in the ethane pyrolysis; the evidence (14) there seems conclusive that the dissociation of C_2H_6 is first-order and that of C_2H_5 second-order. Two explanations may tentatively be put forward to explain this

apparently paradoxical result:

(i) The number of effective degrees of freedom in the radical (C_2H_5 or CH_2OCH_3) may be larger than in the corresponding molecule (C_2H_6 or CH_3OCH_3) because of less symmetry (cf. Laidler and Wojciechowski (32).

(ii) When a radical decomposes in the presence of a very large excess of its parent molecule there may exist an abnormally effective mechanism for energy transfer, involving atom abstraction. Some support for this interpretation is provided by the conclusion of Purnell and Quinn (33) that the ethyl radical decomposition is not in its first-order region when it is in the presence of butane and in the absence of the parent molecule ethane.

On the basis of these arguments there remains no valid objection to concluding that the reaction is of the type $^2\beta\mu_{3/2}$. Very strong evidence that the initiating reaction is in fact in its second-order region has been obtained from a study of the reaction in the presence of hydrogen sulphide, and is described in detail in Part II, C. This evidence excludes the Benson-Jain $^1\beta\beta_{3/2}$ mechanism. It is consistent with a mechanism in which the chain-ending step involves the recombination of two β radicals, in the low pressure region ($^2\beta\beta H_{3/2}$), and also with a $^2\beta\mu_{3/2}$ mechanism. These are the only two possibilities if initiation is second-order. One

can at once eliminate the second of these two possibilities by the fact that the reaction shows only a very slight effect of inert gases (26); the $^2p\mu_{3/2}$ mechanism would predict a substantial positive inert gas effect, since inert gases will increase the rate of initiation but will have no effect on the rate of termination. With a $^2p\beta_{3/2}$ mechanism, on the other hand, no strong inert-gas effect is to be expected, since both initiation and termination will be affected by the addition of inert gas, and the two effects will approximately cancel.

Chain-ending Steps

Initially, before any formaldehyde has decomposed, the radicals present in the system are CH_3, CH_3O, CH_2OCH_3 and H; only CH_3 and CH_2OCH_3 are involved in chain-propagating steps, and their concentrations are very much greater than those of the other two radicals. The CH_3 radical is certainly a β radical, and CH_2OCH_3 may be either β or μ and may indeed play both roles. The following chain-ending steps are therefore possible;

[17a] $CH_3 + CH_3 + M \rightarrow C_2H_6 + M$

[18a] $CH_3 + CH_2OCH_3 + M \rightarrow CH_3CH_2OCH_3 + M$

[19a] $2CH_2OCH_3 + M \rightarrow CH_3OCH_2CH_2OCH_3 + M$

A choice between these possibilities can be made by carrying out calculations of the concentrations of the radicals, and finding out which chain-ending steps will occur with greatest velocity. Such calculations lead to the conclusion that reaction [17a] occurs somewhat more rapidly than either of the other processes [16a] and [19a]. The over-all reaction mechanism is therefore concluded to be, for the most part,

[11a] $M + CH_3OCH_3 \rightarrow CH_3 + CH_3O + M$

[12] $CH_3 + CH_3OCH_3 \rightarrow CH_4 + CH_2OCH_3$

[13] $CH_2OCH_3 \rightarrow CH_2O + CH_3$

[14a] $M + CH_3O \rightarrow CH_2O + H + M$

[15] $H + CH_3OCH_3 \rightarrow H_2 + CH_2OCH_3$

[17a] $CH_3 + CH_3 + M \rightarrow C_2H_6 + M$

It should be noted that reaction [14a] is almost certainly in its second-order region, but this has no effect on the over-all behaviour. As discussed earlier, it is not certain whether reaction [13] is first-order or second-order, and this again makes no difference as far as the over-all order is concerned.

Application of the steady-state treatment to the above mechanism gives rise to the following approximate

expressions for the radical concentrations:

$$[CH_3] = \left(\frac{2k_{11a}}{k_{17a}}\right)^{1/2} [CH_3OCH_3]^{1/2}$$

$$[CH_2OCH_3] = \frac{k_{12}}{k_{13}} \left(\frac{2k_{11a}}{k_{17a}}\right)^{1/2} [CH_3OCH_3]^{3/2}$$

The over-all rate is given by

$$v = k_{12} \left(\frac{2k_{11a}}{k_{17a}}\right)^{1/2} [CH_3OCH_3]^{3/2}$$

Values of frequency factors and activation energies for the various elementary processes are given in Table 1, which refers to a temperature of 800°K. The use of these values in the expressions for the radical concentrations leads to the conclusion that the concentrations at 800°K, and with [M] taken as 10^{-5} moles per cc, are as follows:

$[CH_3] = 1.8 \times 10^{-13}$ moles cc^{-1} $[CH_2OCH_3] = 3.1 \times 10^{-15}$ moles cc^{-1}

The methyl radical is therefore predominant, and reaction [17a] is therefore concluded to be the main chain-ending step. One cannot, however, exclude the possibility that reactions [18a] and [19a] also play a small role in the process. It may be noted that the value of 10^{-5} taken for [M] corresponds to the upper range of the pressures employed ($\sim$500 mm Hg); at

Table 1

Kinetic Parameters for the Uninhibited Reaction

Reaction	Frequency Factor (sec^{-1}, $cc.\ mole^{-1}\ sec^{-1}$ or $cc^2\ mole^{-2}\ sec^{-1}$)	Activation Energy (kcal. per mole)	Rate Constant at 800°K (sec^{-1}, $cc.\ mole^{-1}\ sec^{-1}$ or $cc^2\ mole^{-2}\ sec^{-1}$)	Reference
12a	1×10^{10}	74.0	5.8×10^{-3}	estimated (see Appendix I)
12	3×10^{12}	9.5	7.8×10^{8}	Trotman-Dickenson and Steacie (34)
13	7×10^{10}	19.0	4.6×10^{5}	Marcus, Darwent and Steacie (30); Trotman-Dickenson (29)
17a	7×10^{14}	-13.5	3.5×10^{10}	estimated (see Appendix I)

lower pressures the methyl radicals are predominant a fortiori.

Except at the very beginning of the reaction there will be significant amounts of the formyl radical HCO, which arises from the decomposition of the formaldehyde produced as an intermediate. In a personal communication Professor S.W. Benson has suggested to us that for the main part of the reaction the principal chain-ending step is

$$[20] \qquad CH_3 + HCO \longrightarrow CH_4 + CO.$$

According to Professor Benson this reaction will occur more rapidly than reaction [17a] except at the very beginning of reaction. We are unable, however, to agree with this suggestion, for two main reasons. In the first place, our work with hydrogen sulphide (Part II, C) leads unequivocally to the conclusion that the initial dissociation of dimethyl ether is, under our experimental conditions, in its second-order region. This being so, reaction [20], being of the type pp, leads to second-order kinetics, in disagreement with experiment; only with a first-order initiation process does this lead to the correct 3/2-order kinetics. In the second place, our calculations of radical concentrations and rates lead us to the conclusion that reaction [17a] actually occurs considerably more rapidly than reaction [20]. We calculate the third-order rate constant for reaction [17a] to be, at 800°K,

3.5×10^{10} cc^2 mole^{-2} sec^{-1} so that, with the concentration of M taken as 10^{-6}, the rate of reaction [17a] can be expressed as

$$v_{17a} = 3.5 \times 10^{12} [CH_3]^2$$

The concentration of CHO radicals is calculated to be somewhat less than that of CH_3, but for the purpose of the present estimate it will be assumed that the concentrations are the same. Since reaction [20] is a hydrogen atom abstraction reaction its frequency factor is expected to be about 10^{11} cc. mole^{-1} sec^{-1} and its activation energy will be at least 5 kcal per mole. On this basis we calculate that the rate of reaction [20] would be, at 800°K,

$$v_{20} = 4.3 \times 10^9 [CH_3][CHO].$$

Even with equal CH_3 and CHO concentrations the rate of reaction [20] is therefore considerably less than that of reaction [17a]. It is to be noted that the high rate of reaction [17a] is due to the fact that the complex formed from two methyl radicals has a very long life, so that the third-body recombination process occurs almost as rapidly as the second-order reaction with no activation energy.

The calculations do not, however, exclude the possibility that the recombination reaction

[21a] $CH_3 + CHO + M \rightarrow CH_3CHO + M$

plays a significant role in the reaction. Our conclusion is, in fact, that chain-ending may occur by reactions [17a], [18a], [19a] and [21a], with [17a] being most important.

The over-all Reaction

As a check on the proposed mechanism, with [17a] as the chain-ending step, calculations may be made of the absolute rate, frequency factor and activation energy of the reaction on the basis of the mechanism. Using the parameters given in Table 1 the calculated over-all values are

$$k = 0.045 \text{ cc}^{1/2} \text{ mole}^{-1/2} \text{ sec}^{-1}$$

$$A = 1.6 \times 10^{13} \text{ cc}^{2} \text{ mole}^{-2} \text{ sec}^{-1}$$

$$E = 53.3 \text{ kcal. mole}^{-1}$$

The calculated rate constant is less than the experimental value ($0.27 \text{ cc}^{1/2} \text{ mole}^{-1/2} \text{ sec}^{-1}$), as is the frequency factor but the activation energy is in good agreement with the experimental value of 54.9 kcal. mole^{-1}. The error undoubtedly lies in the rather long extrapolations required to calculate the low-pressure rate constants for the initiation and termination steps.

B. The Reaction Inhibited by Nitric Oxide and Propylene

INTRODUCTION

Publications from this laboratory (37-42) have provided evidence for the view that maximally inhibited reactions proceed not by molecular mechanisms but by processes in which the inhibitor is involved both in initiation and in termination. Detailed mechanisms have now been worked out for the decompositions of ethane (40), propane (41), butane (42) and other substances, and a specific scheme has been proposed for the dimethyl ether decomposition (37).

[22] $CH_3OCH_3 + NO \rightarrow CH_3OCH_2 + HNO$

[13] $CH_3OCH_2 \rightarrow CH_3 + CH_2O$

[12] $CH_3 + CH_3OCH_3 \rightarrow CH_4 + CH_2OCH_3$

[23] $HNO \rightarrow H + NO$

[25] $H + CH_3OCH_3 \rightarrow H_2 + CH_3OCH_2$

[24] $CH_3OCH_2 + NO \rightarrow CH_3OCH_2NO$

The rate expression which this scheme leads to is

$$v = \left(\frac{2k_{22}k_{13}}{k_{24}}\right)[CH_3OCH_3] + k_{22}[CH_3OCH_3][NO]$$

This part is concerned with an experimental study of the effects of nitric oxide and propylene on the decomposition of dimethyl ether, and with the formulation of reaction mechanisms. The mechanism previously proposed (37) has been found to require some revisions.

A considerable amount of previous experimental work has been done on the inhibited dimethyl ether decomposition. The reaction inhibited by nitric oxide was first studied by Staveley and Hinshelwood (43), who found that the rate is very considerably reduced by small amounts of nitric oxide, and that a limiting rate is reached with nitric oxide pressures between about 0.5 mm and 12 mm. They reported an activation energy of 62 kcal per mole for the maximally inhibited reaction, which they considered to be a molecular reaction. Gay and Travers (44) found, from a study of the products of the inhibited decomposition, that introduction of an increased quantity of nitric oxide into the reaction led to an increased amount of carbon monoxide in the products.

Thompson and Meisner (45) studied the absorption spectra of the products of the retarded decomposition of dimethyl ether, and found that during the course of the reaction the NO lines disappeared and that NH lines appeared; they suggested the formation of formaldoxime ($CH_2 = NOH$). A frozen mixture of the products gave a positive test for the

nitroso group.

Goldanskii (46) has reviewed the work done on inhibited organic decompositions prior to 1946. Based on an inhibition scheme postulated by Rice and Polly (47), he proposed the following mechanism for the dimethyl ether decomposition in the presence of nitric oxide:

[11]	CH_3OCH_3	→	$CH_3 + CH_3O$
[25]	$CH_3O + CH_3OCH_3$	→	$CH_3 +$ products
[12]	$CH_3 + CH_3OCH_3$	→	$CH_4 + CH_2OCH_3$
[13]	CH_2OCH_3	→	$CH_2O + CH_3$
[17]	$CH_3 + CH_3$	→	C_2H_6 or $C_2H_4 + H_2$
[26]	$CH_3 + NO$	→	CH_3NO
[27]	$CH_3OCH_3 + NO$	→	$CH_3NO + CH_3O$
[28]	$2CH_3NO$	→	Products

From this mechanism, Goldanskii was able to predict approximately the shapes of the pressure-time curves observed experimentally. The kinetic parameters, however, were for the most part estimates which are now known to be in error. The calculations were also based on some approximations which were very sensitive to small changes in the kinetic parameters, and the derived rate expression predicts second-order dependence

on other pressure. This mechanism must therefore be rejected.

Ree, Yang and Eyring (46) have recently proposed mechanisms from which they obtain a rate equation predicting a hyperbolic decrease of the reaction rate with the concentration of the inhibitor in the system. Thus, they are not concerned with the mechanism of the residual maximally inhibited reaction. Their mechanism, which they assume to be perfectly general, is interesting however from the point of view of the reactions postulated for inhibitor action. Along with a Rice-Herzfeld (24) mechanism they suppose the following reactions to be taking place.

$$[i] \qquad \beta + I \longrightarrow (\beta I)$$

$$[j] \qquad (\beta I) \longrightarrow \beta + I$$

$$(\beta I) \underset{[-r]}{\overset{[r]}{\rightleftharpoons}} C \longrightarrow \text{Prod.}$$

$$[t] \qquad (\beta I) + M \longrightarrow \beta + \text{Prod.} + I$$

where β represents a β-radical, (βI) is a complex formed between the β-radical and inhibitor (e.g. CH_3NO), C is an isomeric compound of (βI) (e.g. $CH_2 = NOH$) and I is the inhibitor. A similar scheme applies for μ radicals.

The over-all mechanism would not apply for the case of maximal inhibition; however, some of the steps (i, j, r, -r) are almost identical to some suggested below for inhibition

of dimethyl ether by nitric oxide.

Reaction [t] involves abstraction of a hydrogen atom by (βI) followed by a rearrangement and subsequent decomposition. If this reaction occurs at all it would probably be quite slow. It was not considered to be important in the mechanism postulated for the inhibited dimethyl ether pyrolysis.

Recently Imai and Toyama (49) have studied the effect of nitric oxide on the pyrolysis of dimethyl ether. They found that the rate was first decreased by small amounts of nitric oxide, but that it increased linearly as larger quantities of nitric oxide were added. In this accelerated region the order was unity with respect to both nitric oxide and ether. These authors suggested that the inhibited decomposition is a molecular process, and that large quantities of nitric oxide catalyse the molecular decomposition.

Chain branching reactions involving oximes and nitric oxide have been suggested by Norrish and Pratt (50) to account for the acceleration in paraffin pyrolyses when large quantities of NO are added. An example considered is a system containing ethyl radicals and nitric oxide. The suggested branching is said to be due to reactions such as:

[29] $NO + C_2H_5 \rightarrow C_2H_5NO$

[30] $C_2H_5NO \rightarrow CH_3CHNOH$

[31] $NO + CH_3CHNOH \rightarrow (CH_3CHN) + HNO_2$

[32] $(CH_3CHN) \rightarrow CH_3 + HCN$

[33] $HNO_2 \rightarrow OH + NO$

The inhibited rate, according to these workers, corresponds to a situation where the branching has not yet become significant. The usual Rice-Herzfeld (24) mechanism for paraffin pyrolyses are presumed to be occurring as well. Rate laws derived from such schemes have been shown to fit the experimental curves for the pyrolysis of n-pentane observed by Blackmore and Hinshelwood (51), but such a mechanism can be criticized in that these reactions add complications which are not required to explain the observed phenomena. As will be discussed in detail below, the mechanism postulated in this part, as well as in publications from this laboratory (37-42), adequately explain the acceleration at high nitric oxide pressures. The initiation reaction involving the abstraction of a hydrogen atom from the substrate becomes rate determining at sufficiently high pressures of NO. The subsequent fate of the radicals is therefore no longer important in defining the over-all rate of the decomposition.

RESULTS

Isotopic Mixing

Table 2 summarizes the results obtained using 1:1

Table 2

Isotopic Mixing Experiments

Expt. No.	CH_3OCH_3 Pressure (mm)	NO Pressure (mm)	CD_4 Pressure (mm)	Total Pressure Increase (mm)	Approximate % Decomposition	Ratio CD_3H/CD_4 in products
1	314	0	0	141	22.2	2.44
2	312	0	0	96	15.4	2.53
3	311	0	0	58	9.3	2.52
4	308	0	0	35	5.7	2.51
5	305	0	0	18	3	2.44
6	299	5.5	0	115	19.2	2.41
7	294	5.4	0	39	6.6	2.48
8	296	5.4	0	23	4.2	2.47
9	297	5.5	0	13	2.2	2.46
10	297	5.5	0	10	1.7	2.44
11	297	5.5	0	4	0.7	2.39
12	436	0	43	105	12.1	0.03
13	427	4.5	46	18	2.1	0.0
14	428	4.5	51	6	0.7	0.03
15	422	4.7	50	3	0.4	0.03

For experiments no. 1 to 11 inclusive the reaction temperature was 550°C, and for the remaining experiments the temperature was 500°C.

mixtures of CD_3OCD_3 and CH_3OCH_3. The average CD_3H/CD_4 ratio was 2.49 ± 0.04 for the uninhibited runs and 2.44 ± 0.03 for the inhibited runs. The extent of decomposition was determined from pressure measurements, and the methane ratios determined mass spectrometrically. The results from mixtures of ~10% CD_4 and ~90% CH_3OCH_3 in the absence of NO, and in the presence of ~1% NO (sufficient for maximal inhibition), are also shown in Table 2.

The Over-all Kinetics of the Reaction Inhibited by Nitric Oxide

Preliminary experiments were carried out to determine the quantity of nitric oxide required to reduce the rate of decomposition of dimethyl ether to a minimum. The results are summarised in Fig. 9. The curve shows that the relative rate drops sharply to a minimum with the addition of about 1.5 mm of nitric oxide. Further addition of nitric oxide has no effect on the rate until an amount greater than 10 mm has been added, and the rate then increases linearly with increasing nitric oxide pressure. Figure 9 also shows that no matter what pressure of ether was used the same minimum rate is obtained relative to the rate of the uninhibited reaction; ether pressures varying from 130 mm to 479 mm were used to obtain the points lying along the flat portion of the curve. Nitric oxide pressures between 2 mm and 10 mm were used in

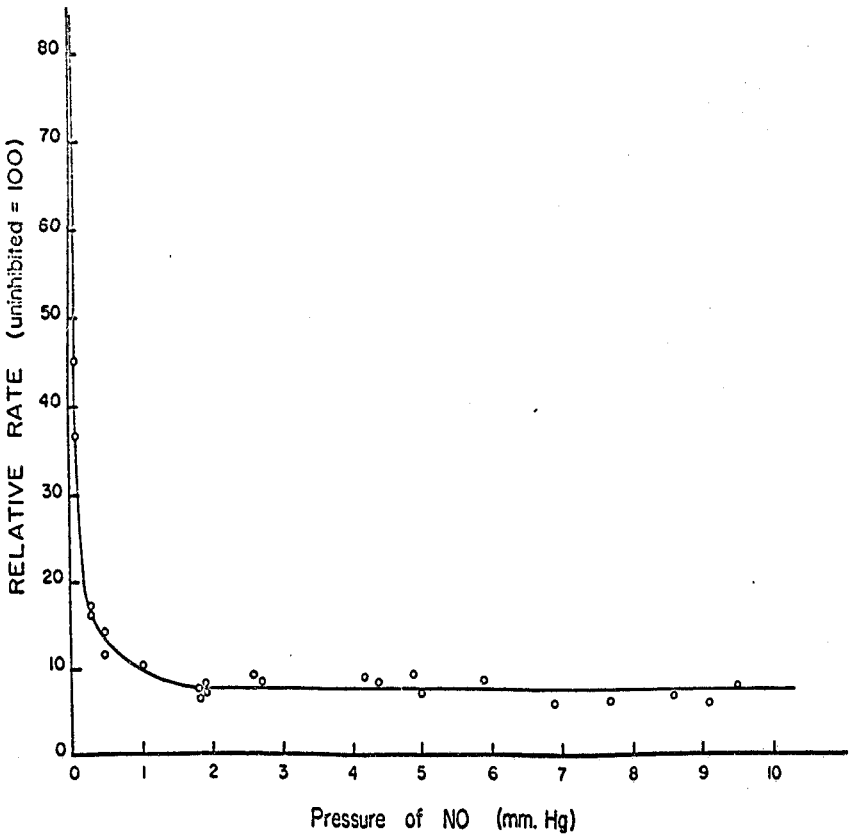

Figure 9. Relative rate (uninhibited rate = 100) against nitric oxide pressure, at 520°C.

subsequent investigations of the maximally inhibited reaction.

Figure 10 shows a typical pressure-time curve for the maximally inhibited decomposition and a similar curve for the uninhibited reaction. The ether pressure was the same (126 mm) in both cases. The curve for the inhibited reaction initially is completely different in shape from that of the uninhibited reaction. However, after a certain 'inhibition time' the rate of the inhibited reaction increases and approaches that of the uninhibited reaction. This is apparently due to the fact that the nitric oxide has been used up.

Figure 11 shows plots of the logarithm of the initial rate versus the logarithm of the ether pressure. About 5 mm of nitric oxide were used in all cases. The lines drawn have slopes of 1.5 at all temperatures. The initial rates become increasingly more difficult to measure as the temperature is lowered; the accuracy is therefore not as good at the lower temperatures, and the points become more scattered.

The activation energy, obtained from the Arrhenius plot shown in Fig. 12, was 64.6 kcal $mole^{-1}$. This is in satisfactory agreement with the activation energy of 62 kcal reported by Staveley and Hinshelwood (43). The three-halves order rate constant may be expressed as

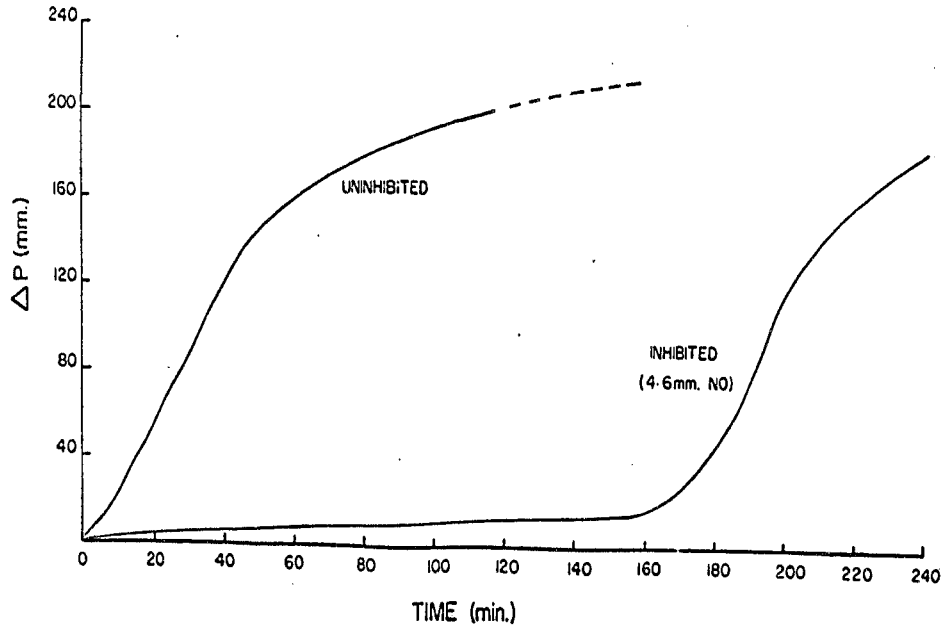

Figure 10. Typical pressure-time curves for the uninhibited reaction and for the reaction maximally inhibited by nitric oxide, at 520°C. The initial ether pressure was 126 mm. in each case.

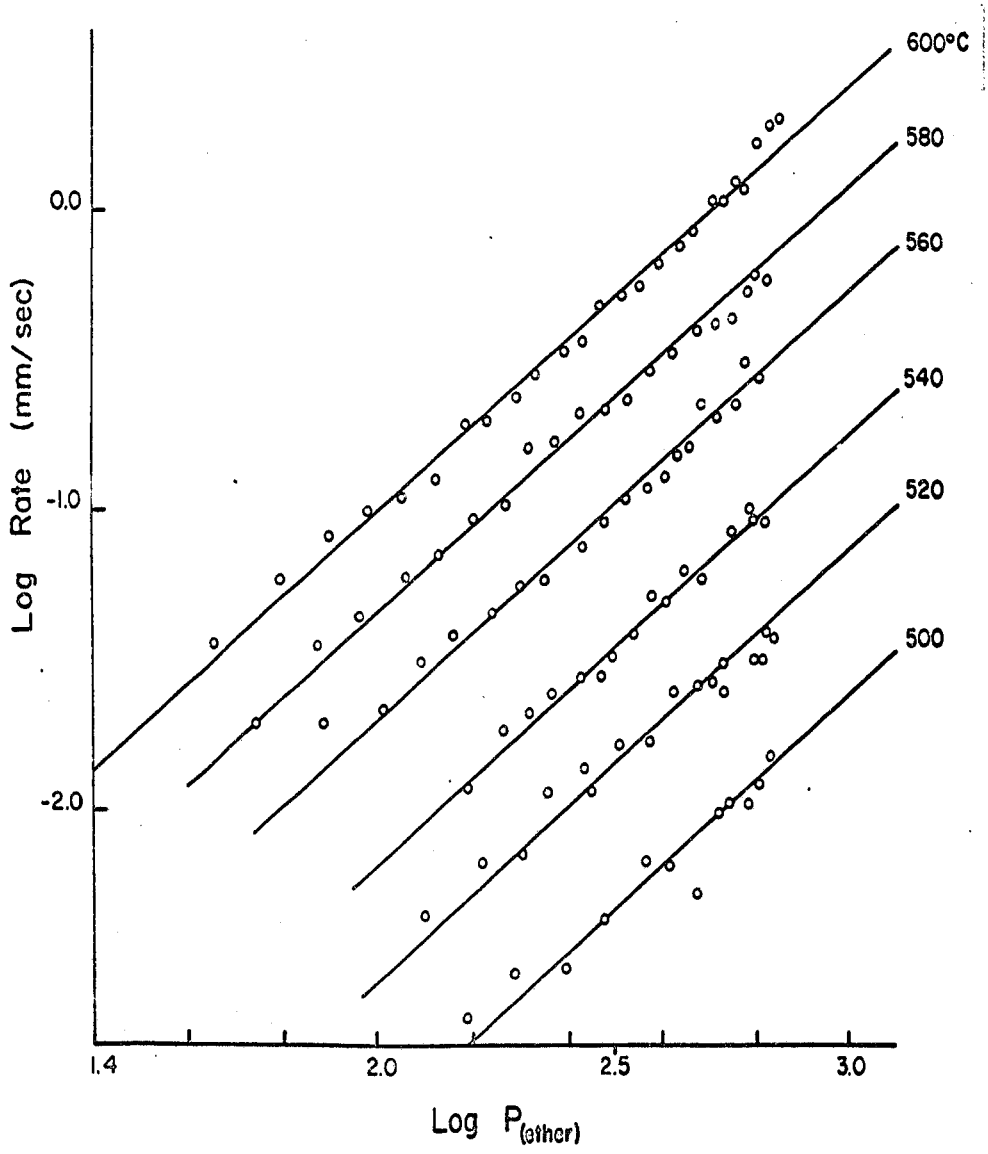

Figure 11. Double logarithmic plots of initial rate against ether pressure, for the maximally inhibited reaction at various temperatures. The lines have slopes of 1.5.

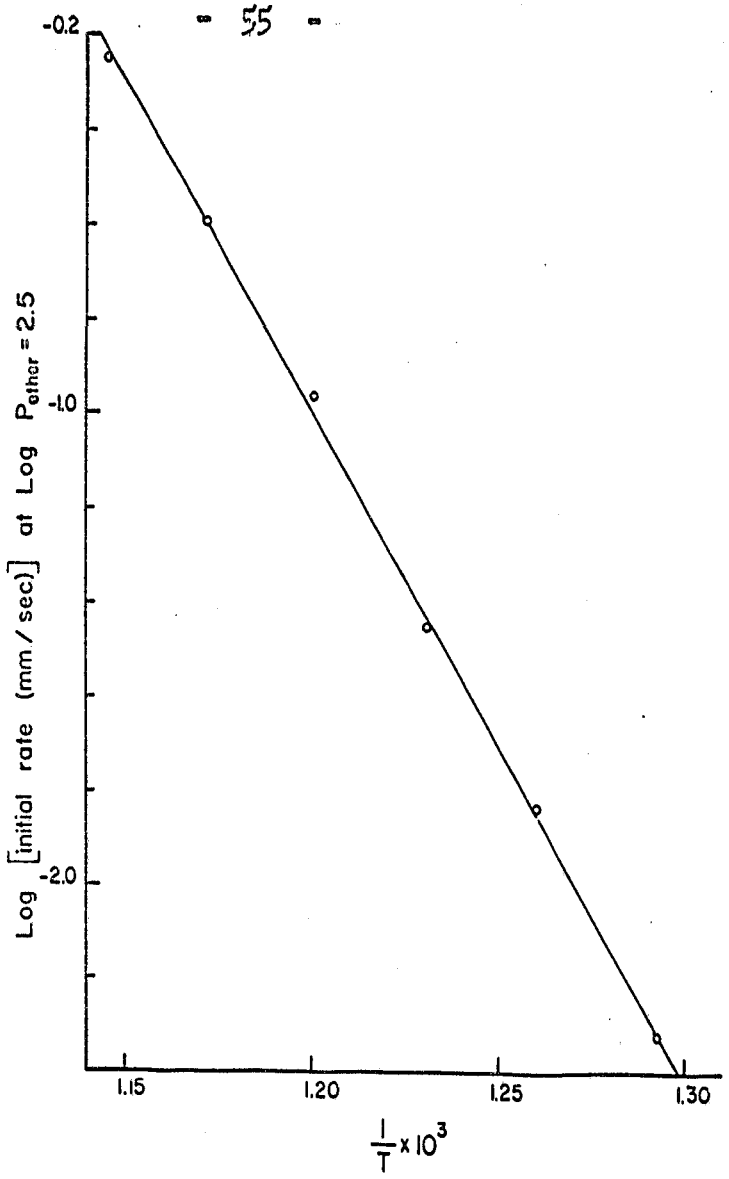

Figure 12. Arrhenius plot for the reaction maximally inhibited by nitric oxide.

$$k = 1.2 \times 10^{16} e^{-64,600/RT} cc^{1/2} mole^{-1/2} sec^{-1}.$$

The effect of the 'inhibition time' with varying amounts of nitric oxide is shown in Fig. 13. As the pressure of nitric oxide is increased the time required to reach the rate corresponding to the uninhibited rate steadily increases. More time is evidently required for the consumption of larger quantities of nitric oxide. The curves also demonstrate how the initial rate increases with large quantities (i.e. > 10 mm) of nitric oxide.

The Reaction Accelerated by Nitric Oxide

Some runs were carried out using high pressures of nitric oxide. Figure 14 shows a plot of the logarithm of the initial rate against the logarithm of the pressure of nitric oxide. The curves corresponding to different ether pressures all show some curvature at low nitric oxide pressures, but tend to linearity as the nitric oxide pressure is increased. The slopes of the linear portions of the curves are all unity. In the maximally inhibited region the order is obviously zero with respect to nitric oxide. The curvature therefore shows the gradual shift to first order in nitric oxide as the nitric oxide pressure is increased. In subsequent studies in this region where the decomposition is sensitised by high pressures of nitric oxide, care was taken to ensure that at

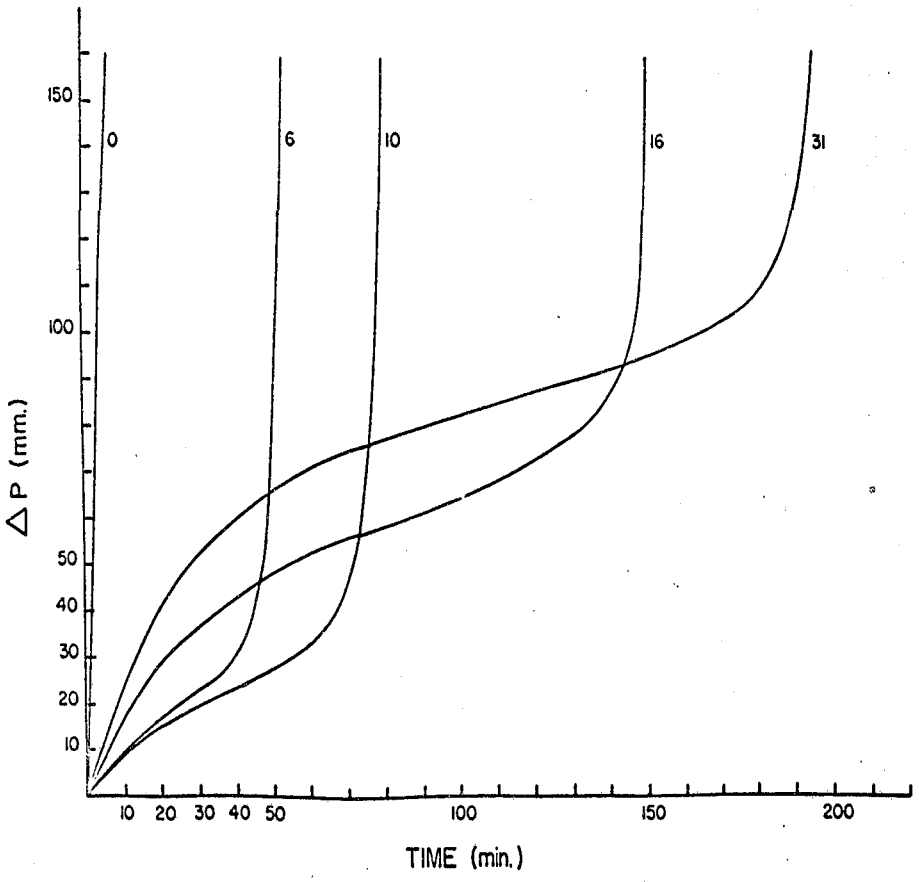

Figure 13. Pressure-time curves for various pressures (mm. Hg) of nitric oxide, which are indicated on the curves; the ether pressures were 470-485 mm, and the temperature 520°C.

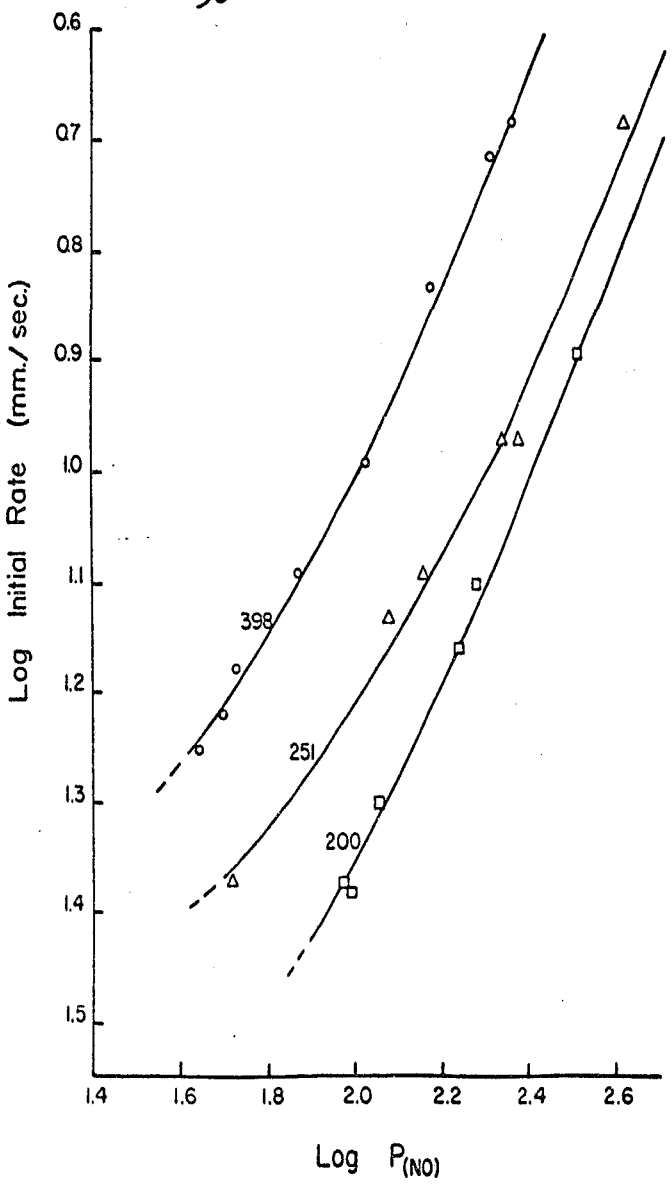

Figure 14. Double logarithmic plot of initial rate against nitric oxide pressure, for the accelerated reaction and for three different pressures of dimethyl ether which are indicated on the curves.

least 250 mm of nitric oxide (corresponding to log $P_{NO} = 2.4$ in Fig. 14) was used.

Rates were determined for the accelerated reaction for pressures of dimethyl ether varying from approximately 75 mm to 425 mm Hg, and over the temperature range from 510 to 570°C. As will be shown in the discussion, the over-all rate expression for the inhibition by nitric oxide can be expressed by

$$v = k[CH_3OCH_3][NO] + k'[CH_3OCH_3]^{3/2}$$

In the accelerated region, i.e. when [NO] is very large, the first term in the expression predominates and the reaction in first-order with respect to both ether and nitric oxide; this was shown experimentally. To avoid the tedious procedure of maintaining a constant nitric oxide pressure, while studying the change in rate with variation of ether pressure, the logarithm of the rate minus the logarithm of the nitric oxide pressure was plotted against the logarithm of the ether pressure. Figure 15 shows the results of such plots. The lines drawn all have slopes of approximately unity. The fact that the slopes are all slightly greater than unity (~ 1.1) shows that the second term in the above expression is not completely negligible even at nitric oxide pressures as high as 350 to 450 mm.

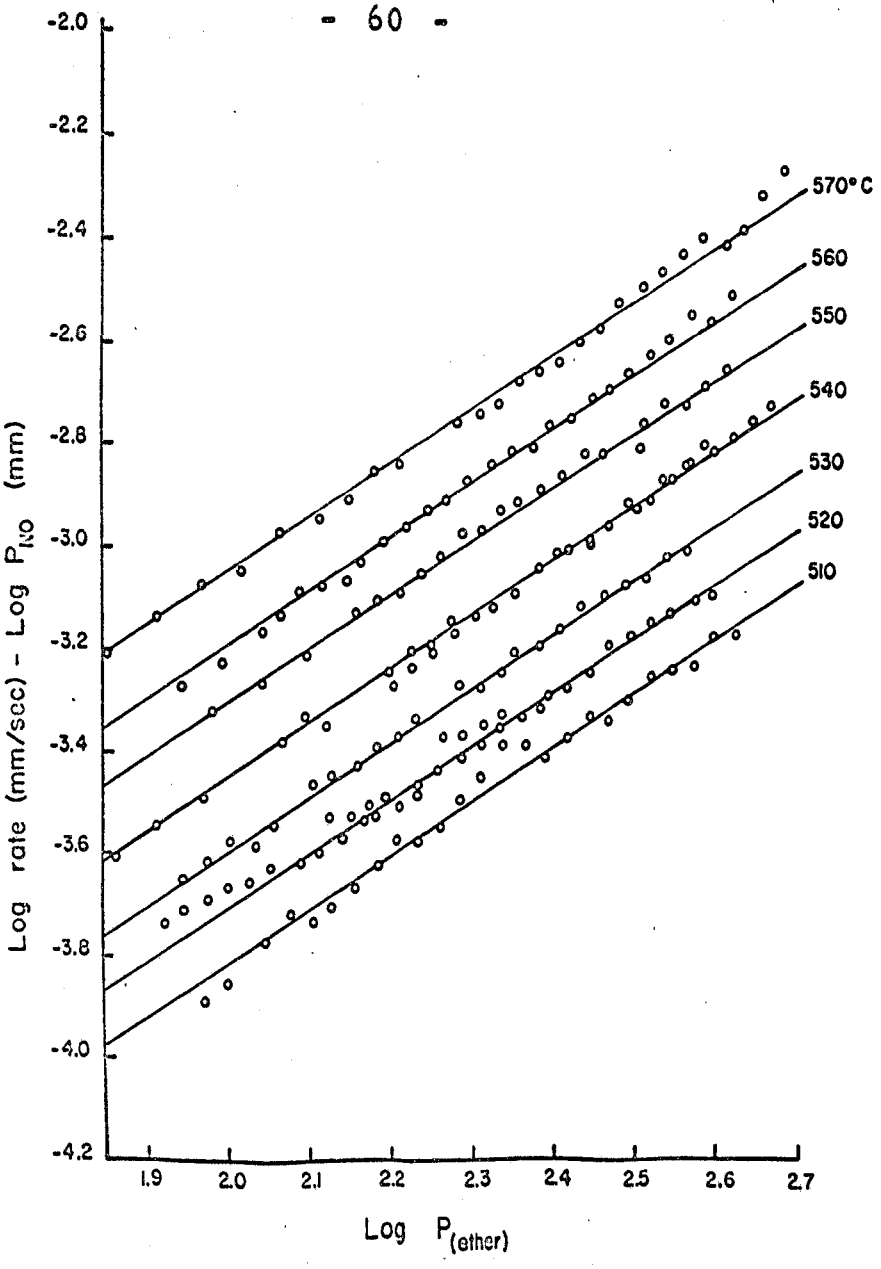

Figure 15. Double logarithmic plots of initial rate against ether pressure, for the reaction accelerated by nitric oxide.

An Arrhenius plot of the data is shown in Fig. 16. The line drawn shows some curvature at the low temperatures, but is linear for temperatures above 530°C. The activation energy calculated from a least-squares treatment of the linear portion of the curve was found to be 43.4 kcal per mole, and the frequency factor was 9.6×10^{13} cc. $mole^{-1}$ sec^{-1}. This is an approximation to the true Arrhenius factor since, as was pointed out, the slopes of the curves of log v - log P_{NO} against log P_{ether} were slightly greater than unity. An approximate second-order rate expression can be written as $k \approx 1 \times 10^{14}\ e^{-43,400/RT}$ cc. $mole^{-1}$ sec^{-1}.

The Reaction Inhibited by Propylene

The inhibition curve showing the variation of relative rate with pressure of propylene is compared in Fig. 17 with the corresponding curve using nitric oxide as the inhibitor. About 70 mm of C_3H_6 are required at 520° to give a limiting rate. The relative rate in the maximally inhibited region is independent of ether pressure, as was also found in the case of inhibition by nitric oxide. In this case ether pressures varying from 168 mm to 513 mm are plotted along the flat portion; the variation was always well within the experimental error. The amount of propylene required to attain a limiting rate varied slightly with temperature. However, even at the highest temperature

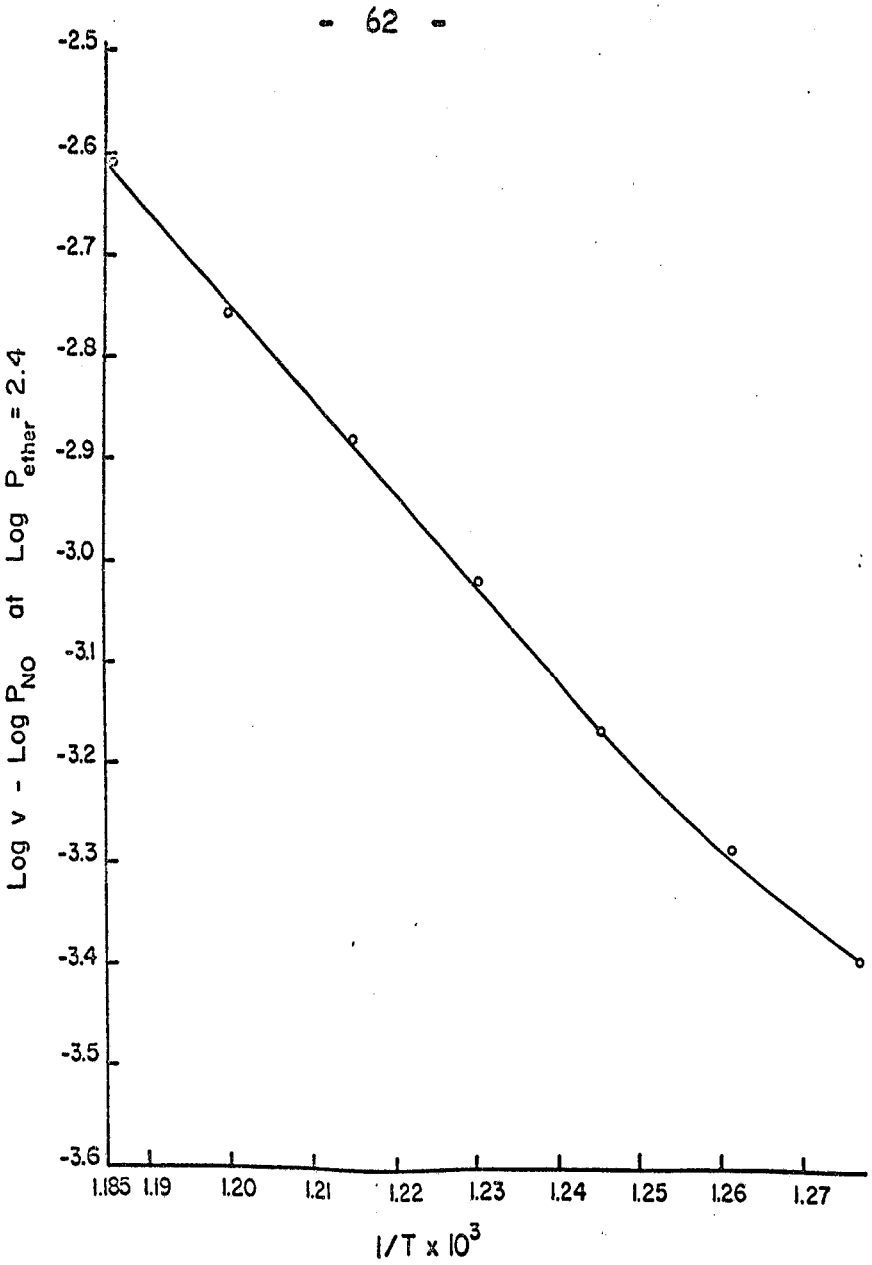

Figure 16. Arrhenius plot for the reaction accelerated by nitric oxide.

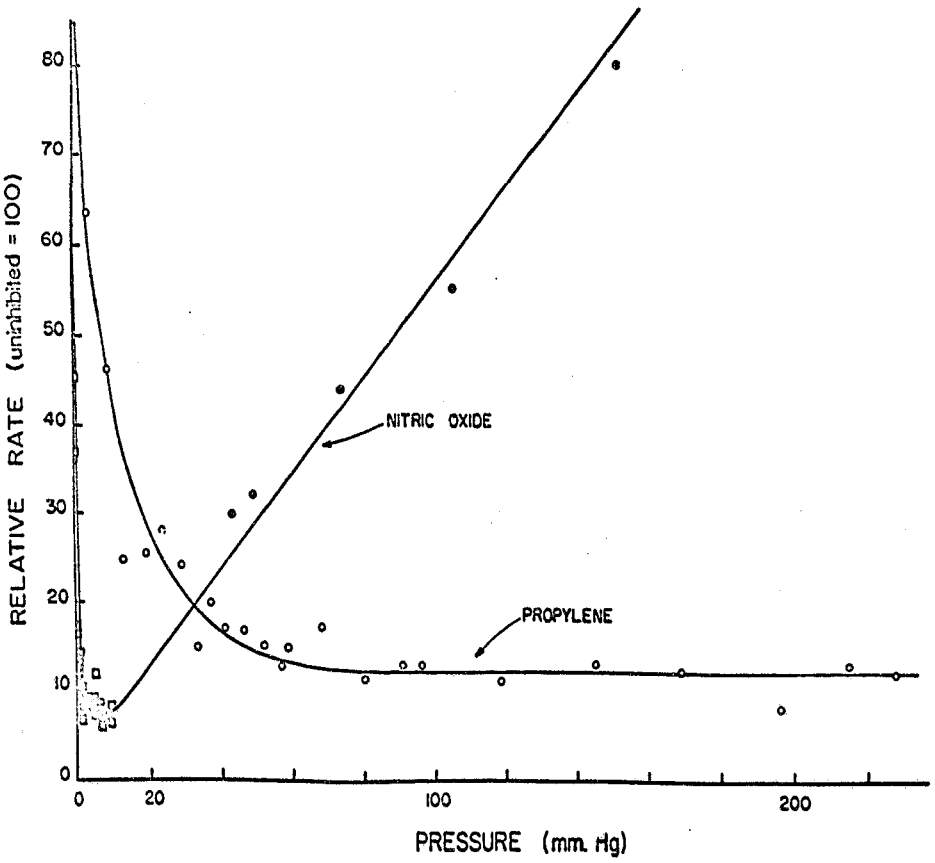

Figure 17. Relative rate (uninhibited rate = 100) against propylene and nitric oxide pressures, at 520°C. The filled circles indicate an initial ether pressure of 398 mm. Points along the flat portions were obtained for various pressures of dimethyl ether.

studied about 85 mm of propylene was found to be sufficient for maximal inhibition. The propylene-inhibition curve differs in shape from the inhibition curve for nitric oxide in the region studied. Even pressures of propylene of about 200 mm failed to increase the rate of the decomposition, whereas pressures greater than 10-15 mm of nitric oxide produced a pronounced increase in rate. Care was taken in subsequent experiments in the fully inhibited region to maintain the propylene pressure at greater than 90 mm.

A typical pressure-time curve for the maximally inhibited reaction is shown in Fig. 18. The shape of the curve indicates that the system reaches equilibrium before an appreciable quantity of propylene is used up. The pressure-time relation for propylene therefore does not show the same behaviour as does that for nitric oxide; this can be seen by comparing Fig. 18 with Fig. 10. The small quantity of nitric oxide necessary for maximal inhibition can be consumed before equilibrium is established between the other and its products, but since much larger quantities of propylene must be used, a very long time would be required for all of the propylene to be used up, and the system comes to equilibrium before this can happen.

Figure 19 shows plots of the logarithm of the inflexion-point rate against the logarithm of the other pressure,

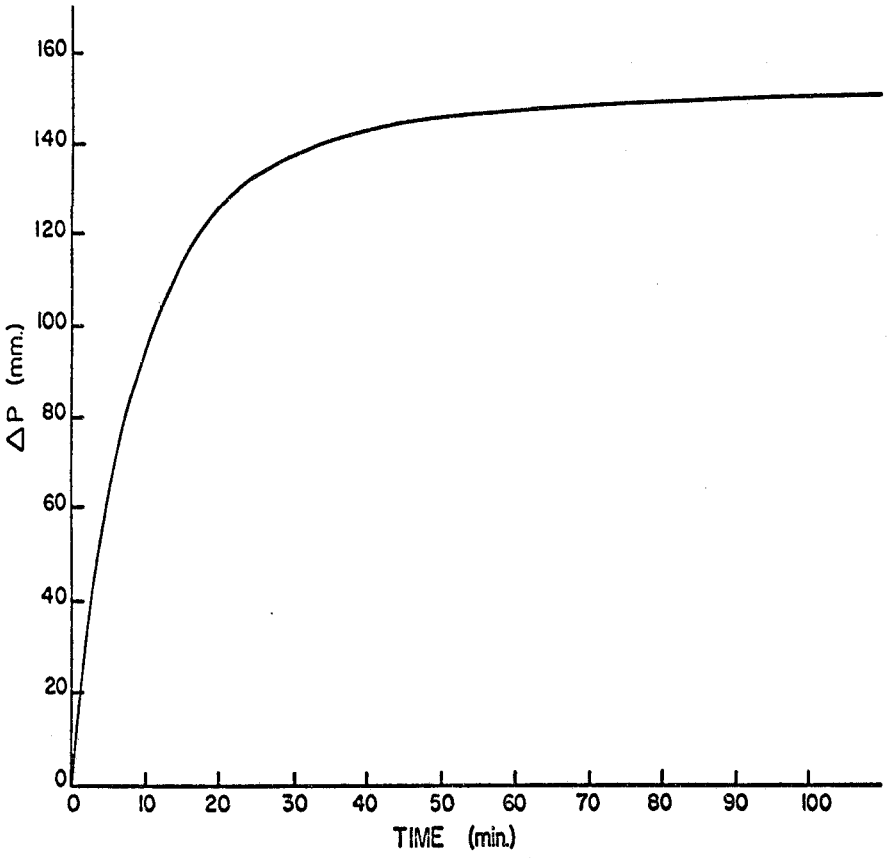

Figure 18. A typical pressure-time curve for the reaction maximally inhibited by propylene; the initial ether pressure was 94 mm., the propylene pressure 107 mm., and the temperature 600°C.

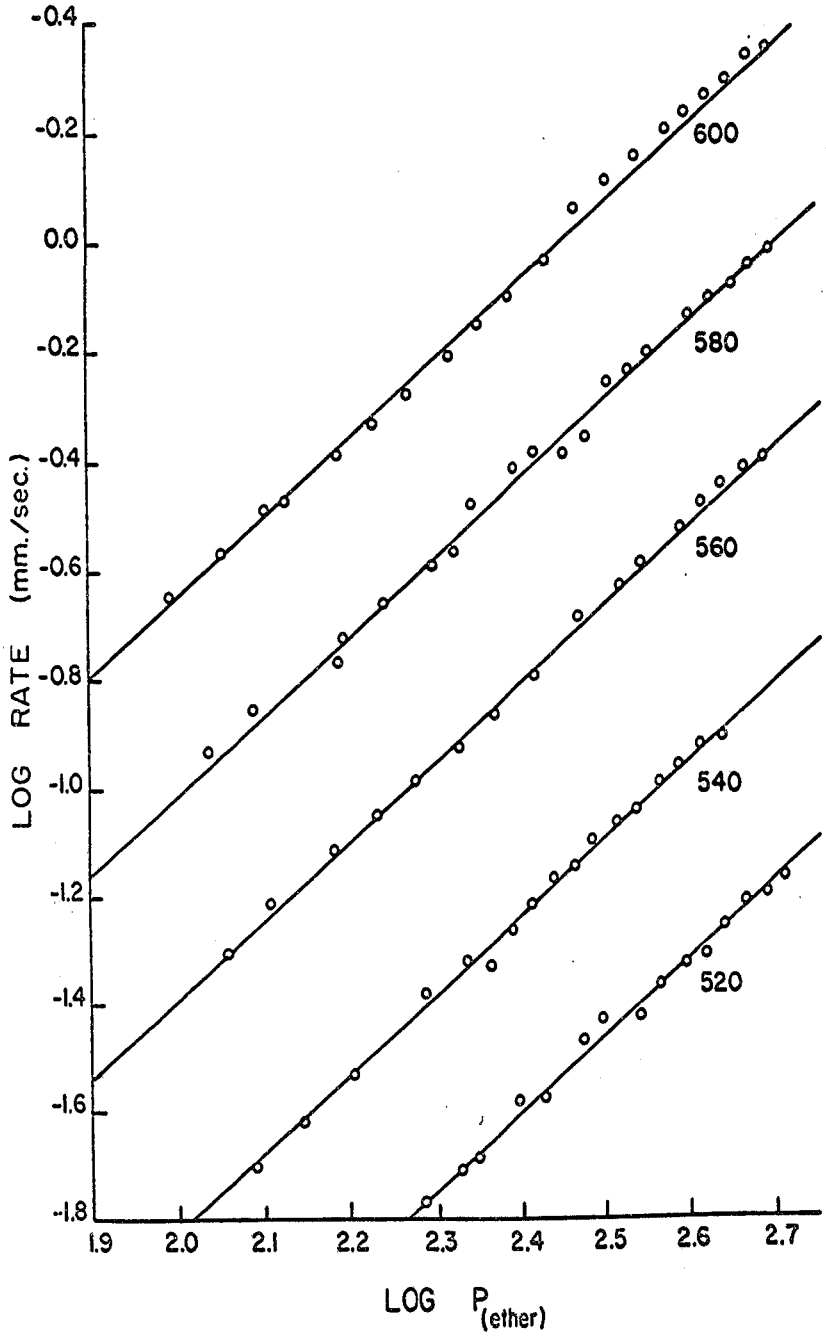

Figure 19. Double logarithmic plots of inflexion point rate against ether pressure for the reaction maximally inhibited by propylene.

at temperatures between 520 to 600°C. The inflexion-point rates were used in this case because initial rates could not be measured very accurately especially at the higher temperatures.

The order, determined from the slopes of the lines in Fig. 19, was three-halves over the complete temperature and pressure ranges studied.

Figure 20 shows the Arrhenius plot for this system. The line drawn is the best fit determined by a least-squares treatment. The activation energy is 61.7 kcal per mole and the rate constant can be expressed as

$$k = 4.6 \times 10^{15} e^{-61,700/RT} \; CO^{1/2} \; mole^{-1/2} \; sec^{-1}.$$

DISCUSSION

Isotopic Mixing

Since the CD_3H/CD_4 ratio for the inhibited reaction is approximately the same as in the uninhibited reaction (see Table 2) it can be concluded that in the region of maximum inhibition the reaction is almost entirely a chain process. The suggestion made by previous workers (43,49) that the inhibited reaction is entirely molecular must therefore be considered invalid for the dimethyl ether pyrolysis. The very low value obtained for the CD_3H/CD_4 ratio, in the case

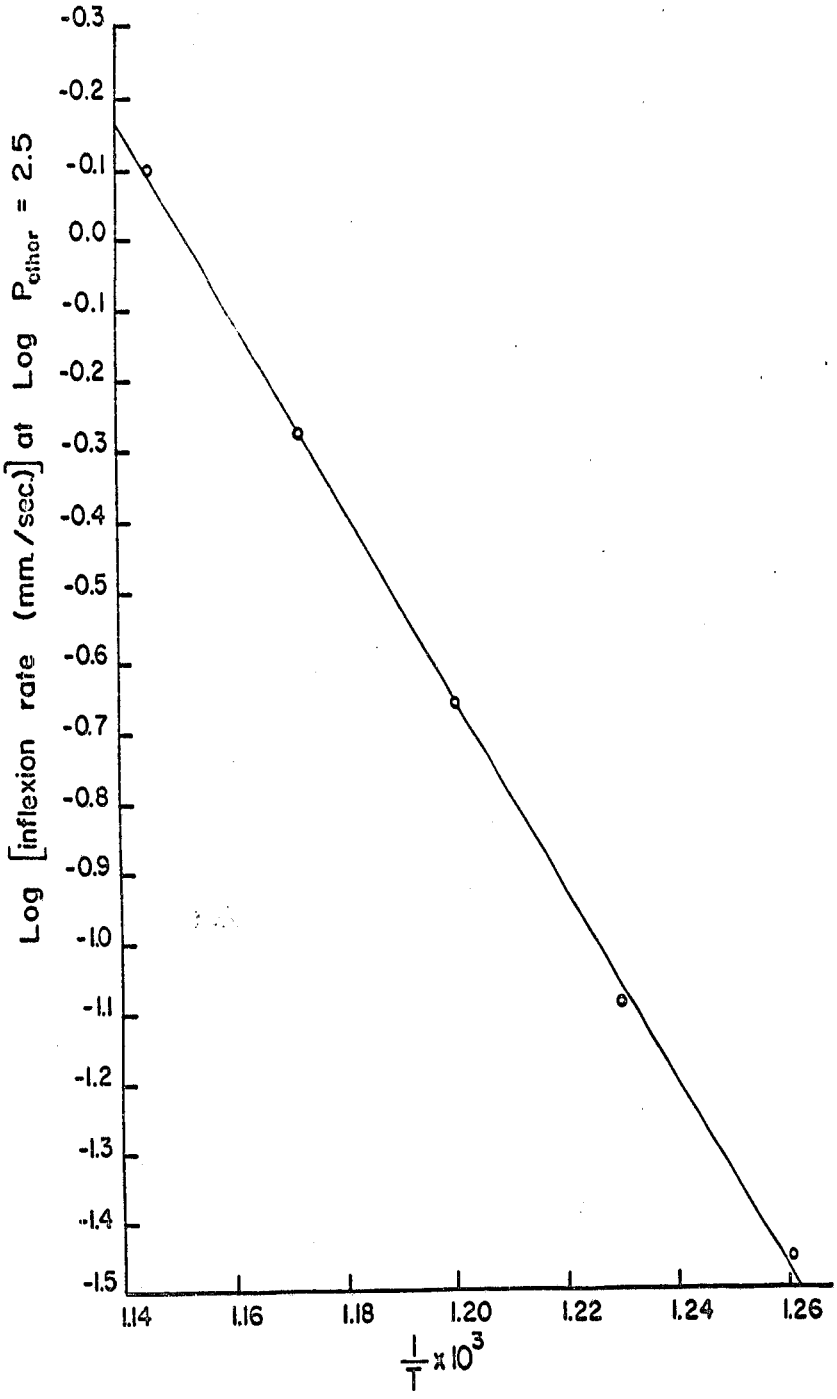

Figure 20. Arrhenius plot for the reaction maximally inhibited by propylene.

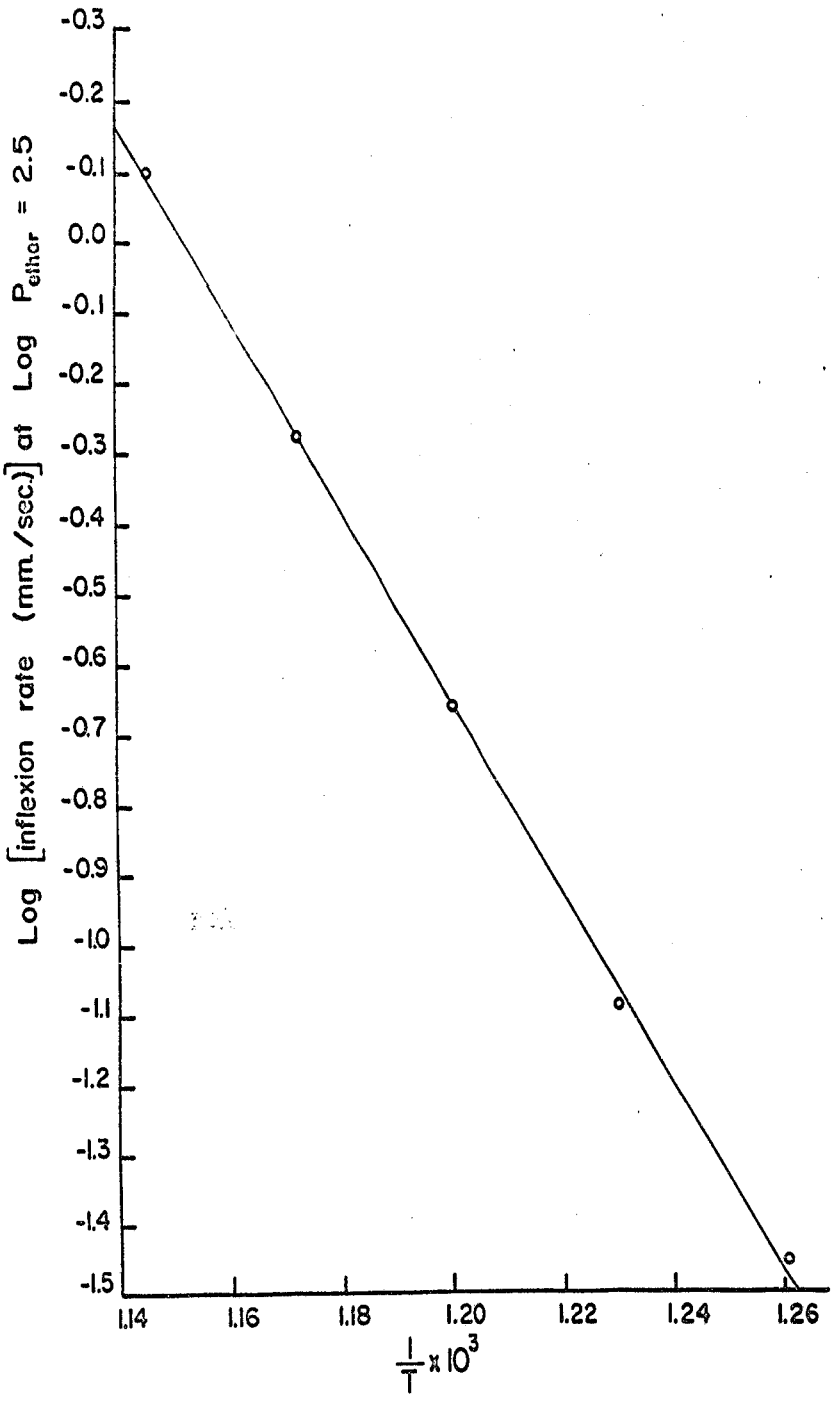

Figure 20. Arrhenius plot for the reaction maximally inhibited by propylene.

of CD_4, CH_3OCH_3, and NO mixtures, indicates that secondary processes are unimportant under these experimental conditions.

The Reaction Fully Inhibited by Nitric Oxide

The participation of nitric oxide in the initiation reaction in the dimethyl ether decomposition has been suggested by Wojciechowski and Laidler (37). Experimentally (see Fig. 10) nitric oxide effectively removes the induction period that is present in the uninhibited decomposition, and this suggests a direct reaction between NO and dimethyl ether. Initiation could therefore occur by either

[22] $CH_3OCH_3 + NO \rightarrow HNO + CH_3OCH_2$

or

[22'] $CH_3OCH_3 + NO \rightarrow CH_3ONO + CH_3$.

As far as the energetics of these reactions are concerned reaction [22'] is favoured. Reaction [22] is endothermic by about 43 kcal. (assuming $D(CH_3OCH_2 - H)$ to be approximately 92 kcal. per mole as discussed later), [22'] is endothermic by about 39 kcal/mole. On the other hand [22'] is a displacement reaction, while [22] is an abstraction reaction and would probably be favoured on steric grounds. Both reactions give similar rate expressions in the over-all scheme, as will be shown below for convenience it will be assumed that initiation is by [22].

If reaction [22] is the correct initiation reaction, the HNO will dissociate to produce H and NO. In hydrocarbon systems in which H atoms are present in large concentrations the reverse step also occurs. However in the decomposition of ether the hydrogen-atom concentration is quite low since the CH_3 radical is the principal chain carrier. The concentrations of HNO is therefore low; the HNO largely dissociates and an equilibrium is established between CH_3, NO, CH_3NO and CH_2NOH,

$$HNO \longrightarrow H + NO$$

$$CH_3 + NO \rightleftharpoons CH_3NO \rightleftharpoons CH_2NOH$$

If on the other hand reaction [22'] is the correct one, the CH_3ONO can react with CH_3 radicals, as was shown by Jost and Phillips (52), as follows:

$$CH_3 + CH_3ONO \longrightarrow CH_3NO + CH_3O$$

The same equilibria as above would then be established.

The over-all order being three-halves, the chain-ending steps must involve reaction between a β radical and either HNO or CH_3NO, of which the latter is present in much larger amounts. Isomerization of CH_3NO to CH_2NOH is known to occur (53), and the latter probably reacts with CH_3 more rapidly than does CH_3NO, since the process $CH_3 + CH_3NO \longrightarrow C_2H_6 + NO$ probably involves a fairly high activation energy

(see Appendix II). The chain-ending step is therefore best written as

$$CH_3 + CH_2NOH \rightarrow CH_3CH_2\text{-}NOH \rightarrow C_2H_6 + NO.$$

This reaction is quite exothermic and can probably occur with no activation energy. The disappearance of nitric oxide is accounted for by the breakdown of CH_2NOH.

The mechanism to which these considerations leads is:

[22]	$CH_3OCH_3 + NO$	$\rightarrow$	$HNO + CH_2OCH_3$
[13]	CH_2OCH_3	$\rightarrow$	$CH_2O + CH_3$
[12]	$CH_3 + CH_3OCH_3$	$\rightarrow$	$CH_4 + CH_2OCH_3$
[23a]	$H + HNO$	$\rightarrow$	$H + NO + H$
[15]	$H + CH_3OCH_3$	$\rightarrow$	$H_2 + CH_2OCH_3$
	$H + CH_3 + NO$	$\underset{[-26a]}{\overset{[26a]}{\rightleftharpoons}}$	$CH_3NO + H$
	CH_3NO	$\underset{[-34]}{\overset{[34]}{\rightleftharpoons}}$	$CH_2NOH \rightarrow$ products (HCN, etc.)
[35]	$CH_3 + CH_2NOH$	$\rightarrow$	$CH_3CH_2NOH \rightarrow C_2H_6 + NO$

Application of the conventional steady-state treatment yields the following expressions for the radical concentrations:

$$[H] = \frac{k_{22}}{k_{15}} [NO]$$

$$[HNO] = \frac{k_{22}}{k_{23a}} [NO]$$

$$[CH_2NOH] = \left(\frac{k_{22}k_{26a}k_{34}}{k_{-26a}k_{-34}k_{35}}\right)^{1/2} [CH_3OCH_3]^{1/2}[NO]$$

$$[CH_3NO] = \left(\frac{k_{22}k_{26a}k_{-34}}{k_{-26a}k_{34}k_{35}}\right)^{1/2} [CH_3OCH_3]^{1/2}[NO]$$

$$+ \frac{k_{22}}{k_{34}} [CH_3OCH_3][NO]$$

$$[CH_3] = \left(\frac{k_{22}k_{-26a}k_{-34}}{k_{26a}k_{34}k_{35}}\right)^{1/2} [CH_3OCH_3]^{1/2}$$

$$[CH_3OCH_2] = \frac{k_{12}}{k_{13}} \left(\frac{k_{22}k_{-26a}k_{-34}}{k_{26a}k_{34}k_{35}}\right)^{1/2} [CH_3OCH_3]^{3/2}$$

$$+ \frac{2k_{22}}{k_{13}} [CH_3OCH_3][NO]$$

The rate is given by

$$\frac{-d[CH_3OCH_3]}{dt} = 2k_{22}[CH_3OCH_3][NO]$$

$$+ k_{12}\left(\frac{k_{22}k_{-26a}k_{-34}}{k_{26a}k_{34}k_{35}}\right)^{1/2} [CH_3OCH_3]^{3/2}$$

At low NO concentrations the first term can be neglected in comparison to the second term, and the rate expression then predicts three-halves-order kinetics with respect to ether. However, when the nitric oxide concentration is large the first term can no longer be neglected and in fact the rate becomes first order with respect to both NO and ether concentration. This is in agreement with the experimental facts.

A calculation can be made to determine whether CH_3 radicals or CH_3OCH_2 radicals are present in greater amounts:

$$\frac{[CH_3]}{[CH_3OCH_2]} = \frac{k_{13}}{k_{12}} \frac{1}{[CH_3OCH_3]}$$

Use of the kinetic parameters listed in Table 3, and with $[CH_3OCH_3]$ equal to 10^{-5} moles per cc. gives rise to, at 600°C

$$\frac{[CH_3]}{[CH_3OCH_2]} = 59$$

Consequently the CH_3 radical should be involved in termination rather than the CH_3OCH_2 radical.

The activation energy for the maximally inhibited reaction predicted by the mechanism is:

$$E = E_{12} + \frac{1}{2}(E_{22} + E_{.26a} + E_{.34} - E_{26a} - E_{35})$$

Agreement with the experimental value of 64.6 kcal. per mole

Table 3

Kinetic Parameters for Inhibition by Nitric Oxide

Reaction	Frequency Factor sec^{-1} or $cc.\ mole^{-1}\ sec^{-1}$	Activation Energy $kcal.\ mole^{-1}$	k at 800°K sec^{-1} or $cc.\ mole^{-1}\ sec^{-1}$	Reference
[22]	1×10^{14}	43.4	1.3×10^{2}	see text
[12]	3×10^{11}	9.5	7.8×10^{8}	see Part II A
[13]	7×10^{10}	19.0	4.6×10^{5}	see Part II A
[23]*	2.1×10^{16}	48.0	1.6×10^{3}	Laidler, Sagert and Wojciechowski (41)
[26]*	1×10^{11}	0	1×10^{11}	(54)
[-26]*	1×10^{15}	50	21	A from (55) and E estimated (see Appendix II)
[34]	1×10^{13}	40	1.2×10^{2}	(56)
[-34]	1×10^{13}	55	9.1×10^{-3}	Estimated (see Appendix II)
[35]	1×10^{10}	0	1×10^{10}	Assumed

* The values given relate to the high-pressure region.

Table 3

Kinetic Parameters for Inhibition by Nitric Oxide

Reaction	Frequency Factor sec^{-1} or $cc.\ mole^{-1}\ sec^{-1}$	Activation Energy $kcal.\ mole^{-1}$	k at 800°K sec^{-1} or $cc.\ mole^{-1}\ sec^{-1}$	Reference
[22]	1×10^{14}	43.4	1.3×10^{2}	see text
[12]	3×10^{11}	9.5	7.8×10^{8}	see Part II A
[13]	7×10^{10}	19.0	4.6×10^{5}	see Part II A
[23]*	2.1×10^{16}	48.0	1.6×10^{3}	Laidler, Sagert and Wojciechowski (41)
[26]*	1×10^{11}	0	1×10^{11}	(54)
[-26]*	1×10^{15}	50	21	A from (55) and E estimated (see Appendix II)
[34]	1×10^{13}	40	1.2×10^{2}	(56)
[-34]	1×10^{13}	55	9.1×10^{-3}	Estimated (see Appendix II)
[35]	1×10^{10}	0	1×10^{10}	Assumed

* The values given relate to the high-pressure region.

is obtained if a value of 64.8 kcal. is taken for $E_{-26a} + E_{-34} - E_{26a} - E_{35}$. The significance of this value is that it implies that formaldoxime, CH_2NOH, is 64.8 kcal. more stable than $CH_3 + NO$. This is a reasonable conclusion; further discussion is to be found in Appendix II.

The predicted frequency factor is

$$A = A_{12}\left(\frac{A_{22}A_{-26a}A_{-34}}{A_{26a}A_{34}A_{35}}\right)^{1/2} = 3 \times 10^{15}\ cc^{1/2}mole^{-1/2}\ sec^{-1}$$

This is in satisfactory agreement with the experimental value of $1.2 \times 10^{16}\ cc^{1/2}\ mole^{-1/2}\ sec^{-1}$.

The Reaction Accelerated By Nitric Oxide

When large quantities of nitric oxide are used the rate of decomposition of dimethyl ether is considerably enhanced. The reaction has been found to be first-order with respect to both NO and CH_3OCH_3 in this region. This result is predicted by the mechanism given above for the fully inhibited reaction. As the quantity of NO is increased the first term in the over-all rate expression (i.e. $2k_{22}[CH_3OCH_3][NO]$) predominates. Thus the ratio of the two terms is given by

$$\frac{\text{term 1}}{\text{term 2}} = \frac{2k_{22}[CH_3OCH_3][NO]}{k_{12}\left(\frac{k_{22}k_{-26a}k_{-34}}{k_{26a}k_{34}k_{35}}\right)^{1/2}[CH_3OCH_3]^{3/2}}$$

This ratio is found to be approximately 73 after substitution of the values for the rate constants and the values $[NO] = [CH_3OCH_3] = 10^{-5}$ moles per cc. If $2k_{22}[CH_3OCH_3][NO]$ is the dominant term when [NO] is large, a second-order rate constant can be calculated which corresponds to k_{22}. The calculated second-order rate constant from Fig. 16 is given by

$$k_{22} = 1 \times 10^{14} e^{-43,400/RT} \text{ cc. mole}^{-1} \text{ sec.}^{-1}$$

The abstraction of a hydrogen atom from dimethyl ether by nitric oxide therefore has an activation energy of 43.4 kcal. per mole, and the frequency factor is, to a good approximation, 1×10^{14} cc. mole^{-1} sec^{-1}. The reason for the approximation is explained above. Using the value of 48.6 kcal. for D(H-NO) (57), and the activation energy of 43.4 kcal. determined above, an estimate of 92.0 kcal. mole^{-1} for $D(CH_3OCH_2\text{-}H)$ can be made.

It is well established that increased quantities of nitric oxide increase the proportion of carbon monoxide in the products (44). This is also true in the decomposition of acetaldehyde (58) and diethyl ether (59). This result has previously been explained as being due to oxidation reactions, but it can be explained by the mechanism postulated above. Carbon monoxide is a major product in the decomposition of formaldehyde, which itself is one of the major products in

This ratio is found to be approximately 73 after substitution of the values for the rate constants and the values $[NO] = [CH_3OCH_3] = 10^{-5}$ moles per cc. If $2k_{22}[CH_3OCH_3][NO]$ is the dominant term when [NO] is large, a second-order rate constant can be calculated which corresponds to k_{22}. The calculated second-order rate constant from Fig. 16 is given by

$$k_{22} = 1 \times 10^{14} e^{-43,400/RT} \text{ cc. mole}^{-1} \text{ sec.}^{-1}$$

The abstraction of a hydrogen atom from dimethyl ether by nitric oxide therefore has an activation energy of 43.4 kcal. per mole, and the frequency factor is, to a good approximation, 1×10^{14} cc. $mole^{-1}$ sec^{-1}. The reason for the approximation is explained above. Using the value of 48.6 kcal. for D(H-NO) (57), and the activation energy of 43.4 kcal. determined above, an estimate of 92.0 kcal. $mole^{-1}$ for $D(CH_3OCH_2\text{-}H)$ can be made.

It is well established that increased quantities of nitric oxide increase the proportion of carbon monoxide in the products (44). This is also true in the decomposition of acetaldehyde (58) and diethyl ether (59). This result has previously been explained as being due to oxidation reactions, but it can be explained by the mechanism postulated above. Carbon monoxide is a major product in the decomposition of formaldehyde, which itself is one of the major products in

the other decomposition. From the mechanism postulated above the rate of formation of formaldehyde is given by

$$\frac{d[CH_2O]}{dt} = k_{13}[CH_3OCH_2]$$

$$= 2k_{22}[CH_3OCH_3][NO] + k_{12}\left(\frac{k_{22}^2 k_{26a} k_{34}}{k_{26a} k_{34} k_{35}}\right)^{1/2}[CH_3OCH_3]^{3/2}$$

The rate expression thus includes a term involving [NO], and therefore the proportion of formaldehyde (and hence of CO) should increase with increasing amounts of nitric oxide. On the other hand, the rate of formation of methane is not increased by adding nitric oxide, since

$$\frac{d[CH_4]}{dt} = k_{12}[CH_3][CH_3OCH_3]$$

$$= k_{12}\left(\frac{k_{22}^2 k_{26a} k_{34}}{k_{26a} k_{34} k_{35}}\right)^{1/2}[CH_3OCH_3]^{3/2}$$

which does not contain a term involving [NO].

The Reaction Fully Inhibited by Propylene

An analogous mechanism can be written for inhibition by propylene by assuming that the allyl radical (C_3H_5) is capable of abstracting hydrogen atoms and is therefore the counterpart of NO in the previous scheme. That C_3H_5 can abstract hydrogen atoms is well established experimentally

(39, 60-63). Consequently, following the dissociation of propylene,

[36] $C_3H_6 \rightarrow C_3H_5 + H$,

the initiation reaction may be written as

[37] $CH_3OCH_3 + C_3H_5 \rightarrow C_3H_6 + CH_3OCH_2$

Experimentally there is an appreciable induction period in the propylene-inhibited reactions. This is required since an appreciable concentration of C_3H_5 radicals must first be formed. In the nitric oxide case the nitric oxide can abstract hydrogen atoms immediately and consequently there is no appreciable induction period.

The over-all mechanism for the propylene-inhibited decomposition may therefore be written as:

[37] $CH_3OCH_3 + C_3H_5 \rightarrow C_3H_6 + CH_3OCH_2$

[13] $CH_3OCH_2 \rightarrow CH_2O + CH_3$

[12] $CH_3 + CH_3OCH_3 \rightarrow CH_4 + CH_3OCH_2$

[36] $C_3H_6 \rightarrow C_3H_5 + H$

[15] $H + CH_3OCH_3 \rightarrow H_2 + CH_3OCH_2$

[38] $CH_3 + C_3H_6 \rightarrow CH_4 + C_3H_5$

[39] $CH_3 + C_3H_5 \rightarrow CH_4 + H_2C{=}C{=}CH_2$

The steady-state treatment yields the following expressions for the radical concentrations:

$$[H] = \frac{k_{36}[C_3H_6]}{k_{15}[CH_3OCH_3]}$$

$$[CH_3] = \left(\frac{k_{37}k_{36}}{k_{38}k_{39}}\right)^{1/2} [CH_3OCH_3]^{1/2}$$

$$[CH_3OCH_2] = \frac{k_{36}}{k_{13}}[C_3H_6] + \frac{k_{38}}{k_{13}}\left(\frac{k_{37}k_{36}}{k_{38}k_{39}}\right)^{1/2}[CH_3OCH_3]^{1/2}[C_3H_6] + \frac{k_{12}}{k_{13}}\left(\frac{k_{37}k_{36}}{k_{38}k_{39}}\right)^{1/2}[CH_3OCH_3]^{3/2}$$

$$[C_3H_5] = \left(\frac{k_{36}k_{38}}{k_{37}k_{39}}\right)^{1/2} \frac{[C_3H_6]}{[CH_3OCH_3]^{1/2}}$$

The over-all rate is

$$v = -\frac{d[CH_3OCH_3]}{dt} = \left(\frac{k_{37}k_{36}k_{38}}{k_{39}}\right)^{1/2} [C_3H_6][CH_3OCH_3]^{1/2} + k_{36}[C_3H_6] + k_{12}\left(\frac{k_{37}k_{36}}{k_{38}k_{39}}\right)^{1/2}[CH_3OCH_3]^{3/2}$$

The second term in this expression is negligible in comparison to the third term. The ratio of the third term to the first term is, using the values in Tables 3 and

The steady-state treatment yields the following expressions for the radical concentrations:

$$[H] = \frac{k_{36}[C_3H_6]}{k_{15}[CH_3OCH_3]}$$

$$[CH_3] = \left(\frac{k_{37}k_{36}}{k_{38}k_{39}}\right)^{1/2} [CH_3OCH_3]^{1/2}$$

$$[CH_3OCH_2] = \frac{k_{36}}{k_{13}}[C_3H_6] + \frac{k_{38}}{k_{13}}\left(\frac{k_{37}k_{36}}{k_{38}k_{39}}\right)^{1/2}[CH_3OCH_3]^{1/2}[C_3H_6] + \frac{k_{12}}{k_{13}}\left(\frac{k_{37}k_{36}}{k_{38}k_{39}}\right)^{1/2}[CH_3OCH_3]^{3/2}$$

$$[C_3H_5] = \left(\frac{k_{36}k_{38}}{k_{37}k_{39}}\right)^{1/2} \frac{[C_3H_6]}{[CH_3OCH_3]^{1/2}}$$

The over-all rate is

$$v = -\frac{d[CH_3OCH_3]}{dt} = \left(\frac{k_{37}k_{36}k_{38}}{k_{39}}\right)^{1/2} [C_3H_6][CH_3OCH_3]^{1/2} + k_{36}[C_3H_6] + k_{12}\left(\frac{k_{37}k_{36}}{k_{38}k_{39}}\right)^{1/2}[CH_3OCH_3]^{3/2}$$

The second term in this expression is negligible in comparison to the third term. The ratio of the third term to the first term is, using the values in Tables 3 and

4, and with $[CH_3OCH_3] = [C_3H_6]$

$$\frac{\text{term 3}}{\text{term 1}} = \frac{k_{12}}{k_{38}} \frac{[CH_3OCH_3]}{[C_3H_6]} = 2 \text{ at } 800^\circ K$$

Consequently the third term will predominate and the over-all order is predicted to be three-halves with respect to ether, in agreement with experiment.

Reaction [39] shows that the allyl radical is used up in forming stable products. As pointed out above one cannot observe by direct pressure measurement when all of the C_3H_5 has been consumed, as is possible with NO, because a thermodynamic equilibrium is presumably established long before the very large quantity of allyl radicals has disappeared by reaction [39]. The propylene constitutes a reservoir supplying C_3H_5 radicals to the system by reaction [36].

The predicted activation energy is

$$E = E_{12} + \frac{1}{2}(E_{37} + E_{36} - E_{38} - E_{39})$$

$$= 62.2 \text{ kcal. mole}^{-1}$$

in good agreement with the experimental value of 61.7 kcal. mole^{-1}.

The predicted frequency factor is given by

$$A = A_{12}\left(\frac{A_{37}A_{36}}{A_{38}A_{39}}\right)^{1/2} = 4.2 \times 10^{14} \text{ cc}^{1/2} \text{ mole}^{-1/2} \text{ sec.}^{-1}$$

Table 4

Kinetic Parameters for Inhibition by Propylene

Reaction	Frequency Factor sec^{-1} or $mole^{-1}\ sec^{-1}$	Activation Energy kcal. $mole^{-1}$	k at 800°K sec^{-1} or cc. $mole^{-1} sec^{-1}$	Reference
[37]	1.0×10^{12}	38.0	4.1	Estimated
[36]	1.0×10^{15}	78.0	4.7×10^{-7}	Estimated from Semaro (64)
[38]	5.2×10^{10}	7.7	4.1×10^{8}	Trotman-Dickenson and Steacie (65)
[39]	1.0×10^{10}	3.0	1.5×10^{9}	Estimated

whereas the experimental value is

$$A = 4.6 \times 10^{15} \text{ cc}^{1/2} \text{ mole}^{-1/2} \text{ sec}^{-1}.$$

The agreement is quite satisfactory in view of the uncertainties in the individual factors.

Induction Period

The induction period in the uninhibited reactions is associated with a gradual increase in rate at the beginning of the reaction; this results in the familiar S-shaped pressure-time curves. This type of curve was observed in the uninhibited reaction (see part II A), in the reaction inhibited by propylene, and in the reaction accelerated by large quantities of nitric oxide. In the latter case an induction period was evident only at low pressures and temperatures. The situation is quite different in the case of the reaction fully inhibited by nitric oxide. Here there is no evidence of any induction period at high pressures and temperatures. However, as the pressures and temperature are lowered there is a pronounced time lag before there is any pressure change in the reaction vessel. Thus the pressure-time curve exhibits a flat portion initially, followed by a sudden increase; Fig. 21 shows this effect.

The S-shaped curves can perhaps be explained by

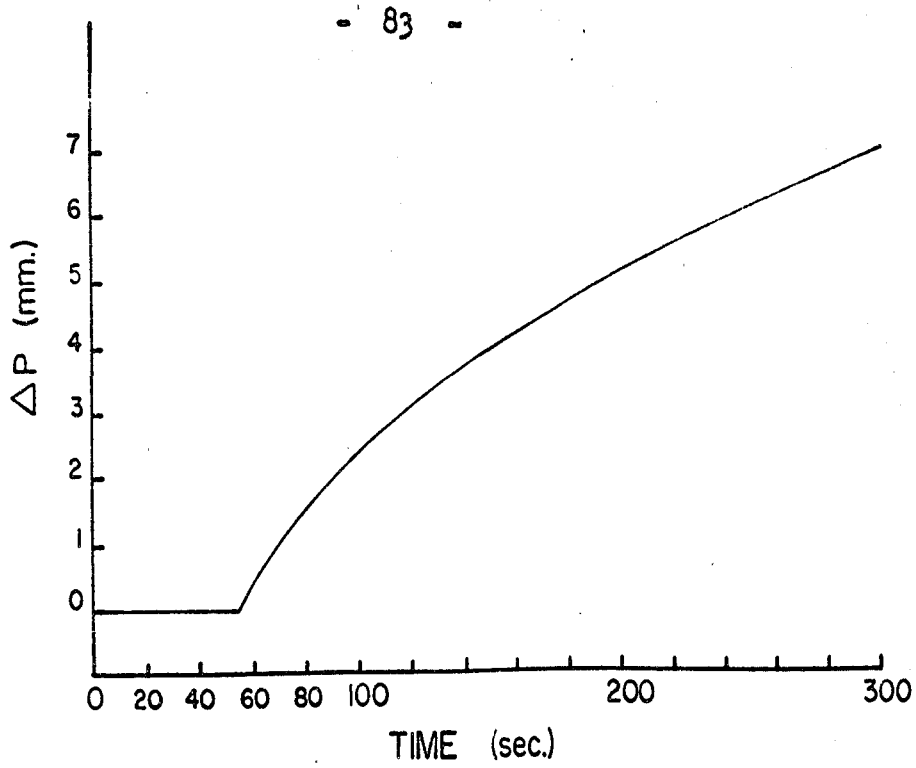

Figure 21. Typical pressure-time curve for the reaction maximally inhibited by nitric oxide, particularly at low pressures and temperatures; this curve was obtained at 520° with an ether pressure of 591 mm. and a nitric oxide pressure of 4.8 mm.

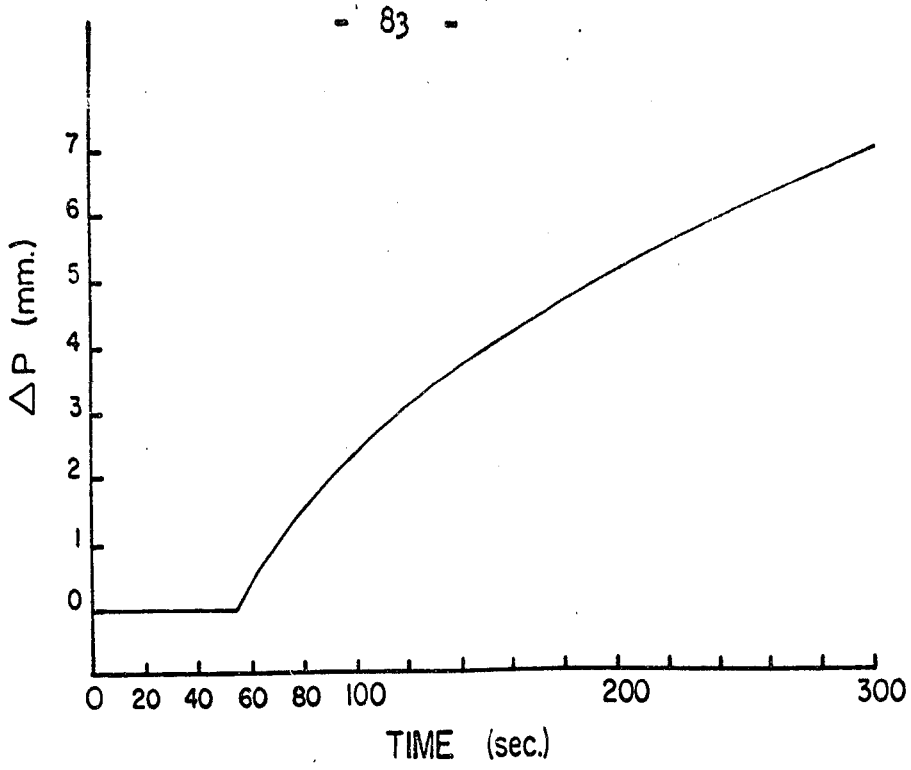

Figure 21. Typical pressure-time curve for the reaction maximally inhibited by nitric oxide, particularly at low pressures and temperatures; this curve was obtained at 520° with an ether pressure of 591 mm. and a nitric oxide pressure of 4.8 mm.

assuming a gradual approach to steady-state conditions. For the nitric oxide inhibited reaction the shape of the pressure-time curve suggests that there is a time delay before any ether decomposes, after which the reaction proceeds in the manner described above.

assuming a gradual approach to steady-state conditions. For the nitric oxide inhibited reaction the shape of the pressure-time curve suggests that there is a time delay before any ether decomposes, after which the reaction proceeds in the manner described above.

C. The Reaction Accelerated by Hydrogen Sulphide

INTRODUCTION

A number of workers (28, 68-73) have suggested that thiyl radicals (RS) are more reactive than alkyl radicals. Thus thiols generally accelerate free radical reactions involving saturated aldehydes; this has been shown to be the case in the liquid phase (68), in photodecomposition reactions in the gas phase (69,70) and in thermal decompositions in the gas phase (28,71,72,73). Birrell and co-workers (69) observed that various thiols (H_2S, CH_3SH, C_2H_5SH, etc.) catalysed the photodecomposition of acetaldehyde, and in most cases the thiols increased the rate of the decomposition. The rates increased to a plateau with the addition of thiol and remained constant over a range of concentrations. When the thiol concentration was about three-quarters of the acetaldehyde concentration the relative rate (ratio of catalysed to uncatalysed rate) increased further. Hydrogen sulphide was found to be the most effective catalyst, and the catalytic effect decreased with increasing complexity of the thiol. The mechanism proposed for catalysis by methanethiol involved the chain transfer reaction

$$CH_3 + CH_3SH \longrightarrow CH_3S + CH_4$$

followed by

$$CH_3S + CH_3CHO \rightarrow CH_3SH + CH_3 + CO$$

and termination by

$$2CH_3S \rightarrow CH_3SSCH_3$$

Such a simple mechanism could not, however, explain the effects observed for other thiols.

More recently Imai and Toyama have postulated mechanisms to explain the acceleration by hydrogen sulphide and methanethiol of the decomposition of acetaldehyde (71,72,73). The effect of hydrogen sulphide on the decomposition of dimethyl ether was also studied (28). These workers suggest that the catalytic effect of hydrogen sulphide is essentially due to reaction of methyl radicals with hydrogen sulphide, with the production of hydrosulphide (SH) radicals which in turn abstract hydrogen atoms from the substrate. These reactions are suggested to be faster than the reaction between methyl radicals and the substrate. For the thermal decomposition of dimethyl ether in the presence of hydrogen sulphide the rate increased with increasing concentration of hydrogen sulphide and reached a limit where further addition of hydrogen sulphide had no effect. The maximum amount of hydrogen sulphide which was added was approximately 67%, and the reactions were carried out over the temperature range of 360 to 440°C. The mechanism

suggested for the reaction in the presence of sufficient hydrogen sulphide to ensure 'limiting' acceleration was as follows:

[11] $CH_3OCH_3 \rightarrow CH_3 + CH_3O$

[40] $CH_3O + H_2S \rightarrow CH_3OH + HS$

[41] $CH_3 + H_2S \rightarrow CH_4 + HS$

[42] $CH_3OCH_3 + HS \rightarrow H_2S + CH_3OCH_2$

[13] $CH_3OCH_2 \rightarrow CH_2O + CH_3$

[43] $HS + HS \rightarrow$ products

The rate equation to which this mechanism leads is

$$-\frac{d[CH_3OCH_3]}{dt} = \frac{d[CH_4]}{dt} = k_{42}\left(\frac{k_{11}}{k_{43}}\right)^{1/2}[CH_3OCH_3]^{3/2}$$

and a three-halves-order dependence on other concentrations was obtained experimentally. The results led to a rate constant of

$$k = 1.82 \times 10^{15}\, e^{-51,000/RT}\ cc^{1/2}\ mole^{-1/2}\ sec^{-1}.$$

In the light of recent work (Part II D) in this laboratory on the action of inhibitors on the thermal decomposition of dimethyl ether, it was thought that a mechanism similar to inhibition mechanisms could be applied to the reaction accelerated by hydrogen sulphide. It also seemed

necessary to extend the experimental investigation to higher temperatures and higher pressures of H_2S. The fact that there was in increase in relative rate at very high pressures of H_2S (> 50% added H_2S) indicated that the mechanism postulated by Imai and Toyama (23) is not sufficient to describe the reaction completely.

RESULTS

Preliminary experiments were carried out with hydrogen sulphide alone in the reaction vessel at 600°C. It was found that the total pressure decreased by approximately 1% to a limit. This slight pressure change is insignificant compared to the pressure change for the decomposition of dimethyl ether in the presence of H_2S, and was therefore ignored.

Rates were calculated from the slopes of the pressure-time curves at the inflexion point, and the results were found to be fully reproducible over the entire range of pressure and temperature. The induction period for the reaction in the presence of H_2S was generally quite short, so that the inflexion point occurred in all cases at less than 10% decomposition. The rates can therefore be considered to be initial rates to a very close approximation.

In order to verify the experimental results of previous workers (23) the rate of decomposition of dimethyl

ether was measured for various added amounts of hydrogen sulphide. A plot of relative rate (i.e., the rate in the presence of H_2S divided by the rate in the absence of H_2S) is shown in Fig. 23. The curves drawn have been calculated from Fig. 24, to be considered later. For a given pressure of ether the relative rate increases to a plateau with an increasing concentration of hydrogen sulphide. In this region the order with respect to hydrogen sulphide is obviously zero. As still greater quantities of H_2S are added the relative rate increases linearly. It is apparent from the curves shown in Fig. 23 that the length of the plateau depends on the pressure of ether; the lower the ether pressure, the shorter the plateau. This suggests that the effects depend only on the proportion of H_2S relative to ether, rather than on the absolute amount of H_2S. This result differs from that found in the nitric oxide inhibited decomposition of dimethyl ether (Part II B). A plot of relative rate against the percentage of hydrogen sulphide (Fig. 24) shows this dependence more clearly. Points were determined at three different temperatures - 400, 520, 530°C. Within the experimental error, the plateau occurs at approximately the same relative rate in all cases, although there appears to be a slight increase with decreasing temperature, i.e. the plateau seems to be higher for the low temperatures.

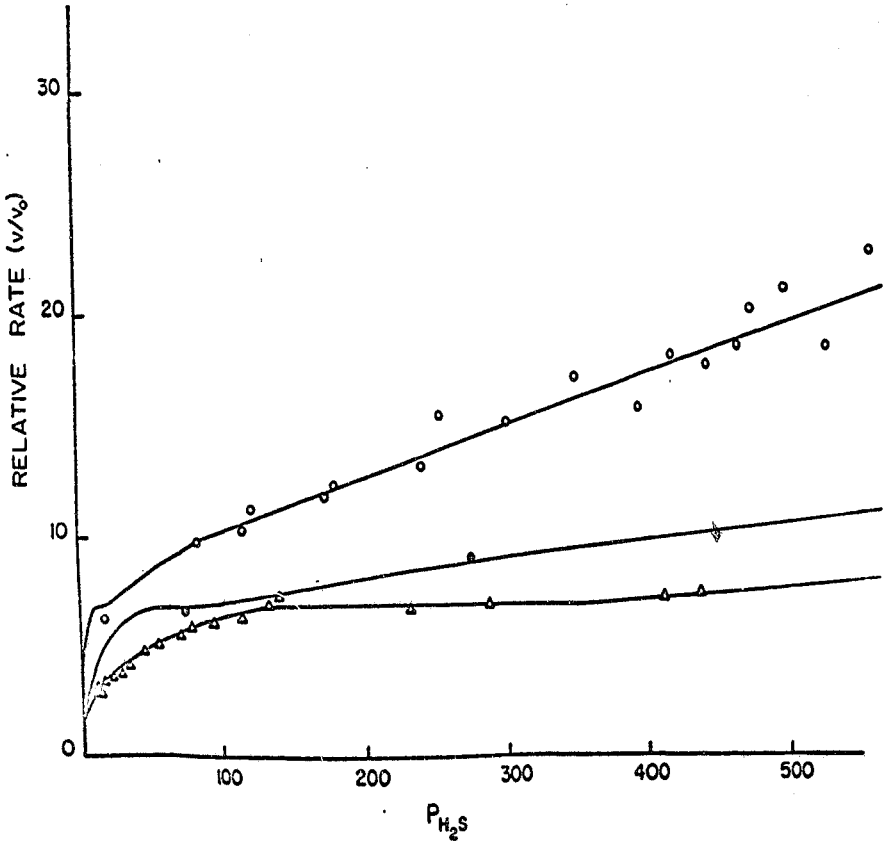

Figure 23. Relative rate (v/v_0) against pressure of hydrogen sulphide for three different pressures of ether: Δ - 300 mm., ⊕ - 100 mm., and O - 20 mm. of ether. The solid lines have been calculated from Figure 24.

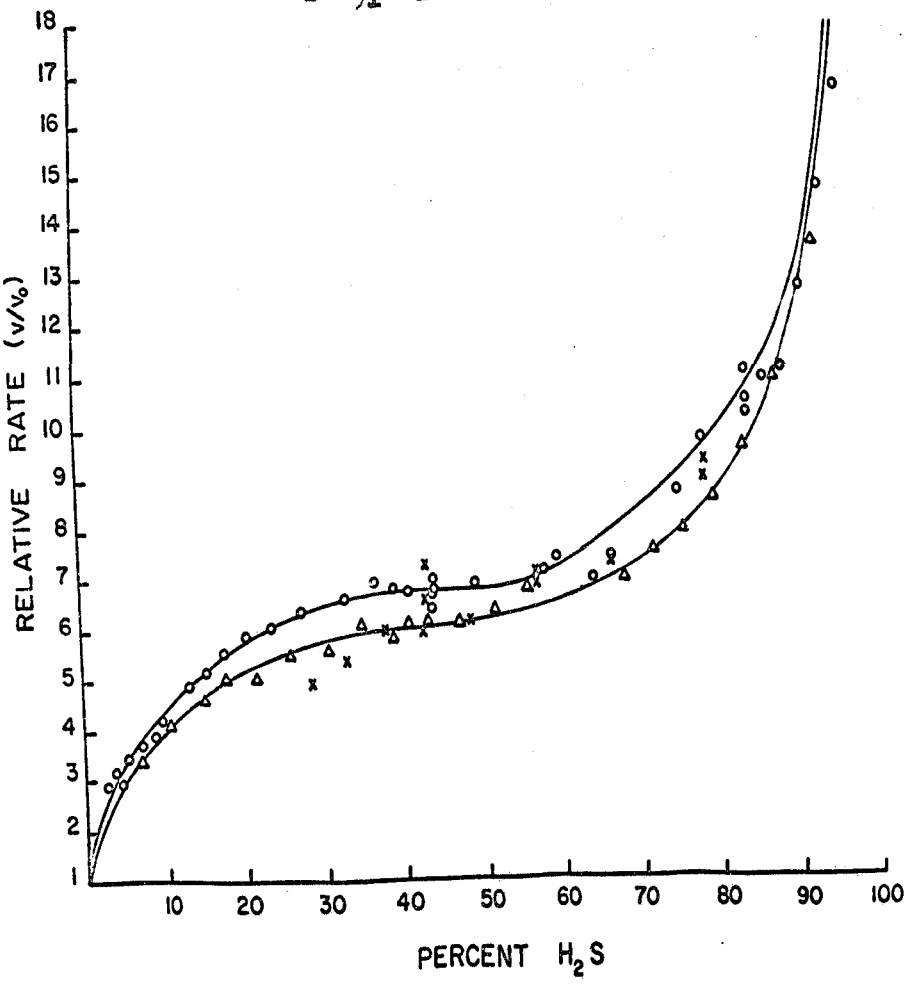

Figure 24. Relative rate (v/v_0) against the percentage of hydrogen sulphide for three different temperatures; Δ - 530°C, 0 - 520°C and X - 480°C.

Kinetic measurements were carried out with about 40% added H_2S, and with about 75 to 99% added H_2S. Hydrogen sulphide in the amount of 40% was sufficient to ensure 'limiting' acceleration (independent of H_2S), while over 75% H_2S ensured that the reaction was in the region dependent on the percentage of hydrogen sulphide.

A typical pressure-time curve is shown in Fig. 25. Curve A is an actual tracing of the record obtained for the decomposition of 90 mm. of dimethyl ether in the absence of H_2S. Curve B is a similar tracing showing the decomposition of 85 mm. of dimethyl ether in the presence of 475 mm. of H_2S. Both runs were carried out at 510°C. The accelerating effect of the added H_2S is readily seen.

Figure 26 shows plots of the logarithm of the rate against the logarithm of the ether pressure, for the reaction in the plateau region where about 40% H_2S was added. All of the lines have slopes of 1.5. The corresponding Arrhenius curve is shown in Fig. 27. The three-halves-order rate constant may be expressed as $k = 1.06 \times 10^{14} e^{-53,200/RT}$ $cc^{1/2}$ $mole^{-1/2}$ sec^{-1}. This is to be compared with $k = 1.82 \times 10^{15} e^{-51,800/RT}$ $cc^{1/2}$ $mole^{-1/2}$ sec^{-1} obtained by Imai and Toyama (20).

The kinetic measurements made with 75 to 99% H_2S are shown in Figs. 28, 29 and 30. Figure 28 is a double

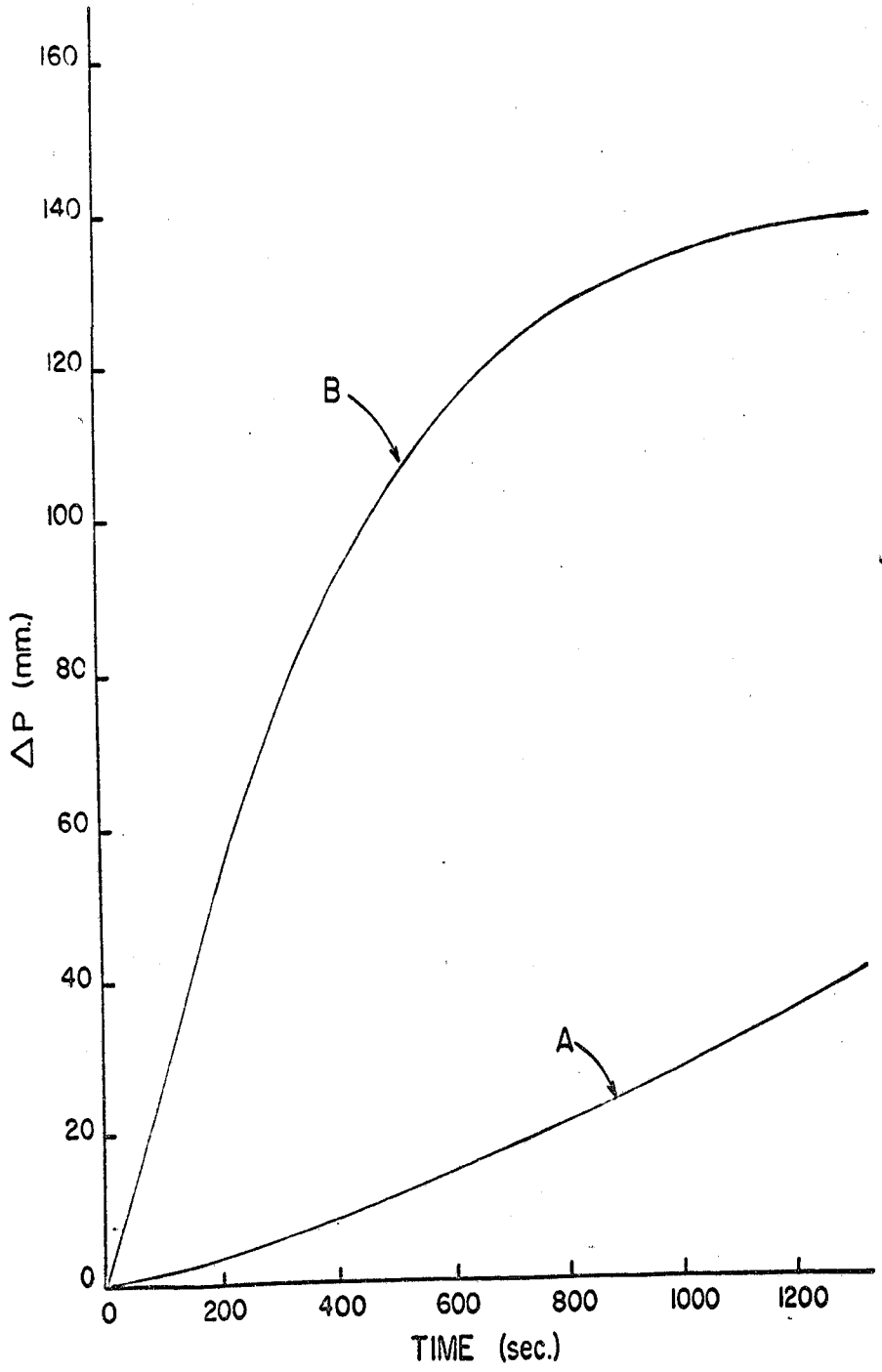

Figure 25. Typical pressure-time curves. Curve A is a tracing of the record obtained for the decomposition of 90 mm. of ether in the absence of hydrogen sulphide. Curve B is a similar tracing showing the decomposition of 85 mm. of ether in the presence of 475 mm. of H_2S. The temperature in both cases was 510°C.

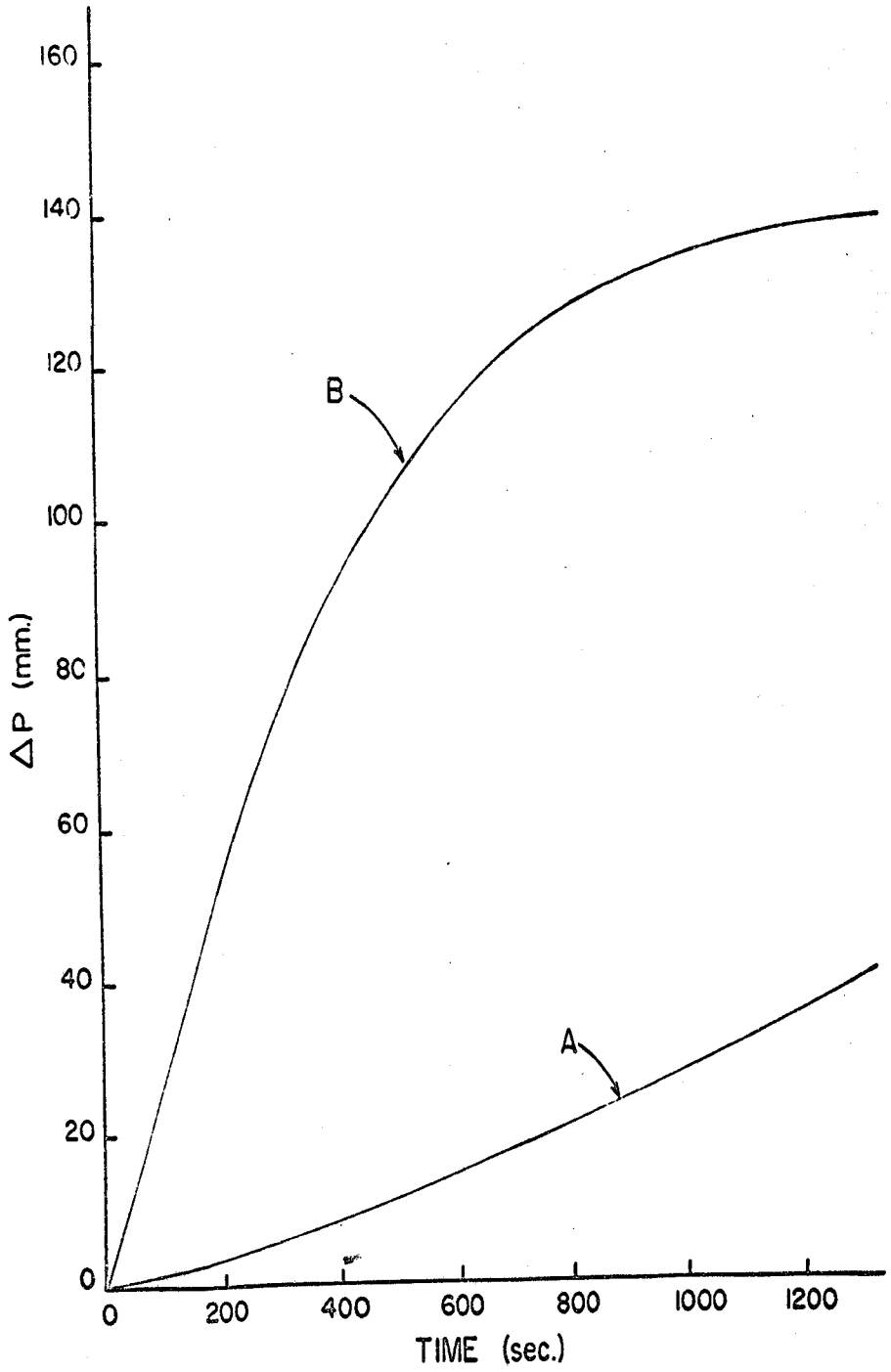

Figure 25. Typical pressure-time curves. Curve A is a tracing of the record obtained for the decomposition of 90 mm. of ether in the absence of hydrogen sulphide. Curve B is a similar tracing showing the decomposition of 85 mm. of ether in the presence of 475 mm. of H_2S. The temperature in both cases was 510°C.

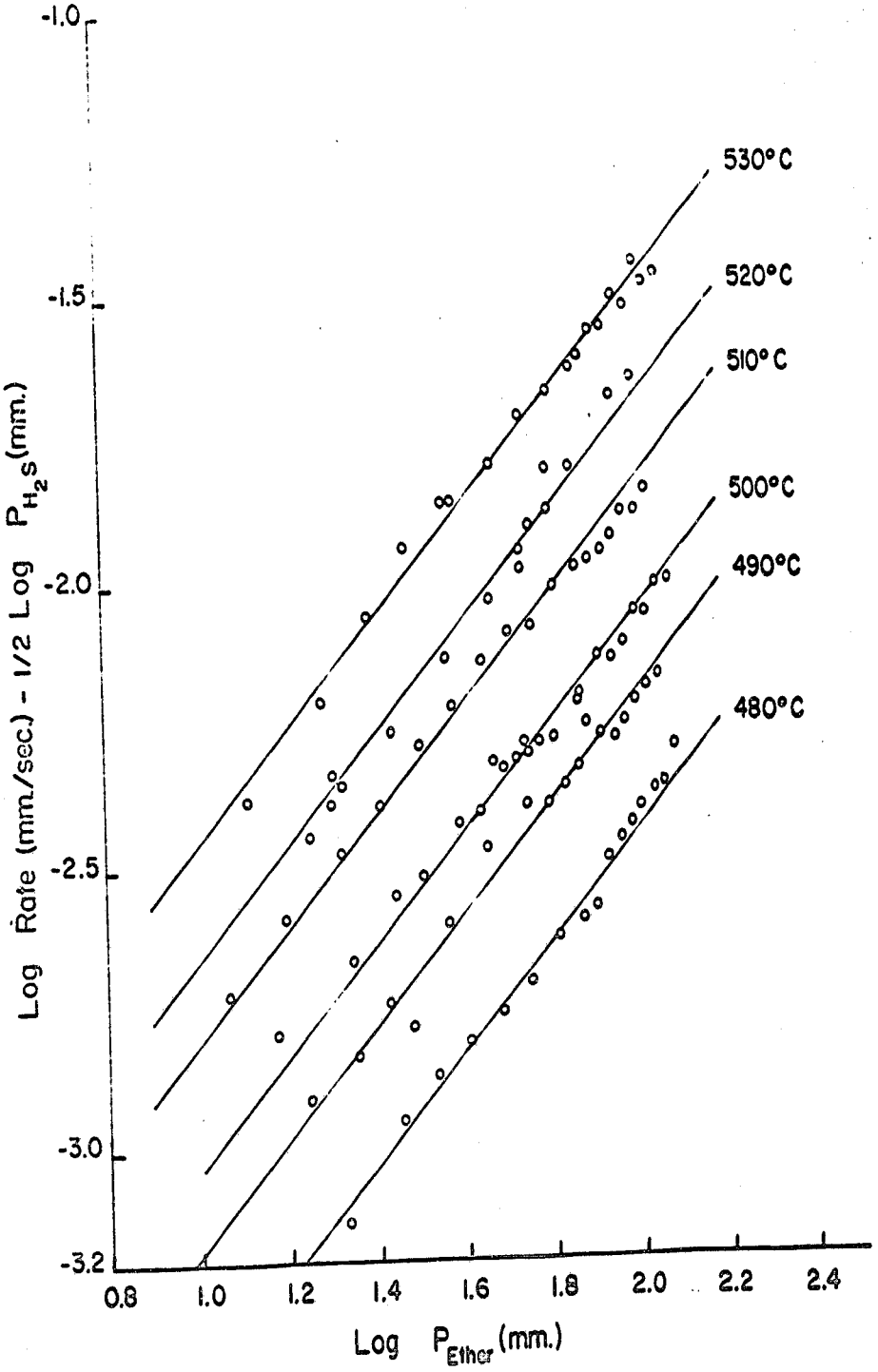

Figure 26. Double logarithmic plot of inflexion rate against ether pressure for various temperatures. The lines all have slopes of 1.5. These curves were determined for the decomposition in the presence of about 40% H_2S (i.e. the plateau region).

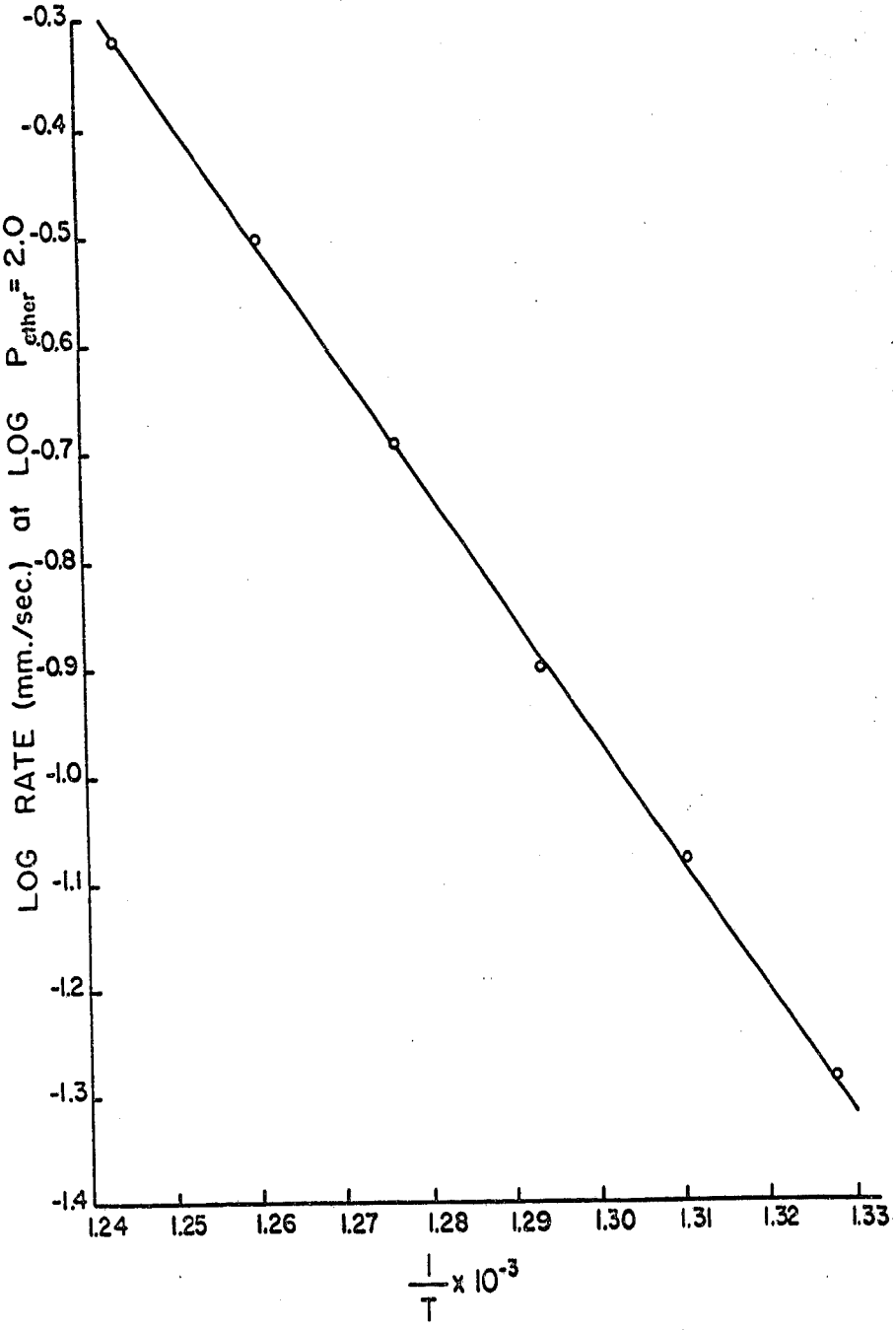

Figure 27. Arrhenius plot for the decomposition in the presence of about 40% H_2S (i.e. the plateau region).

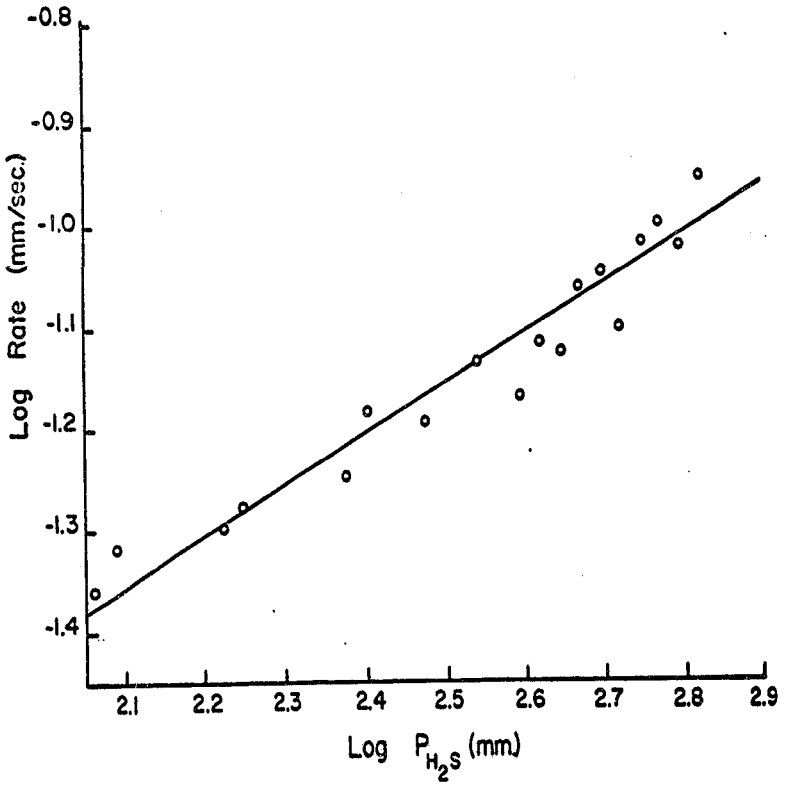

Figure 28. Double logarithmic plot of inflexion rate against pressure of hydrogen sulphide at 520°C. The ether pressure was constant at about 20 mm. The slope of the line is 0.5.

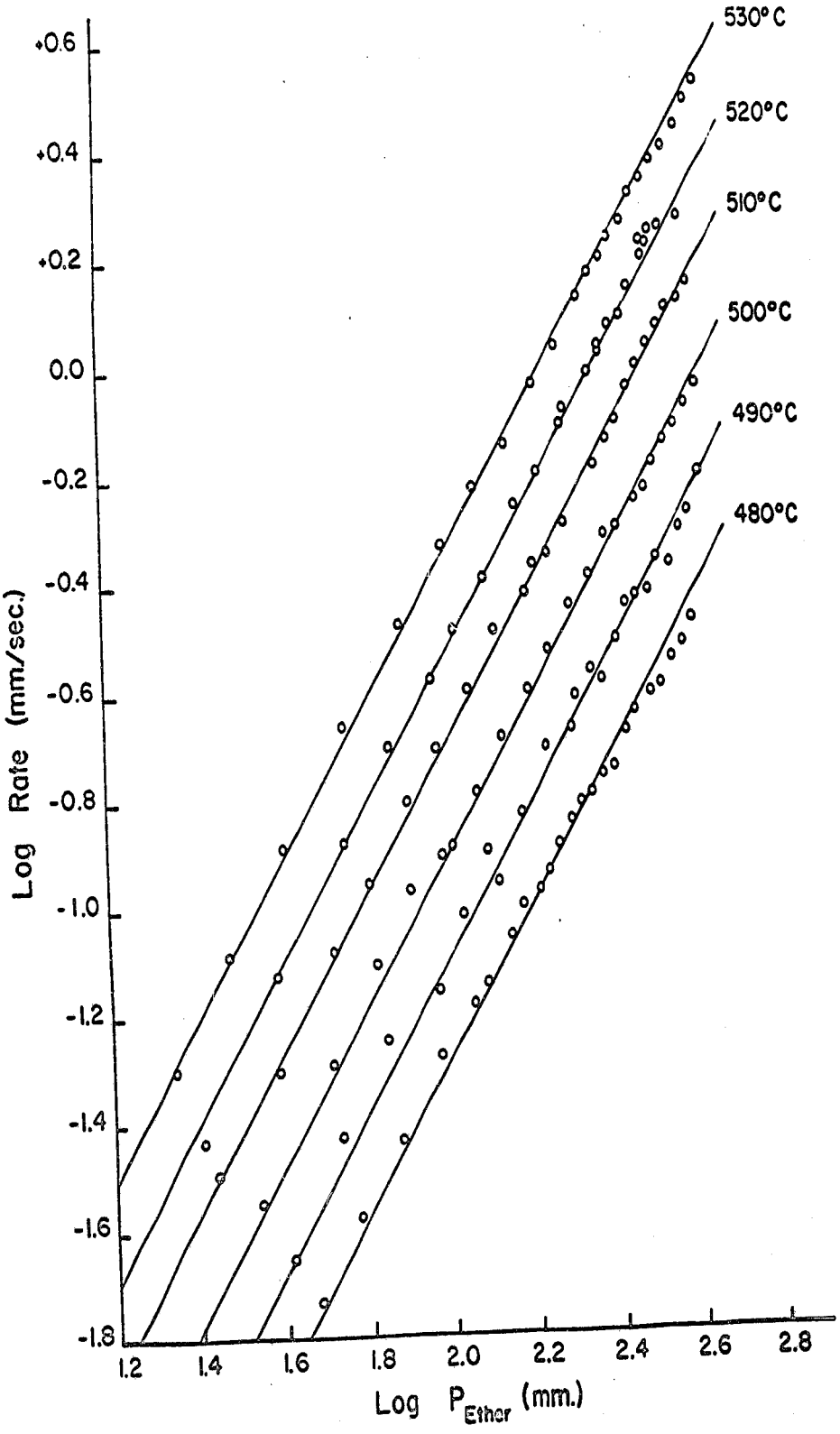

Figure 29. Double logarithmic plot of inflexion rate against ether pressure for various temperatures. The lines all have slopes of 1.5. These curves were determined for the decomposition in the presence of 75-99% H_2S.

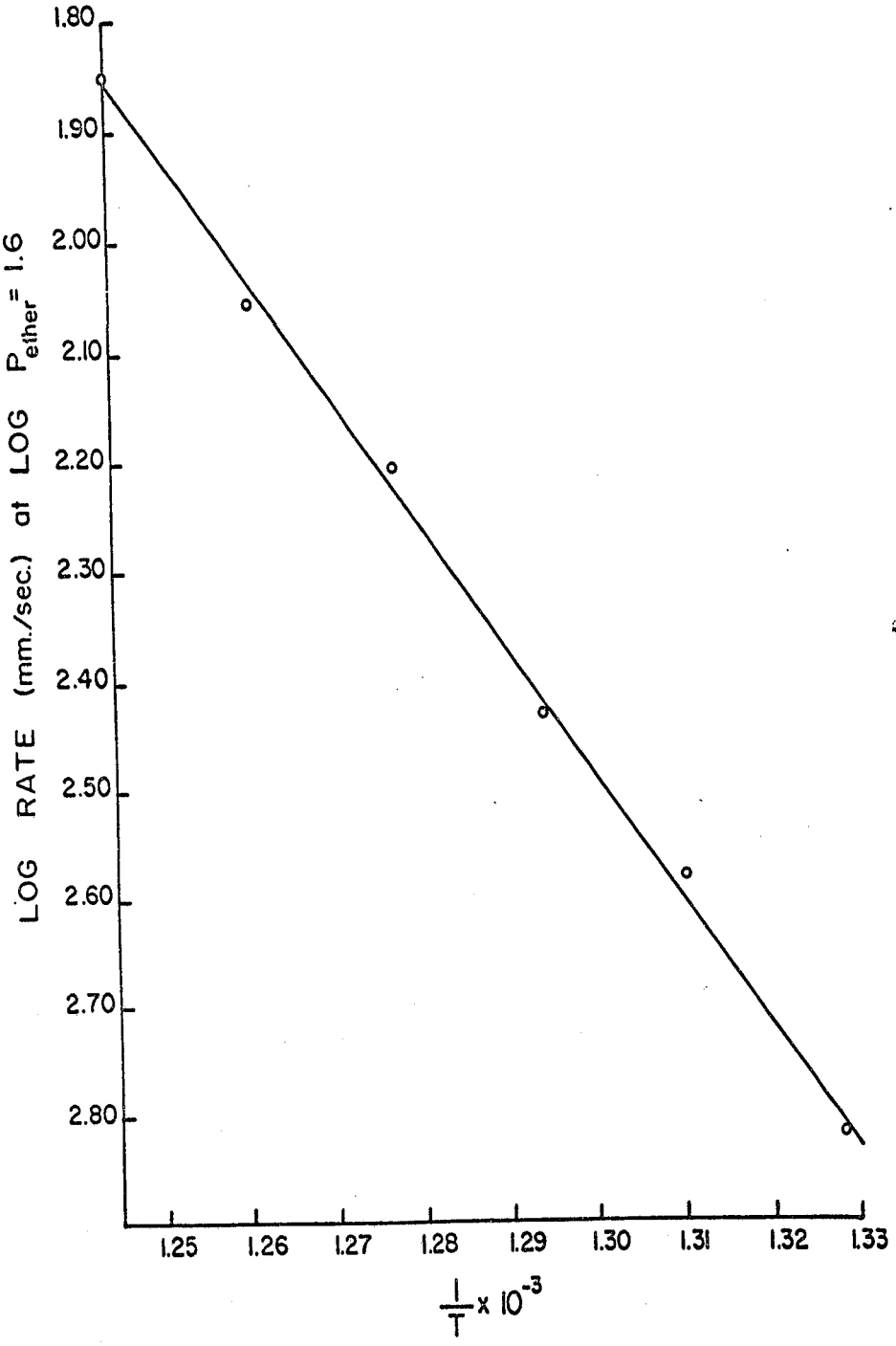

Figure 30. Arrhenius plot for the decomposition in the presence of 75-99% H_2S.

logarithmic plot of rate against pressure of hydrogen sulphide, for a constant ($\sim$ 20 mm) pressure of dimethyl ether. The line drawn has a slope of 0.5, showing that the order with respect to H_2S pressure is one-half in the region of very high percentages of H_2S. The logarithm of the rate minus one-half the logarithm of the hydrogen sulphide pressure is plotted against the logarithm of the ether pressure in Fig. 29. A plot of this kind enabled the dependence on ether pressure to be determined, without the tedious task of holding the H_2S pressure constant. All of the lines drawn in Fig. 29 have slopes of unity. The corresponding Arrhenius plot is shown in Fig. 30. The calculated activation energy for the reaction accelerated by very high percentages of hydrogen sulphide is 52.5 kcal $mole^{-1}$. The rate constant may be expressed by $k = 4.98 \times 10^{14}\ e^{-52,500/RT}\ cc^{1/2}\ mole^{-1/2}\ sec^{-1}$.

DISCUSSION

The fact that the rate of decomposition of dimethyl ether in the presence of hydrogen sulphide relative to the rate in the absence of hydrogen sulphide depends on the proportion of H_2S to ether (see Figs. 23 and 24) suggests that competitive reactions are involved in the process. At these temperatures it is well known that dimethyl ether decomposes to form methyl and methoxy radicals. Hydrosulphide

radicals are almost certainly formed from the decomposition of hydrogen sulphide. This is suggested by the fact that there is a slight decrease in pressure when H_2S alone is present in the reaction vessel at 600°C. The thermal decomposition of hydrogen sulphide has in fact been studied in the temperature range employed in this research (74). The evidence suggests that the decomposition proceeds mainly by heterogeneous processes at temperatures below 600°C. The radical HS would probably be formed in large quantities, and can also be produced from reactions such as

$$CH_3 + H_2S \rightarrow CH_4 + HS$$

Consequently, during the decomposition of dimethyl ether in the presence of hydrogen sulphide, there should be a plentiful supply of hydrosulphide radicals. These could initiate the ether decomposition by abstraction of a hydrogen atom,

$$CH_3OCH_3 + HS \rightarrow H_2S + CH_3OCH_2$$

The over-all rate expression for the thermal decomposition of pure dimethyl ether is of the form (Part II A, (75))

$$v_0 = k[CH_3OCH_3]^{3/2}$$

The shape of the curves shown in Figs. 23 and 24 suggests

radicals are almost certainly formed from the decomposition of hydrogen sulphide. This is suggested by the fact that there is a slight decrease in pressure when H_2S alone is present in the reaction vessel at 600°C. The thermal decomposition of hydrogen sulphide has in fact been studied in the temperature range employed in this research (74). The evidence suggests that the decomposition proceeds mainly by heterogeneous processes at temperatures below 600°C. The radical HS would probably be formed in large quantities, and can also be produced from reactions such as

$$CH_3 + H_2S \longrightarrow CH_4 + HS$$

Consequently, during the decomposition of dimethyl ether in the presence of hydrogen sulphide, there should be a plentiful supply of hydrosulphide radicals. These could initiate the ether decomposition by abstraction of a hydrogen atom,

$$CH_3OCH_3 + HS \longrightarrow H_2S + CH_3OCH_2$$

The over-all rate expression for the thermal decomposition of pure dimethyl ether is of the form (Part II A, (75))

$$v_0 = k[CH_3OCH_3]^{3/2}$$

The shape of the curves shown in Figs. 23 and 24 suggests

the following relationships:

$$v = k'[H_2S]^n[CH_3OCH_3]^m + k''[CH_3OCH_3]^{3/2}$$

or

$$\frac{v}{v_o} = \frac{k'[H_2S]^n[CH_3OCH_3]^m + k''[CH_3OCH_3]^{3/2}}{k[CH_3OCH_3]^{3/2}}$$

This reduces to

$$\frac{v}{v_o} = \frac{k'}{k} \frac{[H_2S]^n}{[CH_3OCH_3]^{3/2-m}} + \frac{k''}{k}$$

Thus on a plot of relative rate (v/v_o) against the percentage of hydrogen sulphide a plateau would be observed when the proportion of H_2S to CH_3OCH_3 is small and k''/k is the dominant term. However, as the ratio of H_2S to CH_3OCH_3 becomes larger the relative rate should then increase with increasing percentage of hydrogen sulphide.

The rate expression for the reaction in the presence of H_2S should therefore involve two terms - one predicting three-halves-order behaviour with respect to dimethyl ether and no dependence on hydrogen sulphide, the second predicting dependence with respect to both hydrogen sulphide and dimethyl ether. Figures 28, 29 and 30 show that the order is one-half

in H_2S and first in CH_3OCH_3, i.e. n = 1/2 and m = 1, for the reaction with high percentages of H_2S.

The mechanism to which these considerations lead can be written as:

[11a]	$M + CH_3OCH_3$	$\rightarrow$	$CH_3 + CH_3O + M$
[44]	$M + H_2S$	$\rightarrow$	$H + HS + M$
[45]	$H + CH_3OCH_3$	$\rightarrow$	$H_2 + CH_3OCH_2$
[42]	$HS + CH_3OCH_3$	$\rightarrow$	$H_2S + CH_3OCH_2$
[13]	CH_3OCH_2	$\rightarrow$	$CH_2O + CH_3$
[41]	$CH_3 + H_2S$	$\rightarrow$	$CH_4 + HS$
[14a]	$M + CH_3O$	$\rightarrow$	$CH_2O + H + M$
	$HS + HS$	$\underset{[-45]}{\overset{[45]}{\rightleftharpoons}}$	$H_2S + S$
[43a]	$M + HS + HS$	$\rightarrow$	$H_2S_2 + M$

where M represents a third body. Application of the conventional steady-state approximation yields for the radical concentrations:

$$[HS] = \left(\frac{2k_{44}}{k_{43a}}\right)^{1/2} [H_2S]^{1/2} + \left(\frac{2k_{11a}}{k_{43a}}\right)^{1/2} [CH_3OCH_3]^{1/2}$$

$$[CH_3O] = \frac{k_{11a}}{k_{14a}} [CH_3OCH_3]$$

$$[H] = \frac{k_{44}}{k_{15}} + \frac{k_{11a}}{k_{15}}[CH_3OCH_3]$$

$$[CH_3OCH_2] = \frac{k_{42}}{k_{13}}\left(\frac{2k_{44}}{k_{43a}}\right)^{1/2}[CH_3OCH_3][H_2S]^{1/2} + \frac{k_{42}}{k_{13}}\left(\frac{2k_{11a}}{k_{43a}}\right)^{1/2}[CH_3OCH_3]^{3/2} + \frac{k_{11a}}{k_{13}}[CH_3OCH_3][H] + \frac{k_{44}}{k_{13}}[H_2S][H]$$

$$[CH_3] = \frac{k_{11a}}{k_{41}}\frac{[CH_3OCH_3][H]}{[H_2S]} + \frac{k_{42}}{k_{41}}\left(\frac{2k_{44}}{k_{43a}}\right)^{1/2}\frac{[CH_3OCH_3]}{[H_2S]^{1/2}} + \frac{k_{11a}}{k_{41}}\frac{[CH_3OCH_3]}{[H_2S]} + \frac{k_{42}}{k_{41}}\left(\frac{2k_{11a}}{k_{43a}}\right)^{1/2}\frac{[CH_3OCH_3]}{[H_2S}} + \frac{k_{44}}{k_{41}}[H]$$

The rate is given by

$$v = 2k_{11a}[CH_3OCH_3][H] + k_{42}\left(\frac{2k_{44}}{k_{43a}}\right)^{1/2}[H_2S]^{1/2}[CH_3OCH_3] + k_{42}\left(\frac{2k_{11a}}{k_{43a}}\right)^{1/2}[CH_3OCH_3]^{3/2} + k_{44}[H_2S][H]$$

The first and fourth terms in this expression are small in comparison to the second and third terms, and hence may be neglected.

The rate can therefore be written as

$$v = k_{42}\left(\frac{2k_{44}}{k_{43a}}\right)^{1/2}[H_2S]^{1/2}[CH_3OCH_3] + k_{42}\left(\frac{2k_{11a}}{k_{43a}}\right)^{1/2}[CH_3OCH_3]^{3/2}$$

A crude estimate of the percentage of H_2S at which the change in order takes place can be made using the values for k_{11a} and k_{44} from Table 5. The ratio of the first to the second term is

$$\left(\frac{k_{44}}{k_{11a}}\right)^{1/2}\frac{[H_2S]^{1/2}}{[CH_3OCH_3]^{1/2}} = 0.1103 \times \frac{[H_2S]^{1/2}}{[CH_3OCH_3]^{1/2}}$$

This expression becomes greater than unity when the ratio $[H_2S]/[CH_3OCH_3]$ becomes greater than 9.1. Thus the first term in the rate expression predominates when the pressure of hydrogen sulphide exceeds 90%. The transition actually takes place with about 50-70% H_2S. The agreement is therefore quite satisfactory in view of the uncertainties in the rate constants. Consequently, to describe the rate for the plateau region the following expression can be written:

Table 5

Kinetic Parameters

Reaction	Frequency Factor (sec^{-1}, $cc\ mole^{-1}\ sec^{-1}$, or $cc^2\ mole^{-2}\ sec^{-1}$)	Activation energy (kcal $mole^{-1}$)	k at 800°K (sec^{-1}, $cc\ mole^{-1}\ sec^{-1}$ or $cc^2\ mole^{-2}\ sec^{-1}$)	Reference
[11a]	1×10^{18}	74.0	5.8×10^{-3}	See Part II A
[44]	1×10^{18}	81.0	7.0×10^{-5}	estimated (See footnote)
[42]	1×10^{12}	13.0	2.9×10^{8}	assumed
[13]	7×10^{10}	19.0	4.6×10^{5}	See Part II A
[41]	2.5×10^{11}	2.6	1.9×10^{10}	Imai and Toyama (76)
[43a]	1×10^{14}	- 5.6	2.9×10^{12}	estimated (see footnote)
[12]	3×10^{11}	9.5	7.8×10^{8}	See part II A
[17a]	7×10^{14}	- 13.5	3.5×10^{18}	See part II A

The values for reactions [44] and [43a] were calculated in the same manner as in the Appendix I. Four effective degrees of freedom were assumed for HS + SH, by analogy with hydrogen peroxide, and three effective degrees of freedom were taken for $H + H_2S \rightarrow H + HS + H$.

$$v = k_{42}\left(\frac{2k_{11a}}{k_{43a}}\right)^{1/2}[CH_3OCH_3]^{3/2}$$

This expression is identical to that postulated by Imai and Toyama (28). The reason for this is that reaction [44] is unimportant until large relative quantities of hydrogen sulphide are used. Thus with the neglect of reactions [44] and [15], the mechanism is essentially the same as that postulated by Imai and Toyama (28). The reaction in this region is therefore predicted to be three-halves-order with respect to ether, in agreement with experiment. The predicted activation energy is given by $E = E_{42} + \frac{1}{2}(E_{11a} - E_{43a})$. Substitution of the appropriate values given in Table 5 yields $E = 52.8$ kcal $mole^{-1}$, in good agreement with the experimental value of 53.2 kcal $mole^{-1}$. The predicted frequency factor is $A = A_{42}(2A_{11a}/A_{43a})^{1/2} = 1.0 \times 10^{14}$ $cc^{1/2}$ $mole^{-1/2}$ sec^{-1}. This is also in good agreement with the experimental value of 1.06×10^{14} $cc^{1/2}$ $mole^{-1/2}$ sec^{-1}.

In the region of high percentages of H_2S the rate is given by

$$v = k_{42}\left(\frac{2k_{44}}{k_{43a}}\right)^{1/2}[H_2S]^{1/2}[CH_3OCH_3]$$

Experimentally the reaction is one-half-order with respect to hydrogen sulphide and first-order with respect to dimethyl

$$v = k_{42} \left(\frac{2k_{11a}}{k_{43a}}\right)^{1/2} [CH_3OCH_3]^{3/2}$$

This expression is identical to that postulated by Imai and Toyama (28). The reason for this is that reaction [44] is unimportant until large relative quantities of hydrogen sulphide are used. Thus with the neglect of reactions [44] and [15], the mechanism is essentially the same as that postulated by Imai and Toyama (28). The reaction in this region is therefore predicted to be three-halves-order with respect to ether, in agreement with experiment. The predicted activation energy is given by $E = E_{42} + \frac{1}{2}(E_{11a} - E_{43a})$. Substitution of the appropriate values given in Table 5 yields $E = 52.8$ kcal $mole^{-1}$, in good agreement with the experimental value of 53.2 kcal $mole^{-1}$. The predicted frequency factor is $A = A_{42}(2A_{11a}/A_{43a})^{1/2} = 1.0 \times 10^{14}$ $cc^{1/2}$ $mole^{-1/2}$ sec^{-1}. This is also in good agreement with the experimental value of 1.06×10^{14} $cc^{1/2}$ $mole^{-1/2}$ sec^{-1}.

In the region of high percentages of H_2S the rate is given by

$$v = k_{42} \left(\frac{2k_{44}}{k_{43a}}\right)^{1/2} [H_2S]^{1/2} [CH_3OCH_3]$$

Experimentally the reaction is one-half-order with respect to hydrogen sulphide and first-order with respect to dimethyl

other in this region, in agreement with this rate expression. The predicted activation energy is $E = E_{42} + \frac{1}{2}(E_{44} - E_{43a}) = 56.3$ kcal mole^{-1} in fair agreement with the experimental value of 52.5 kcal mole^{-1}. The predicted frequency factor is $A = A_{42}\left(\frac{2A_{44}}{A_{43a}}\right)^{1/2} = 1.0 \times 10^{14}$ cc$^{1/2}$ mole$^{-1/2}$ sec^{-1}, whereas the experimental value is $A = 4.98 \times 10^{14}$ cc$^{1/2}$ mole$^{-1/2}$ sec^{-1}.

The Termination Reaction

Darwent and Roberts (74) concluded, from a study the photolysis of H_2S, that about 13% of the HS radicals disappeared by the reaction $2HS \rightarrow S_2 + H_2$ while about 87% reacted by the process $2HS \rightarrow H_2S + S$ followed by $2S + M \rightarrow S_2 + M$.

In view of this evidence, the equilibrium process

$$HS + HS \underset{[-45]}{\overset{[45]}{\rightleftharpoons}} H_2S + S$$

has been included in the mechanism. The small quantity of S atoms produced may react with H_2S as shown or with CH_3OCH_3

[46] $\quad CH_3OCH_3 + S \rightarrow HS + CH_3OCH_2$

It is suggested that reaction [-45] is faster than [46], and hence [46] can be ignored.

The concentration of HS radicals is large in this system and their combination will give rise to H_2S_2. This reaction will require a third body under these experimental conditions.

The Initiation Reaction

An important conclusion arises from this study with regard to the order of the initiation reaction - the dissociation of the ether molecule into the radicals CH_3 and CH_3O. Consideration of the steady-state equations shows that the only apparent way to obtain the correct pressure dependence in both H_2S and CH_3OCH_3, is by having the initiation in its low-pressure second-order region. This observation is important with reference to the mechanism of the uninhibited reaction, as discussed in Part II A.

The Dissociation Energy of Hydrogen Sulphide

The present work provides a method of estimating the dissociation energy [D(H-SH)] of hydrogen sulphide. The difference between the activation energies for the reaction in the plateau region and the region of high H_2S percentages is given from the over-all rate expression as

$$\Delta E = [E_{42} + \tfrac{1}{2}(E_{11a} - E_{43a})] - [E_{42} + \tfrac{1}{2}E_{44} - E_{43a})]$$

$$= \tfrac{1}{2}[E_{11a} - E_{44}]$$

The experimental difference is 0.7 kcal mole^{-1}. Since E_{11a} is known (Part II A) E_{44} can be calculated as, at high pressures,

$$E_{44} = E_{11a} - 2\Delta E = 85.6 \text{ kcal mole}^{-1},$$

Previous work has led to conflicting values for this dissociation energy; values varying from 81 to 95 kcal mole^{-1} have been reported (77). Johns and Ramsay (78) recently determined the dissociation energy of the hydrosulphide radical and obtained $D(H-S) = 81.4 \pm 2.9$ kcal mole^{-1}. This can be used to calculate a value for D(H-SH), since the heats of formation of S, H and H_2S are known (79). For the process

$SH \longrightarrow S + H$,

$$D(S-H) = \Delta H_f^0(S) + \Delta H_f^0(H) - \Delta H_f^0(SH)$$

$$81.4 = 53.23 + 52.09 - \Delta H_f^0(SH)$$

whence $\Delta H_f^0(SH) = 23.9$ kcal mole^{-1}. For $H_2S \longrightarrow H + SH$

$$D(H-SH) = \Delta H_f^0(H) + \Delta H_f^0(SH) - \Delta H_f^0(H_2S)$$

$$= 52.09 + 23.9 - (-4.82)$$

$$= 80.9 \text{ kcal mole}^{-1}.$$

Cottrell (77) favours a more recent value of 57 kcal mole^{-1} for $\Delta H_f^0(S)$, and Ansdell and Page (80) support this value on the basis of their determination of the electron affinity of the sulphur atom. This value yields $D(H-SH) = 84.65$ kcal

mole^{-1}, in good agreement with our value. On the other hand, Macklo and MacLean (81) prefer a value of 35.2 kcal mole^{-1} for ΔH_f^0(HS), which was determined from a calorimetric study of benzyl mercaptan. This yields D(H-SH) = 92 kcal mole. Palmer and Lossing (82) recently determined ΔH_f^0(HS) $\geqslant$ 33.7 by mass spectrometric techniques, and this leads to an estimate of D(H-SH) $\geqslant$ 90.6 kcal mole^{-1}. The value is therefore still in doubt, but our value of 85.6 kcal mole^{-1} calculated from the difference in activation energies supports the lower values. Admittedly the experimental errors involved in this estimation are large. The value of 85.6 kcal mole^{-1} was taken for the calculations considered above.

The Effect of Temperature on the Relative Rate

The main features of the thermal decomposition of dimethyl ether can be represented by the following scheme (see Part II A):

[11a] $H + CH_3OCH_3 \rightarrow CH_3 + CH_3O + H$

[12] $CH_3 + CH_3OCH_3 \rightarrow CH_4 + CH_3OCH_2$

[13] $CH_3OCH_2 \rightarrow CH_2O + CH_3$

[14a] $H + CH_3O \rightarrow CH_2O + H + H$

[15] $H + CH_3OCH_3 \rightarrow H_2 + CH_3OCH_2$

[17a] $H + CH_3 + CH_3 \rightarrow C_2H_6 + H$

The over-all rate expression derived by means of the usual steady-state approximation is given by

$$v_0 = k_{12} \left(\frac{2k_{11a}}{k_{17a}}\right)^{1/2} [CH_3OCH_3]^{3/2}$$

It was shown above that the rate expression for the reaction in the plateau region ($\sim$ 30 to 50% added H_2S) can be written as

$$v = k_{42} \left(\frac{2k_{11a}}{k_{43a}}\right)^{1/2} [CH_3OCH_3]^{3/2}$$

The relative rate is therefore

$$\frac{v}{v_0} = \frac{k_{42} \left(\frac{2k_{11a}}{k_{43a}}\right)^{1/2} [CH_3OCH_3]^{3/2}}{k_{12} \left(\frac{2k_{11a}}{k_{17a}}\right)^{1/2} [CH_3OCH_3]^{3/2}}$$

which reduces to

$$\frac{v}{v_0} = \frac{k_{42}}{k_{12}} \left(\frac{k_{17a}}{k_{43a}}\right)^{1/2}$$

The predicted activation energy for the relative rate in this region is therefore

$$E = E_{42} - E_{12} + \frac{1}{2}(E_{17a} - E_{43a})$$

Substitution of the appropriate values from Table 5 yields $E = -0.45$ kcal mole^{-1}. This is in good agreement with the experimental value determined by subtracting the activation energy for the reaction in the absence of H_2S from the activation energy for the reaction in the presence of 40% H_2S i.e. 53.2 - 54.9 = - 1.7 kcal mole^{-1}. This explains why the relative rate seems to increase with decreasing temperature. The fact that - 1.7 is so small is indicated from Fig. 24, which shows that the curves for the three temperatures fall very close to one another.

Similarly for the region using high percentages of hydrogen sulphide the relative rate is given by

$$\frac{v}{v_0} = \frac{k_{42}}{k_{12}} \left(\frac{k_{44}k_{17a}}{k_{11a}k_{43a}}\right)^{1/2} \frac{[H_2S]^{1/2}}{[CH_3OCH_3]^{1/2}}$$

The activation energy for the relative rate is predicted to be

$$E = E_{42} - E_{12} + \tfrac{1}{2}(E_{44} + E_{17a} - E_{11a} - E_{43a})$$

$$= 3.85 \text{ kcal mole}^{-1}$$

This is in fair agreement with the experimental value of -2.4 kcal mole^{-1}, considering the uncertainties in the individual activation energies.

Since, in the region of high percentages of hydrogen sulphide, the relative rate increases very rapidly for small changes in the percentage of hydrogen sulphide, this temperature dependence of the relative rate is not very apparent in Fig. 24.

Part III

KINETICS AND MECHANISMS OF THE PYROLYSIS OF DIETHYL ETHER

A. The Uninhibited Reaction

INTRODUCTION

Diethyl ether undergoes pyrolysis to give two sets of products, as represented by the following stoichiometric equations:

$$C_2H_5OC_2H_5 = C_2H_5OH + C_2H_4$$

$$C_2H_5OC_2H_5 = CH_3CHO + C_2H_6$$

Under the usual conditions, at temperatures around 600°C, the acetaldehyde and ethane decompose further into methane, carbon monoxide, ethylene and hydrogen. A number of kinetic studies have been made, the first being by Hinshelwood (83) in 1927. He found that the reaction was close to first-order and observed a 'falling-off' of the rate constant at low ether pressures. The activation energy was found to be 53 kcal mole^{-1}.

The reaction has been investigated over a very wide range of pressure (from 0.1 mm. Hg. (84) to about 300 atm. (85,86,87)). Even at the highest pressure the first-order rate coefficient was found to be still increasing with in-

creasing pressure.

Free radicals were detected in the decomposition by the metallic-mirror technique (18,88). This led to an estimate of 68.6 kcal $mole^{-1}$ for the initial split of the ether molecule into radicals. This is probably too low a value.

Fletcher and Rollefson (89) determined the amount of acetaldehyde at various stages of the ether decomposition, and suggested that radicals from the ether were sensitizing the decomposition of acetaldehyde. A suggestion was made by these authors that ether was decomposing partly by a free-radical mechanism and partly by a molecular reaction.

An alternative to the free-radical scheme postulated by Rice and Herzfeld (24), was made by Hebbert and Laidler (90). The main difference in the two mechanisms was the nature of the initiation reaction. This point is discussed below.

More recently, Freeman (91,92), Freeman, Danby and Hinshelwood (93) and Danby and Freeman (94) have carried out a thorough analytical study of the pyrolysis at 525°C. In the pressure region from about 400 to 1600 mm. the reaction was found to be three-halves-order, but below 400 mm. the order decreased. A logarithmic plot showed that over the low pressure region the order was 1.2 with respect to ether pressure. The free-radical mechanism postulated by Freeman (92) can be written:

creasing pressure.

Free radicals were detected in the decomposition by the metallic-mirror technique (18,88). This led to an estimate of 68.6 kcal $mole^{-1}$ for the initial split of the ether molecule into radicals. This is probably too low a value.

Fletcher and Rollefson (89) determined the amount of acetaldehyde at various stages of the ether decomposition, and suggested that radicals from the ether were sensitizing the decomposition of acetaldehyde. A suggestion was made by these authors that ether was decomposing partly by a free-radical mechanism and partly by a molecular reaction.

An alternative to the free-radical scheme postulated by Rice and Herzfeld (24), was made by Hebbert and Laidler (90). The main difference in the two mechanisms was the nature of the initiation reaction. This point is discussed below.

More recently, Freeman (91,92), Freeman, Danby and Hinshelwood (93) and Danby and Freeman (94) have carried out a thorough analytical study of the pyrolysis at 525°C. In the pressure region from about 400 to 1600 mm. the reaction was found to be three-halves-order, but below 400 mm. the order decreased. A logarithmic plot showed that over the low pressure region the order was 1.2 with respect to ether pressure. The free-radical mechanism postulated by Freeman (92) can be written:

$$C_2H_5OC_2H_5 \rightarrow C_2H_5 + C_2H_5O$$

$$C_2H_5 + C_2H_5OC_2H_5 \rightarrow C_2H_6 + C_2H_4OC_2H_5$$

$$C_2H_4OC_2H_5 \rightarrow C_2H_5 + CH_3CHO$$

$$C_2H_5O \rightarrow CH_3 + HCHO$$

$$C_2H_5 \rightarrow H + C_2H_4$$

$$H + C_2H_5OC_2H_5 \rightarrow H_2 + C_2H_4OC_2H_5$$

$$C_2H_5 + C_2H_4OC_2H_5 \rightarrow \text{products}$$

$$H + C_2H_4OC_2H_5 \rightarrow \text{products}$$

After some approximations the steady state treatment led to a rate expression predicting first-order dependence on ether. In order to explain the three-halves-order behaviour at high pressures it was assumed that the rate constant for the initiation reaction eventually takes the form

$$k = \frac{D[M]}{1 + E[M]} + F[M],$$

where D, E and F are constants, and M represents the ether molecule. When this is substituted into the rate expression the mechanism predicts three-halves-order dependence at high pressures of ether. This assumption is however based on an empirical relationship derived by Jach and Hinshelwood (95) to explain the shapes of rate-pressure curves for the decom-

position of paraffins in the presence of inert gases. Some of their experimental data have been shown to be of questionable validity (15,16), and hence the form of the rate constant (k) above is probably erroneous. This of course invalidates the mechanism suggested by Freeman (92). Danby and Freeman (94) found that the ethanol formation was not inhibited by nitric oxide, and from this they concluded that the process giving rise to C_2H_5OH and C_2H_4 is a molecular one; further evidence for this was obtained in the present work. The production of acetaldehyde and ethane is, however, inhibited by nitric oxide, and is obviously at least in part a chain reaction. The present work leads to the conclusion that it is almost entirely a chain reaction.

The present investigation consists of a further experimental study with the particular object of separating the various components of the reaction and determining their orders and kinetic parameters. A detailed free-radical mechanism is proposed.

EXPERIMENTAL

The experimental procedure was essentially the same as described in Part II A. The diethyl ether was anhydrous reagent grade purchased from Mallinckrodt Chemical Works of Montreal. It was further purified by distillation

in the vacuum system.

In view of the very detailed analytical study made by Danby and Freeman (94), only a few analyses were carried out in the present work; the main object of these was to relate the pressure changes to the amount of ether that had undergone reaction. Fixed fractions of the reaction products were analysed by gas chromatography using a Perkin-Elmer model 154 Vapor Fractometer. Quantitative determinations were made for ether and ethanol on a two-meter Perkin-Elmer 'A' column which contained dodecyl phthalate adsorbed on fire-brick. Calibration curves were made using reagent standards, hence peak heights were used as a quantitative measure of partial pressure. The column temperature was maintained at 30.0 ± 0.5°C.

RESULTS

Typical pressure-time curves for the decomposition are shown in Fig. 31. Curve A is a tracing of the record obtained in the pyrolysis of 102 mm. of diethyl ether at 560°C. Curve B is a curve obtained using approximately the same ether pressure but at a temperature of 620°C. Induction periods were observed only at low temperatures and pressures.

Figure 32 shows double logarithmic plots of rate against ether pressure. All of the lines have slopes of

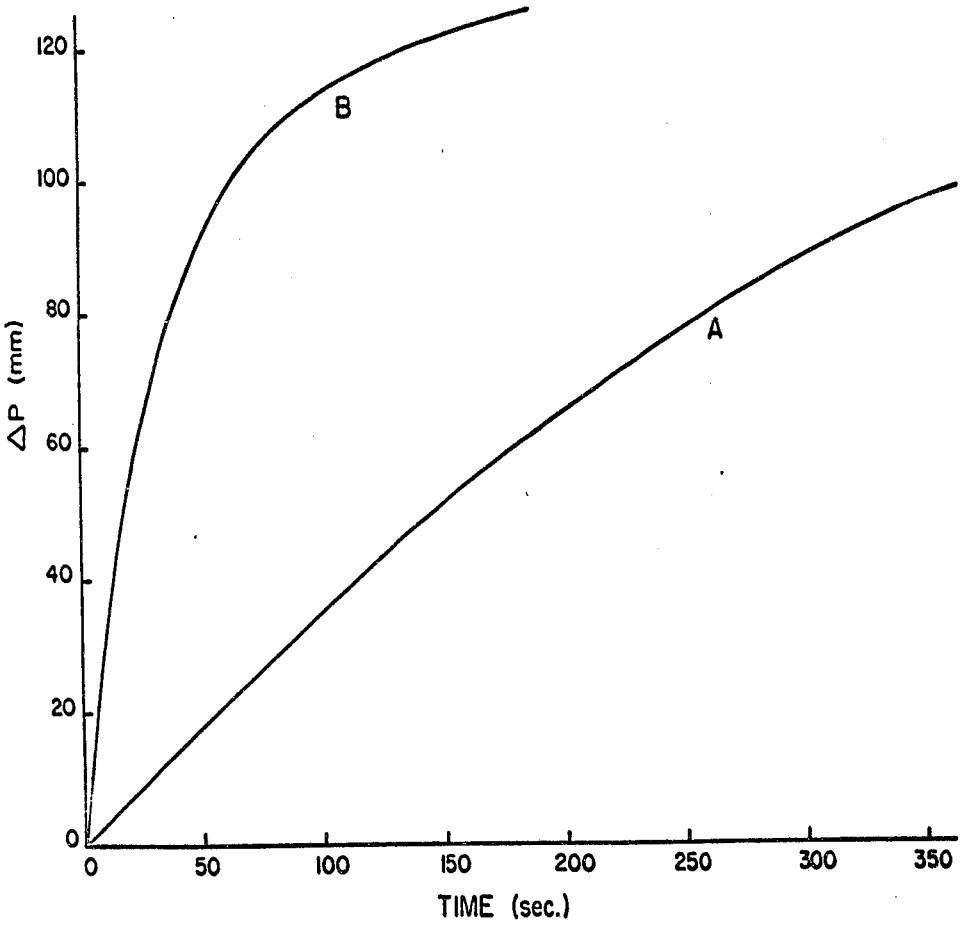

Figure 31. Pressure-time curves for the uninhibited pyrolysis of diethyl ether. Curve A is a tracing of the record obtained in the pyrolysis of 102 mm. of diethyl ether at 560°C. Curve B is a similar tracing obtained using approximately the same ether pressure but at a temperature of 620°C.

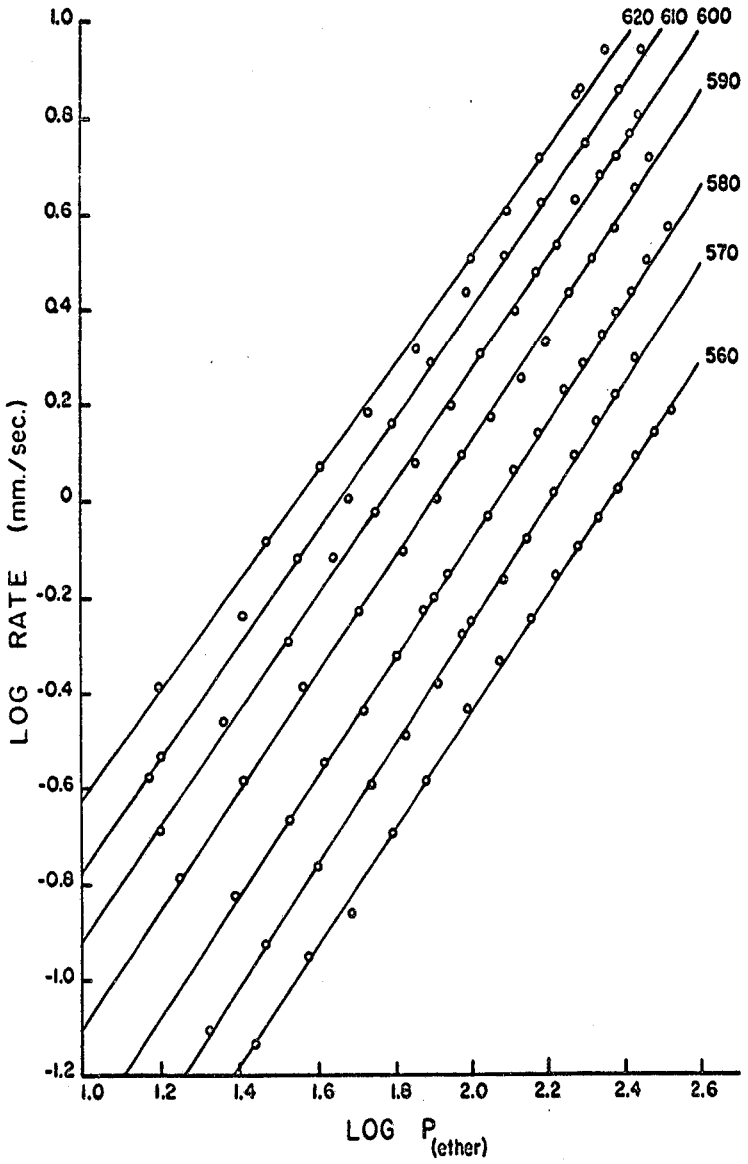

Figure 32. Double logarithmic plots of rate against diethyl ether pressure for the uninhibited reaction. The temperature (°C) is indicated on each curve.

between 1.2 and 1.3. Freeman (92) working at 525°C has shown that the order becomes 3/2 at high pressure. This increase in order has been shown by Fletcher and Rollefson (96) at 521°C. This implies that the over-all rate expression involves at least two terms, each corresponding to a different order. As will be discussed later, the theoretical rate equation is a somewhat complex one, but the behaviour it predicts is closely represented by an equation of the form

$$v = (k_m + k_p)[M] + k'[M]^{3/2} \qquad (1)$$

where M represents ether. The rate constants k_m and k_p relate to molecular and free-radical reactions, respectively.

In order to see whether the results obtained are consistent with this equation, plots were made of $v/[M]$ against $[M]^{1/2}$, and Fig. 33 shows the results of such plots. The slopes and intercepts of the lines were obtained using the method of least squares, and the correlation coefficients and standard errors were calculated using conventional statistical procedures. The intercepts (equal to $k_m + k_p$) and slopes (equal to k') are listed in Table 6. The uncertainty in the intercept (at the 95% level) is taken to be $\pm 2s$, where s is the standard error of the estimate. The uncertainty in the slope was taken to be $\pm 2s/(\text{range})$. There appears to be no standard method for stating the uncertainty

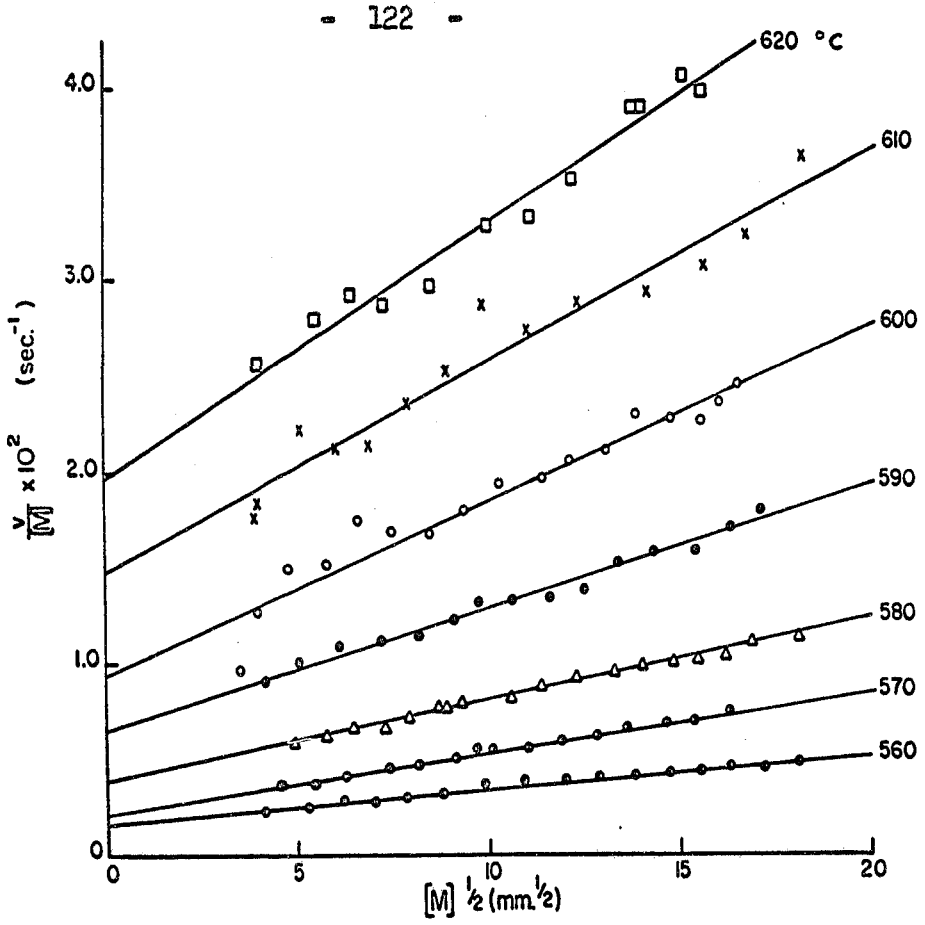

Figure 33. Plots of v/[M] against $[M]^{1/2}$ for the uninhibited pyrolysis of diethyl ether.

Table 6

Rate Constants Derived from Figure 33*

Temperature (°C)	Correlation coefficient	Standard error $\times 10^5$	$10^3(k_m+k_p)$ (sec^{-1})	$10^3 k_p$ (sec^{-1})	$10^4 k'$ ($mm^{-1/2} sec^{-1}$)
560	0.988	12.9	1.65 ± 0.26	1.38 ± 0.26	1.91 ± 0.14
570	0.997	9.3	2.09 ± 0.19	1.60 ± 0.19	3.40 ± 0.11
580	0.997	13.2	3.95 ± 0.26	3.08 ± 0.26	4.34 ± 0.13
590	0.990	37.4	6.53 ± 0.75	4.94 ± 0.75	6.62 ± 0.42
600	0.969	100.0	9.44 ± 2.00	6.78 ± 2.0	9.30 ± 1.10
610	0.974	120.0	14.8 ± 2.4	10.0 ± 2.4	11.2 ± 1.3
620	0.983	89.0	19.8 ± 1.8	11.9 ± 1.8	13.5 ± 1.1

* These rate constants may be corrected by multiplying them by 0.84 (see text).

in a slope; the method used undoubtedly exaggerates the uncertainty.

As will be discussed later, the first-order component of the reaction consists of both a molecular reaction and a free-radical reaction. A procedure for obtaining the rate constants k_m for the molecular reaction, involving inhibition by nitric oxide, is explained in Part III B. Table 6 includes values of k_p, obtained by subtracting these k_m values from $k_m + k_p$.

Figure 34 shows an Arrhenius plot for the first-order chain component (k_p), the uncertainties being shown for each temperature. The rate constant can be expressed as

$$k_r = 1.7 \times 10^{12} e^{-57,600/RT} \text{ sec}^{-1}$$

A similar plot is shown in Fig. 35 for the three-halves-order components of the reaction, and leads to an activation energy of 47.7 kcal mole^{-1} and a frequency factor of 7.6×10^{0} mm$^{-1/2}$ sec^{-1}. Experiments were carried out to relate pressure changes to concentration changes, as measured by vapour-phase chromatography, at various stages of the reaction. Figure 36 shows the results of such measurements, in the form of the relative change in true ether pressure plotted against the relative change in pressure measured using the spiral gauge. The line has a slope of 0.84, which is to be compared with the ratios

in a slope; the method used undoubtedly exaggerates the uncertainty.

As will be discussed later, the first-order component of the reaction consists of both a molecular reaction and a free-radical reaction. A procedure for obtaining the rate constants k_m for the molecular reaction, involving inhibition by nitric oxide, is explained in Part III B. Table 6 includes values of k_r, obtained by subtracting these k_m values from $k_m + k_r$.

Figure 34 shows an Arrhenius plot for the first-order chain component (k_r), the uncertainties being shown for each temperature. The rate constant can be expressed as

$$k_r = 1.7 \times 10^{12} e^{-57,600/RT} \text{ sec}^{-1}$$

A similar plot is shown in Fig. 35 for the three-halves-order components of the reaction, and leads to an activation energy of 47.7 kcal mole^{-1} and a frequency factor of 7.6×10^8 mm$^{-1/2}$ sec^{-1}. Experiments were carried out to relate pressure changes to concentration changes, as measured by vapour-phase chromatography, at various stages of the reaction. Figure 36 shows the results of such measurements, in the form of the relative change in true ether pressure plotted against the relative change in pressure measured using the spiral gauge. The line has a slope of 0.84, which is to be compared with the ratios

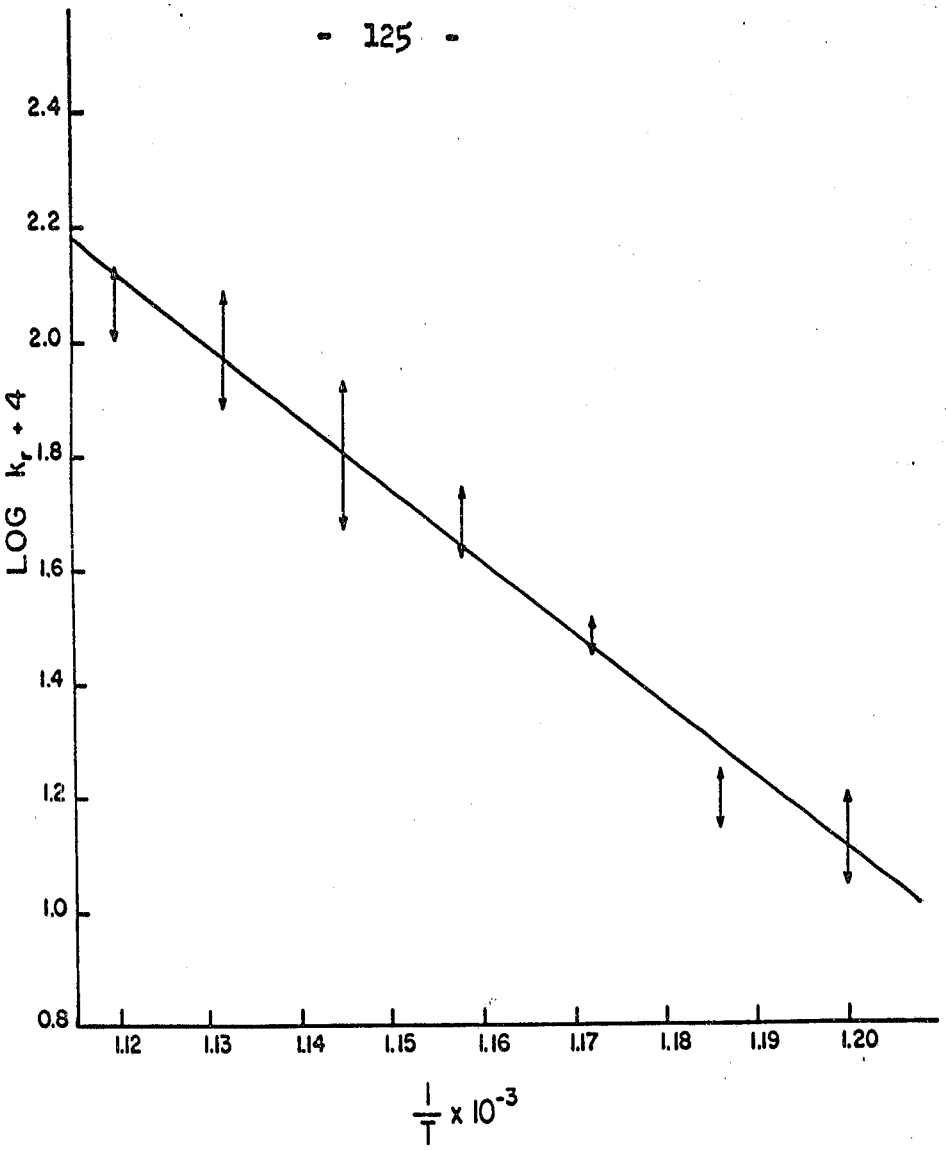

Figure 34. Arrhenius plot for the first-order chain component (k_r) of the uninhibited pyrolysis of diethyl ether.

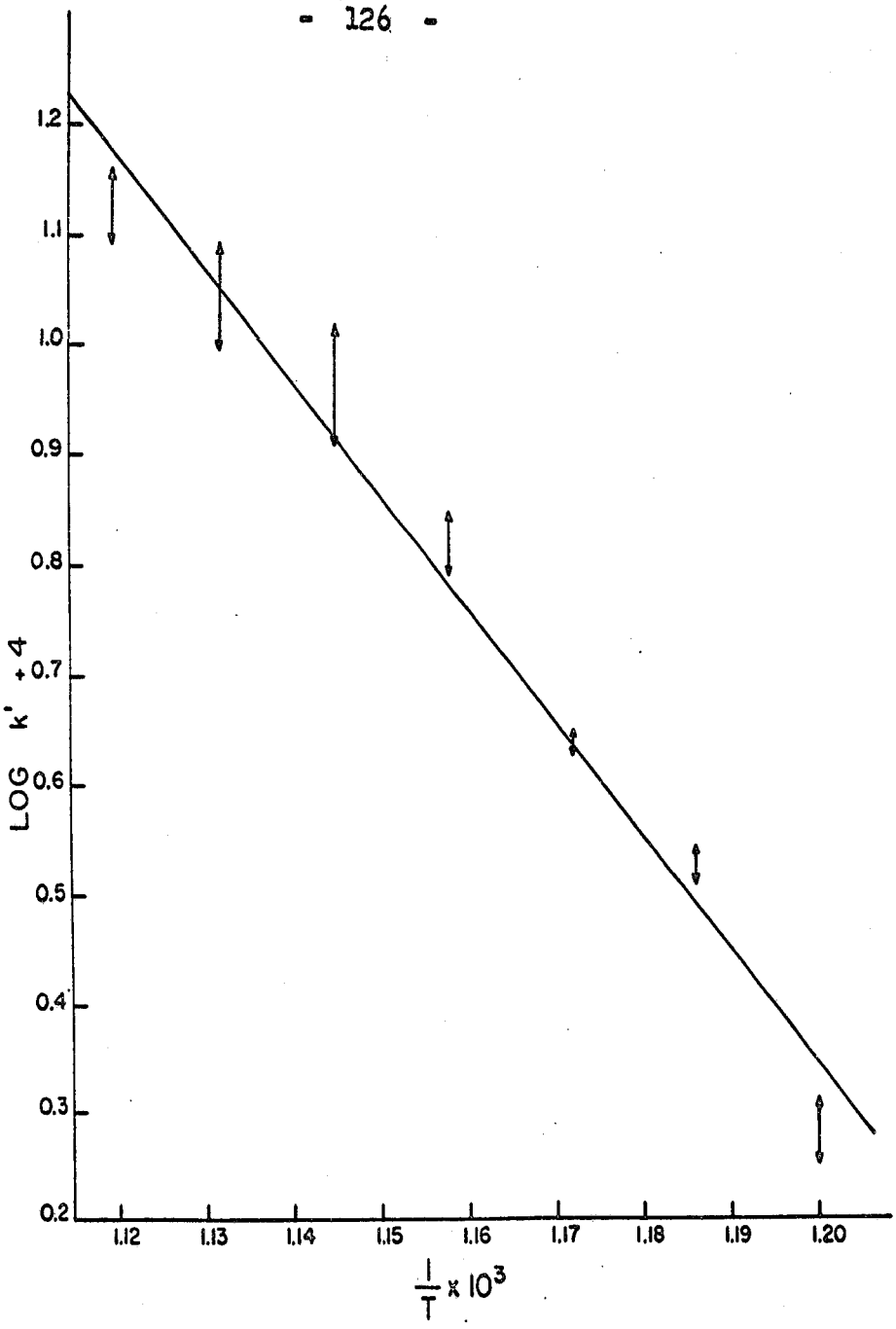

Figure 35. Arrhenius plot for the three-halves-order component (k') of the uninhibited pyrolysis of diethyl ether.

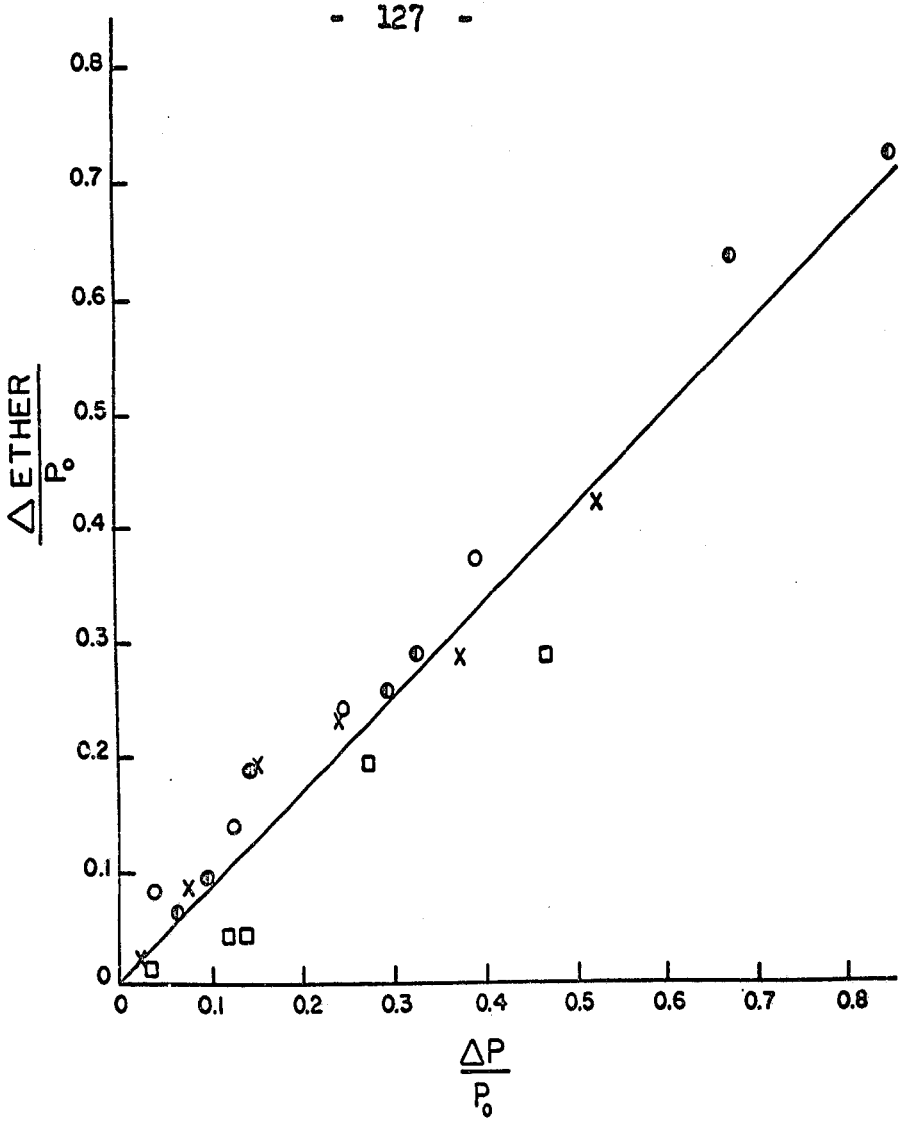

Figure 36. Plot of relative change in true diethyl ether pressure against the relative change in pressure measured using the spiral gauge. × 560°C, ◐ 620°C uninhibited; ○ 560°C □ 620°C inhibited.

of 0.69 to 0.80 determined at 525°C by Danby and Freeman (94).

Use of the factor 0.84 leads to the following expressions for the rate constants:

$$k_r = 1.4 \times 10^{12}\, e^{-57,600/RT} \text{ sec}^{-1}$$

$$k' = 4.8 \times 10^{12}\, e^{-47,400/RT} \text{ cc}^{1/2} \text{ mole}^{-1/2} \text{ sec}^{-1}$$

DISCUSSION

The Chain-propagating Step

It is convenient to consider the chain-propagation reactions first, since there is least uncertainty with regard to these. Abstraction of a hydrogen atom from the diethyl ether molecule will lead to either $CH_3CHOCH_2CH_3$ or $CH_2CH_2OCH_2CH_3$, and the possible reactionsthat result are shown schematically in Fig. 37. Important information is provided by a consideration of the fate of the C_2H_5O radical. It might be thought that this radical would lead to ethanol production by the abstraction reaction

[a] $C_2H_5O + C_2H_5OC_2H_5 \rightarrow C_2H_5OH + C_2H_4OC_2H_5$

However it can easily be shown that this reaction must be unimportant in comparison with

[50]* $C_2H_5O \rightarrow CH_3 + CH_2O$

---

* This reaction is numbered so as to be consistent with the mechanism discussed below.

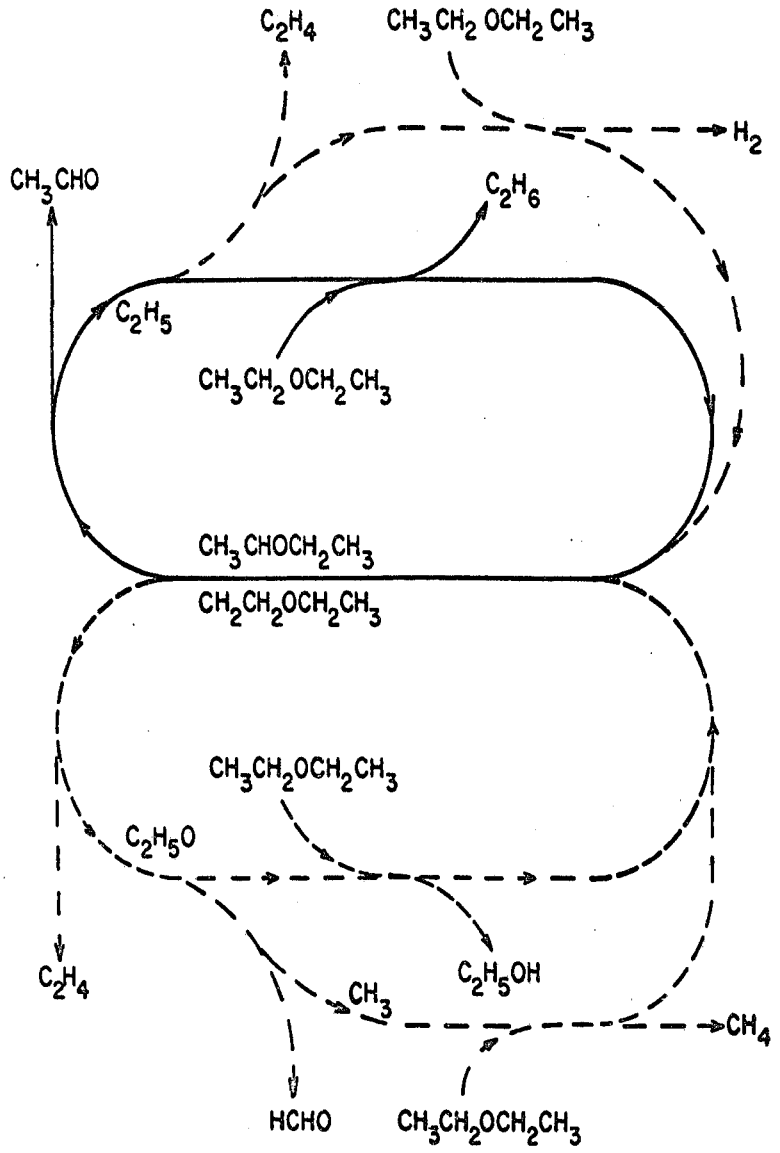

Figure 37. Diagram illustrating the possible processes resulting from the decompositions of the radicals, $CH_2CH_2OC_2H_5$ and $CH_3CHOC_2H_5$.

The former reaction probably has a frequency factor of about 10^{12} cc mole^{-1} sec^{-1} and an activation energy of about 10 kcal per mole; the second reaction will have a frequency factor of at least 10^{13} and its activation energy will be equal to its exothermicity, which has been estimated by Rebbert and Laidler (90) as 10.4 kcal mole^{-1}. At the pressures of the present investigations the value of $[C_2H_5OC_2H_5]$ is of the order of 10^{-5} mole cc^{-1}, so that

$$\frac{v_a}{v_{50}} \approx \frac{10^{12}\, e^{-10,000/RT}}{10^{13}\, e^{-10,400/RT}} \times 10^{-5}$$

which is very much less than unity. It therefore follows that if C_2H_5O were formed in this reaction it would give rise to CH_2O and CH_3, which in turn produces CH_4.

The analytical results of Danby and Freeman (94), however, indicate that the initial rate of formation of methane is considerably smaller than that of acetaldehyde and ethane. From this it follows that the lower cycle in Fig. 37 occurs only to a small extent relative to the upper cycle. This could be due to either of the following causes:

1) The radical $CH_2CH_2OC_2H_5$ is formed to an insignificant extent by abstraction of a hydrogen atom from $C_2H_5OC_2H_5$.

2) The radical $CH_2CH_2OC_2H_5$ is quite stable with respect to decomposition and its main reaction is to abstract a hydrogen

atom from an ether molecule to form $CH_3CHOC_2H_5$.
The first explanation is intrinsically improbable since a great difference in reactivity between the α and β hydrogen atoms is not to be expected. The occurrence of the transfer reaction

$$CH_2CH_2OC_2H_5 + CH_3CH_2OC_2H_5 \rightarrow CH_3CHOC_2H_5 + CH_3CH_2OC_2H_5$$

is, however, quite reasonable, and was in fact mentioned as a possibility by Freeman (91). The breakdown of $CH_2CH_2OC_2H_5$ into C_2H_4 and C_2H_5O probably requires a much higher activation energy than that of $CH_3CHOC_2H_5$ into CH_3CHO and C_2H_5. The concentration of $CH_2CH_2OC_2H_5$ is therefore expected to be high, and this radical is probably involved in chain ending, as discussed below.

It follows that there are two important reasons why ethanol is not produced to any significant extent by chain processes:

1) The radical $CH_2CH_2OC_2H_5$ is unreactive.

2) Any C_2H_5O radicals produced from the breakdown of this radical will dissociate rather than abstract.

Most of the ethanol formed in the reaction must therefore be formed by the molecular split of $C_2H_5OC_2H_5$ into C_2H_5OH and C_2H_4. This is also the conclusion drawn by Danby and Freeman (94) on the basis of their finding that the ethanol production is not inhibited by nitric oxide. Danby and Freeman's analytical

results also show that the initial rate of ethylene formation is not much greater than that of ethanol formation. Most of the ethylene formed initially is therefore produced by the molecular process, and very little from the breakdown of the C_2H_5 formed in the chain processes. This is to be expected from the fact that the breakdown of C_2H_5 into $C_2H_4 + H$ requires an activation energy of 39.5 kcal $mole^{-1}$ (97). Since the abstraction reaction of C_2H_5 requires only about 10 kcal $mole^{-1}$, most of the C_2H_5 molecules will abstract before they acquire the energy to decompose. For the butane decomposition, however, Purnell and Quinn (33) have shown that the C_2H_5 decomposition takes place to a significant extent and is in the intermediate region between first- and second-order kinetics.

The main conclusion is that, as shown schematically in Fig. 37, the chain-propagating reactions are primarily

$$C_2H_5 + CH_3CH_2OCH_2CH_3 \longrightarrow C_2H_6 + CH_3CHOCH_2CH_3$$

and

$$CH_3CHOCH_2CH_3 \longrightarrow CH_3CHO + C_2H_5,$$

with the decomposition of C_2H_5 playing a minor but significant role. Less important chain-propagating processes are

$$C_2H_5 + CH_3CH_2OC_2H_5 \longrightarrow C_2H_6 + CH_2CH_2OC_2H_5$$

$$CH_2CH_2OC_2H_5 \rightarrow C_2H_4 + C_2H_5O$$

$$C_2H_5O \rightarrow CH_3 + CH_2O$$

Since the transfer reaction

$$CH_2CH_2OC_2H_5 + CH_3CH_2OC_2H_5 \rightarrow CH_3CHOC_2H_5 + CH_3CH_2OC_2H_5$$

occurs in addition, the radical $CH_2CH_2OC_2H_5$ is both a β and a μ radical.

Initiation and Termination Steps

In a chain reaction for a decomposition the over-all kinetic behaviour depends only on the order (and not the detailed nature) of the initiation process, on the order of the termination process, and on the nature (β or μ) of the radicals involved in termination. An over-all kinetic study therefore cannot discriminate between the following two possible initiation processes:

$$CH_3CH_2OCH_2CH_3 \rightarrow CH_3 + CH_2OCH_2CH_3$$

and

$$CH_3CH_2OCH_2CH_3 \rightarrow CH_3CH_2O + CH_2CH_3$$

The first of these was the one originally assumed by Rice and Herzfeld (24). Robbert and Laidler (90) presented thermochemical arguments in favour of the second initiation reaction.

but as pointed out by Gowenlock (98) these are by no means conclusive. The second process will be assumed in the present work, but the first would give rise to exactly the same conclusions. In view of the size of the diethyl ether molecule it is safe to conclude, especially with reference to the butane decomposition (16), that the reaction is in its first-order region.

The radicals occurring in the chain-propagating steps are $CH_2CH_2OC_2H_5$, $CH_3CHOC_2H_5$, C_2H_5, CH_3 and H. Of the small radicals C_2H_5 is clearly predominant, since the initial rates of formation of C_2H_6 are much greater than those of CH_4 and H_2. Of the two larger radicals, $CH_2CH_2OC_2H_5$ is present in higher concentrations, as discussed above, and its concentration is probably higher than that of C_2H_5. The C_2H_5 mainly undergoes bimolecular abstraction reactions, and is therefore a β radical. The $CH_2CH_2OC_2H_5$ radical, on the other hand, undergoes both a bimolecular transfer reaction and a unimolecular decomposition; it is therefore both a β radical and a μ radical.

The recombination of $CH_2CH_2OC_2H_5$ radicals is unlikely for steric reasons, so that the predominant chain-ending step is concluded to be

$$C_2H_5 + CH_2CH_2OC_2H_5 \longrightarrow C_4H_9OC_2H_5.$$

This termination process has both ββ and βμ character; the

former leads, according to the rules of Goldfinger, Letort and Niclause (99), to three-halves order kinetics and the latter to first-order kinetics. This chain-ending step therefore explains the observed over-all kinetic behaviour, as will now be shown in detail.

The over-all mechanism

The mechanism proposed is, with some simplifications, as follows:

[1m] $C_2H_5OC_2H_5 \rightarrow C_2H_5OH + C_2H_4$

[47] $C_2H_5OC_2H_5 \rightarrow C_2H_5O + C_2H_5$

[48] $C_2H_5 + C_2H_5OC_2H_5 \rightarrow C_2H_6 + CH_2CH_2OC_2H_5$

[49] $C_2H_5 + C_2H_5OC_2H_5 \rightarrow C_2H_6 + CH_3CHOC_2H_5$

[50] $C_2H_5O \rightarrow CH_3 + CH_2O$

[51] $CH_3 + C_2H_5OC_2H_5 \rightarrow CH_4 + CH_2CH_2OC_2H_5$

[52] $CH_3 + C_2H_5OC_2H_5 \rightarrow CH_4 + CH_3CHOC_2H_5$

[53] $CH_2CH_2OC_2H_5 + C_2H_5OC_2H_5 \rightarrow CH_3CHOC_2H_5 + C_2H_5OC_2H_5$

[54] $CH_2CH_2OC_2H_5 \rightarrow C_2H_4 + C_2H_5O$

[55] $CH_3CHOC_2H_5 \rightarrow CH_3CHO + C_2H_5$

[56] $C_2H_5 + CH_2CH_2OC_2H_5 \rightarrow C_4H_9OC_2H_5$

The reactions $C_2H_5 \rightarrow C_2H_4 + H$, and abstraction reactions by

the H atom, are unimportant and are neglected in the above scheme; their inclusion leads to no important change in the form of the kinetic equations.

Application of the steady-state treatment to the above reaction scheme leads, with the usual approximations, to the following expressions for the radical concentrations:

$$[CH_2CH_2OC_2H_5] = \left(\frac{k_{47}k_{48}(k_{51}+k_{52})}{(k_{51}+k_{52})k_{53}k_{56}[M] + k_{52}k_{54}k_{56}}\right)^{1/2} [M] \quad (2)$$

$$[CH_3CHOC_2H_5] = \frac{(k_{48}+k_{49})}{k_{55}} \left(\frac{(k_{51}+k_{52})k_{47}k_{53}[M] + k_{47}k_{52}k_{54}}{(k_{51}+k_{52})k_{48}k_{56}}\right)^{1/2} [M] \quad (3)$$

$$[C_2H_5] = \left(\frac{(k_{51}+k_{52})k_{47}k_{53}[M] + k_{47}k_{52}k_{54}}{(k_{51}+k_{52})k_{48}k_{56}}\right)^{1/2} \quad (4)$$

$$[CH_3] = \frac{k_{47}}{k_{51}+k_{52}} + \frac{k_{54}}{k_{51}+k_{52}} \left(\frac{k_{47}k_{48}(k_{51}+k_{52})}{(k_{51}+k_{52})k_{53}k_{56}[M] + k_{52}k_{54}k_{56}}\right)^{1/2} \quad (5)$$

where M represents diethyl ether. The ether disappears mainly by reaction [3m], [48] and [49], since the initiation reaction [47] is slow and the methyl radicals are present in much lower concentrations than the ethyl radicals; the over-all rate of

disappearance of ether is therefore given approximately by

$$v = k_{1m}[M] + (k_{48}+k_{49})\left(\frac{(k_{51}+k_{52})\,k_{47}k_{53}[M] + k_{47}k_{52}k_{54}}{(k_{51}+k_{52})k_{48}k_{56}}\right)^{1/2}[M] \qquad (6)$$

At high concentrations of ether this equation predicts three-halves-order kinetics, the limiting rate expression being

$$v_{high} = (k_{48}+k_{49})\left(\frac{k_{47}k_{53}}{k_{48}k_{56}}\right)^{1/2}[M]^{3/2} \qquad (7)$$

At low pressures, on the other hand, the kinetics are first-order, the rate expression being

$$v_{low} = k_{1m}[M] + (k_{48}+k_{49})\left[\frac{k_{47}k_{52}k_{54}}{(k_{51}+k_{52})k_{48}k_{56}}\right]^{1/2}[M] \qquad (8)$$

These conclusions are entirely consistent with the experimental results. It is true that equation (6) is not of exactly the same form as equation (1). Analysis of the experimental results in terms of an equation of the form of (6) would, however, be difficult and it was considered preferable to use equation (1), as described in the Results section. The three-halves and first-order rate constants obtained in this way, being extrapolated values, can be identified with the rate constants in

equations (7) and (8).

Activation Energies

The experimental activation energy corresponding to the three-halves-order kinetics has been seen to be 47.4 kcal mole^{-1}. According to equation (7) the activation energy is

$$E_{high} = E_{48} + \frac{1}{2}(E_{47} + E_{53} - E_{48} - E_{56}) \qquad (9)$$

(E_{48} and E_{49} are assumed to be approximately the same). The value of E_{47} has been estimated by Rebbert and Laidler (90) to be 77.5 kcal, and E_{48} has been measured by Long and Skirrow (100) to be 9.75 kcal. Reaction [53] is assumed to be an abstraction reaction with an activation energy of 10 kcal. The termination reaction [56] is assumed to require no activation energy. Use of these values leads to

$$E_{high} = 46.1 \text{ kcal mole}^{-1}$$

in good agreement with the experimental value.

The experimental activation energy in the low-pressure region is 57.6 kcal mole^{-1}. According to equation (8) the predicted value for the free-radical part of the first-order reaction is

$$E_{low} = E_{48} + \frac{1}{2}[E_{47} + E_{54} - E_{48} - E_{56}]. \qquad (10)$$

the assumption being made that $E_{48} \approx E_{49}$ and $E_{51} \approx E_{52}$. Use of the above values, together with an assumed value of 30 kcal. for E_{54}, leads to

$$E_{low} = 56.5 \text{ kcal mole}^{-1}$$

in reasonable agreement with the experimental value.

B. The Reaction Inhibited by Nitric Oxide

INTRODUCTION

Many previous investigations (20,21,22,43,101,102, 103,104,92,94,93) have shown that small amounts of nitric oxide inhibit the decomposition of diethyl ether, and that larger amounts bring about some acceleration. It was originally supposed that the maximally inhibited reaction, in this and other cases, corresponded to a purely molecular reaction, the effect of the nitric oxide being to remove radicals. Hobbs (102) postulated the following mechanism:

$$C_2H_5OC_2H_5 \rightarrow CH_3 + CH_2OC_2H_5$$

$$CH_3 + C_2H_5OC_2H_5 \rightarrow C_2H_6 + CH_2OC_2H_5$$

$$CH_2OC_2H_5 \rightarrow CH_3 + CH_3CHO$$

$$CH_3 + CH_2OC_2H_5 \rightarrow \text{product}$$

$$NO + CH_2OC_2H_5 \rightarrow \text{product}$$

This leads to a rate expression which predicts first-order dependence on ether, and fails to account for all the products of the decomposition.

More recently, Freeman (92) suggested a similar although more elaborate scheme for the diethyl ether decomposition. This was discussed in Part III A. When nitric oxide was added, it presumably reacted with the large $C_2H_5OC_2H_5$

radicals to form products and thereby stop the chain processes. Thus it was assumed that the maximally inhibited reaction was of a molecular nature. The three-halves-order behaviour which Freeman observed at higher ether pressures was not explained.

For a number of reactions, however, it has been shown that free-radical reactions are still occurring even when there is maximal inhibition, and that molecular processes are unimportant. Specific mechanisms for reactions maximally inhibited by nitric oxide have been proposed for a number of pyrolyses, including those of ethane (40), propane (41), butane (42) and dimethyl ether (Part II B). All of these reactions are found to follow a similar pattern, although there are important differences depending on which radicals are predominant. In all of the mechanisms there is initiation by reaction between a molecule of nitric oxide and a substrate molecule, and termination involves a species (e.g. HNO or CH_3NO) formed from nitric oxide.

In view of the conclusion of Danby and Freeman (94), substantiated in Part II A, that a molecular reaction does play a significant role in the diethyl ether pyrolysis, it was of particular interest to carry out a detailed investigation of the inhibition of this reaction. The present section describes such an investigation, and shows that the maximally inhibited reaction has a first-order molecular component, and a three-halves-order free radical component. The molecular component

is, of course, identical with the one that occurs in the uninhibited reaction. The three-halves order radical component replaces the free-radical components of the uninhibited reaction; different initiation and termination steps are involved, the details of them being discussed below.

EXPERIMENTAL

The experimental procedures were as described in Parts II A and III A.

RESULTS

Preliminary experiments were carried out to determine the range of nitric oxide pressures which would give maximal inhibition. Some of the results are shown in Fig. 38, in which the percentage relative rate is plotted against the nitric oxide pressure. The points correspond to five different temperatures, but a single curve is drawn through the points at 560, 580 and 590°C; this was done because of the scatter at these lower temperatures. At the higher temperatures, 600 and 620°C, there is less experimental scatter and the limiting rates are obviously different. There is less inhibition at the higher temperatures. Figure 38 also shows that the minimum relative rate is independent of the ether pressure; pressures from 12 to 325 mm. were used to obtain

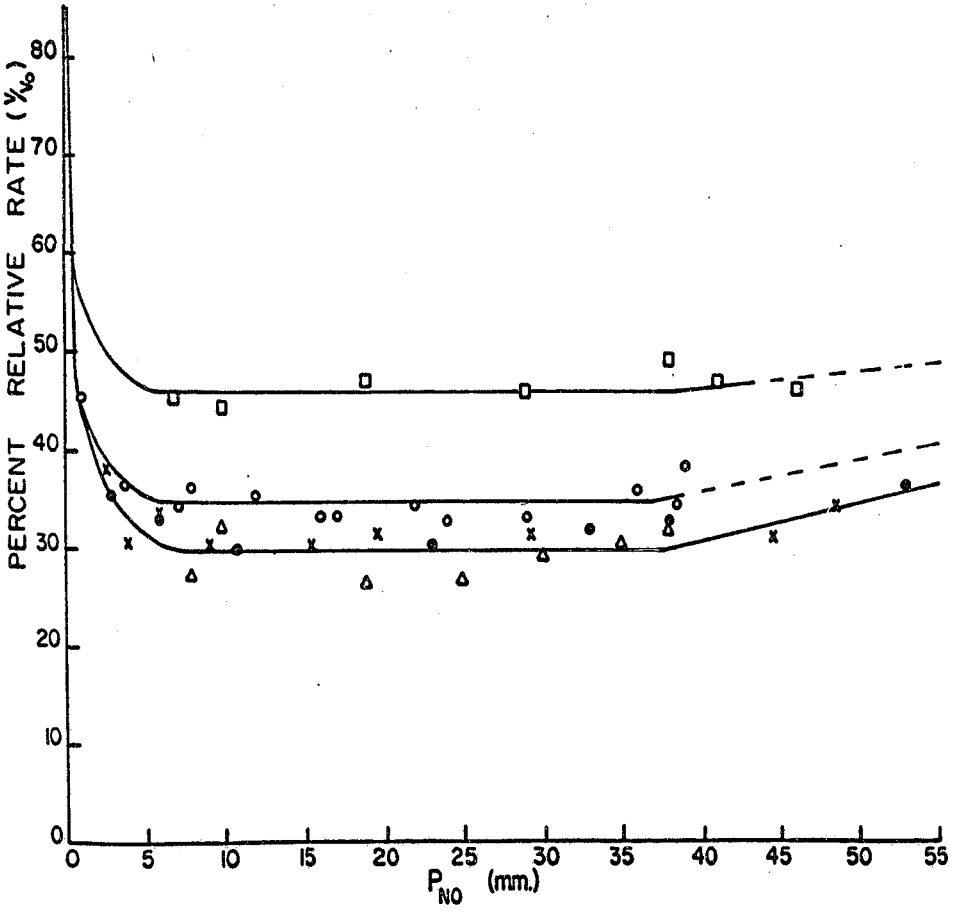

Figure 38. Percent relative rate against nitric oxide.

□ 620°C, ○ 600°C, × 590°C, ● 580°C, Δ 560°C.

points along the flat regions. Nitric oxide pressures between 6 and 40 mm. were used in subsequent studies of the maximally inhibited reaction.

Figure 39 shows some typical pressure-time curves for maximal inhibition. Curve A is a tracing of a record for the decomposition of 95 mm. of diethyl ether in the presence of 31 mm. of NO at 630°C; curves B and C are for approximately the same pressure conditions but at temperatures of 600 and 560°C respectively. Figure 40 shows a record for a run using 355 mm. of ether and 10 mm. of NO at 500°C; there is an initial pressure decrease followed by an increase. As illustrated in Figs. 39 and 40, the 'induction' period becomes more pronounced at low temperatures. Between 560 and 640°C there is effectively no induction period except at low pressures and temperatures.

In order to correlate pressure changes with the disappearance of ether, some analytical studies were made for maximally inhibited reactions. The results were shown in Fig. 36 of Part III A. The appropriate correction has been made in calculating the rate constants quoted below.

Figure 41 shows double logarithmic plots of initial rate against ether pressure at temperatures between 560 and 640°C. At 640°C the order is close to unity (~ 1.1) with no indication of any curvature in the plot. At lower temperatures, on the other hand, the slopes tend to become higher at the

points along the flat regions. Nitric oxide pressures between 8 and 40 mm. were used in subsequent studies of the maximally inhibited reaction.

Figure 39 shows some typical pressure-time curves for maximal inhibition. Curve A is a tracing of a record for the decomposition of 95 mm. of diethyl ether in the presence of 31 mm. of NO at 630°C; curves B and C are for approximately the same pressure conditions but at temperatures of 600 and 560°C respectively. Figure 40 shows a record for a run using 355 mm. of ether and 10 mm. of NO at 500°C; there is an initial pressure decrease followed by an increase. As illustrated in Figs. 39 and 40, the 'induction' period becomes more pronounced at low temperatures. Between 560 and 640°C there is effectively no induction period except at low pressures and temperatures.

In order to correlate pressure changes with the disappearance of ether, some analytical studies were made for maximally inhibited reactions. The results were shown in Fig. 36 of Part III A. The appropriate correction has been made in calculating the rate constants quoted below.

Figure 42 shows double logarithmic plots of initial rate against ether pressure at temperatures between 560 and 640°C. At 640°C the order is close to unity (~ 1.1) with no indication of any curvature in the plot. At lower temperatures, on the other hand, the slopes tend to become higher at the

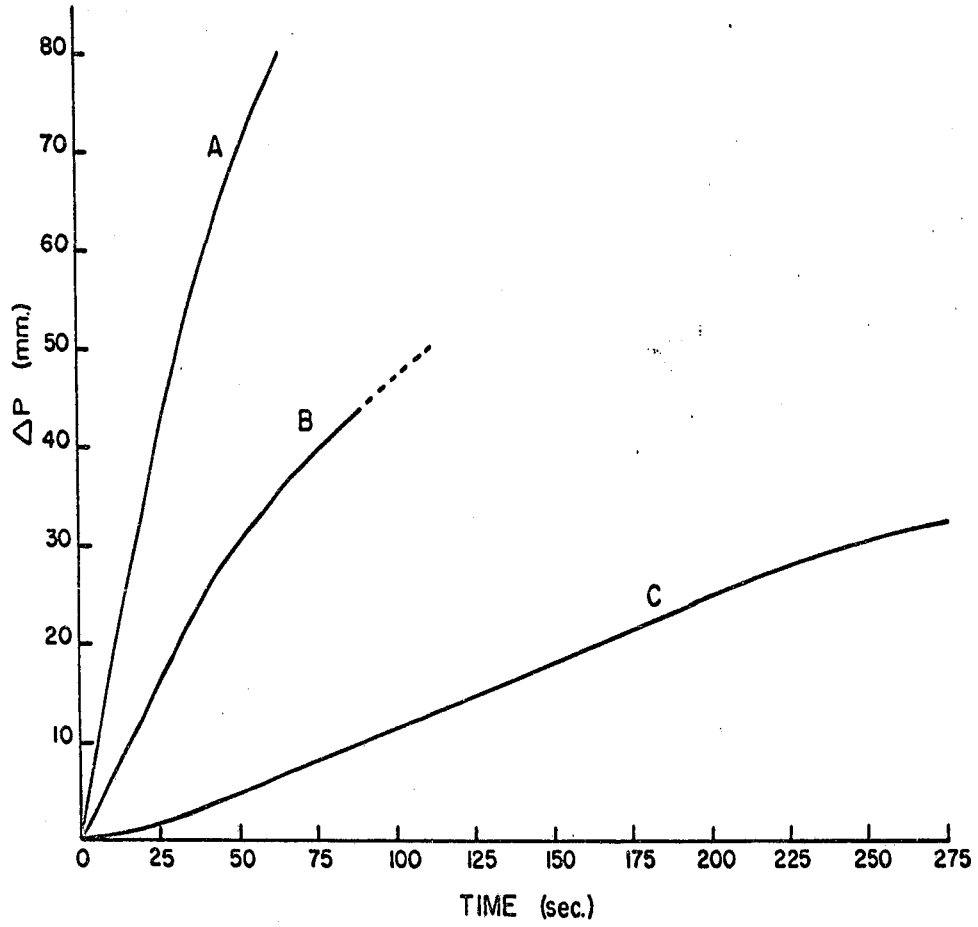

Figure 39. Pressure-time curves for the pyrolysis of diethyl ether maximally inhibited by nitric oxide. Curve A is a tracing of a record obtained in the pyrolysis of 95 mm. of ether in the presence of 31 mm. of nitric oxide at 630°C. Curves B and C are for approximately the same pressure conditions but at temperatures of 600 and 560°C respectively.

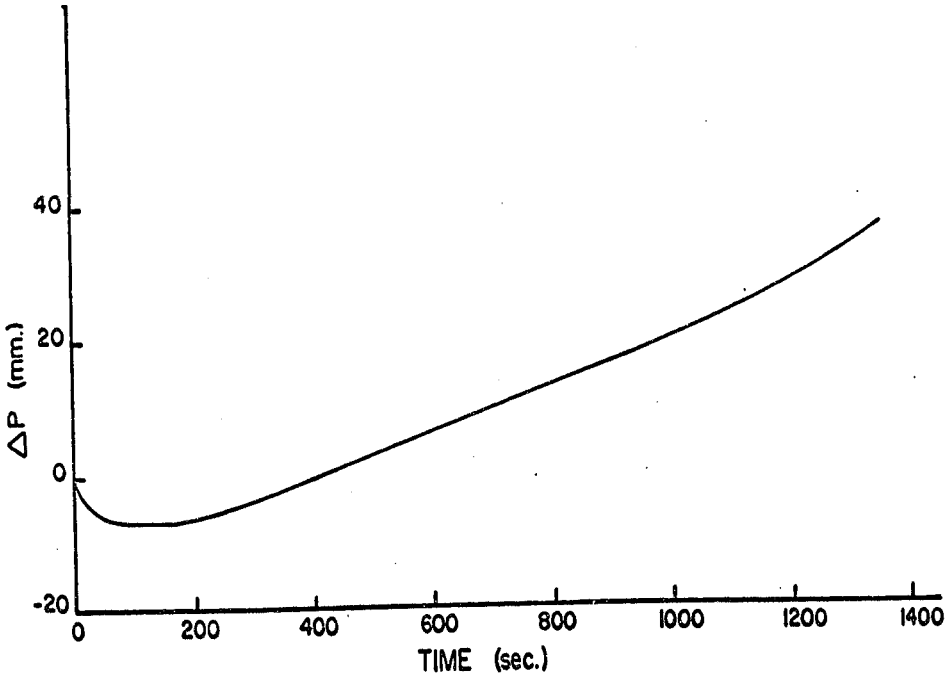

Figure 40. Pressure-time curve for the pyrolysis of diethyl ether. This is a tracing obtained for the pyrolysis of 355 mm. of ether in the presence of 10 mm. of nitric oxide at 500°C.

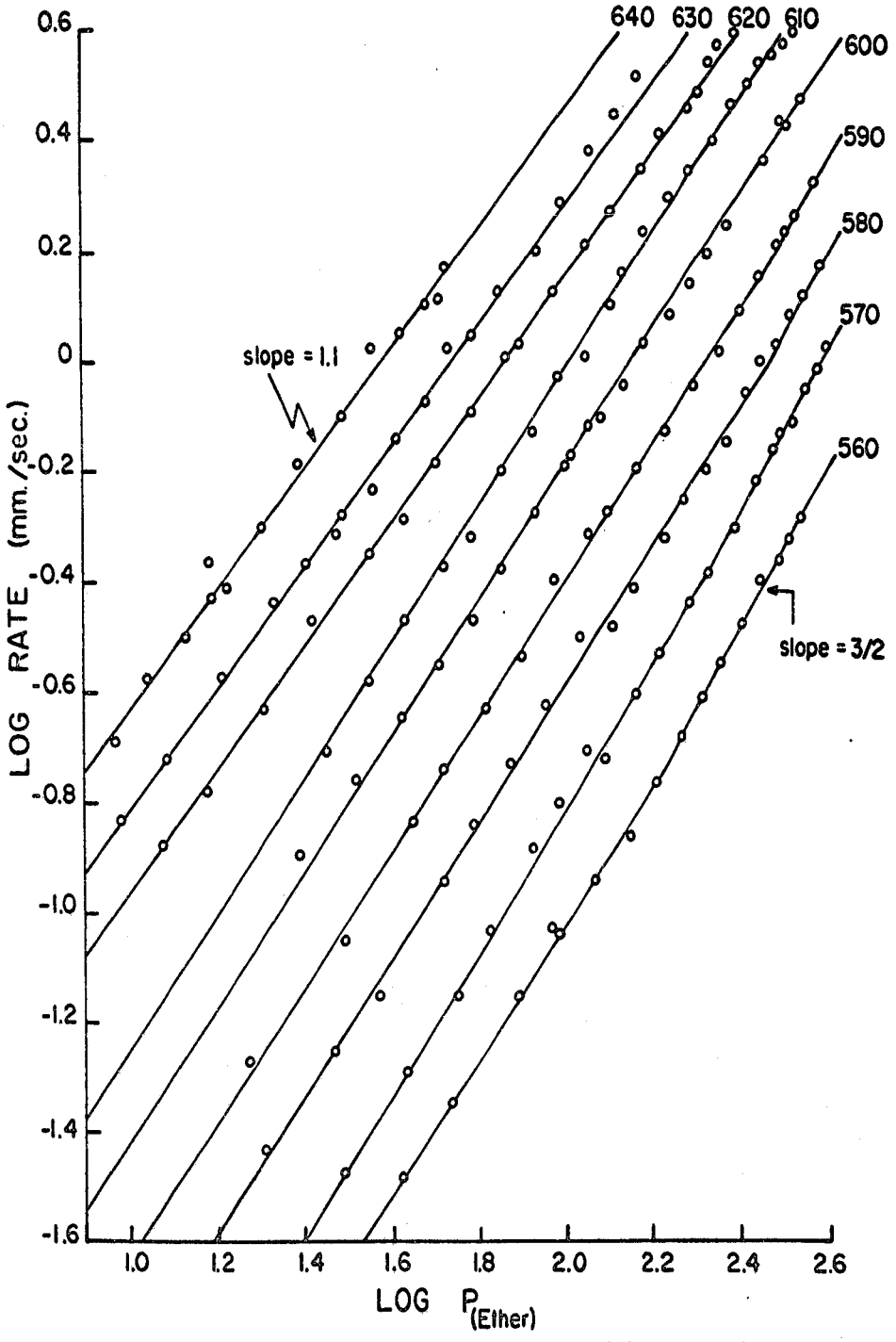

Figure 41. Double logarithmic plots of initial rate against diethyl ether pressure for the reaction maximally inhibited by nitric oxide. The temperature (^{o}C) is indicated on each curve.

higher pressures. At 560 to 590°C the upper portions of the curves have slopes of 1.5.

Figure 42 shows the production of ethanol during the pyrolysis, both in the presence and absence of nitric oxide. The initial pressure and temperature were the same in each case. The initial rates appear to be the same, as found by Danby and Freeman (94), so that ethanol production is apparently not inhibited by nitric oxide. The curves show, however, that the ethanol that is formed decomposes more rapidly in the uninhibited reaction. This is attributed to sensitisation of the ethanol decomposition by the radicals present, their concentration being greater in the uninhibited reaction than in the inhibited one.

The results in Part III A led to the conclusion that the rate law for the uninhibited reaction is of the form

$$v_u = (k_m + k_p)[H] + k'[H]^{3/2} \qquad (I)$$

The term $k_m[H]$, corresponding to the molecular elimination of ethanol and ethylene, will remain intact in the inhibited reaction. The results for the maximally inhibited reaction are consistent with the rate equation

$$v_i = k_m[H] + k''[H]^{3/2} + k'''[H][NO] \qquad (II)$$

A mechanism leading to this rate equation is considered below. The term $k'''[H][NO]$ is responsible for the increase in rate

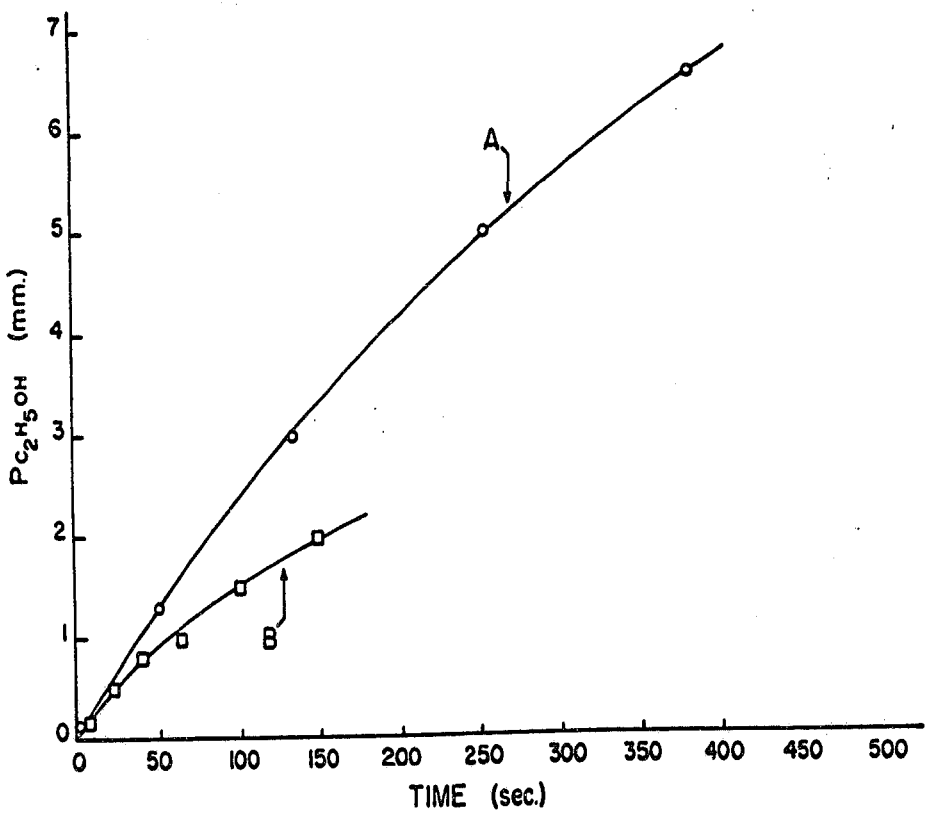

Figure 42. Production of ethanol in the pyrolysis of diethyl ether. Curve A corresponds to the reaction inhibited by nitric oxide, while curve B shows the variation in the uninhibited decomposition. Both curves were obtained at 560°C.

at high NO pressures, and from a study of the reaction in this region the value of k''' can be obtained (21). The remaining two rate constants, k_m and k'', can be obtained by plotting

$$\frac{v_i}{(M)} = k'''(NO)$$

against $(M)^{1/2}$, and such plots are shown in Fig. 43. The results were analyzed using the method of least squares, and the rate constants obtained are listed in Table 7. The high scatter of the points at 640°C is due to the fact that the rates were too rapid to measure accurately.

Figure 44 shows the Arrhenius plot for the first-order rate constant k_m. The point at 640°C was ignored in calculating the activation energy. The rate constant can be expressed as

$$k_m = 2.75 \times 10^{18}\ e^{-83,800/RT}\ sec^{-1}$$

Figure 45 is an Arrhenius plot for the three-halves-order constant k''. Application of the method of least squares led to an activation energy of 54 kcal, but for reasons given below a value of 62 kcal is to be preferred. On this basis the rate constant can be expressed as

$$k'' = 5.5 \times 10^{15}\ e^{-62,000/RT}\ cc^{1/2}\ mole^{-1/2}\ sec^{-1}$$

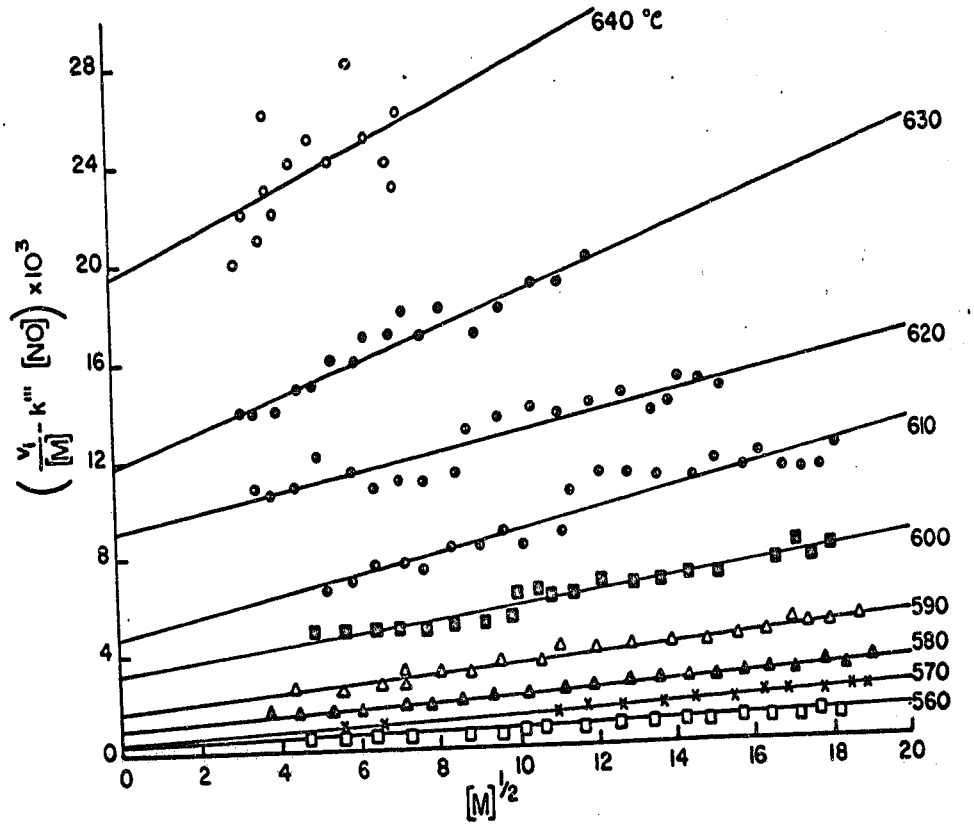

Figure 43. Plots of $v_i/[M] - k'''[NO]$ against $[M]^{1/2}$ for the inhibited pyrolysis of diethyl ether.

Table 7

Rate Constants Derived From Figure 43*

Temperature (°C)	Correlation coefficient	Standard error x 10^5	$10^5 k_m$ (sec^{-1})	$10^5 k''$ ($mm^{-1/2} sec^{-1}$)
525#	1.000	17.5	4.87 ± 0.59	1.82 ± 0.01
560	0.053	5.6	31.2 ± 11.2	4.60 ± 0.56
570	1.000	1.25	37.6 ± 2.5	9.70 ± 0.13
580	0.992	7.34	99.3 ± 14.7	12.3 ± 0.7
590	0.932	30.2	179 ± 60	17.6 ± 3.0
600	0.951	32.4	329 ± 65	25.4 ± 3.2
610	0.941	60.6	474 ± 121	41.9 ± 6.1
620	0.928	59.6	868 ± 119	40.3 ± 7.5
630	0.951	56.4	1180 ± 110	67.7 ± 9.4
640	0.572	170	1950 ± 340	84.3 ± 42.5

* These rate constants may be corrected by multiplying them by 0.84 (see text).

\# Calculated from published data (Freeman (91)).

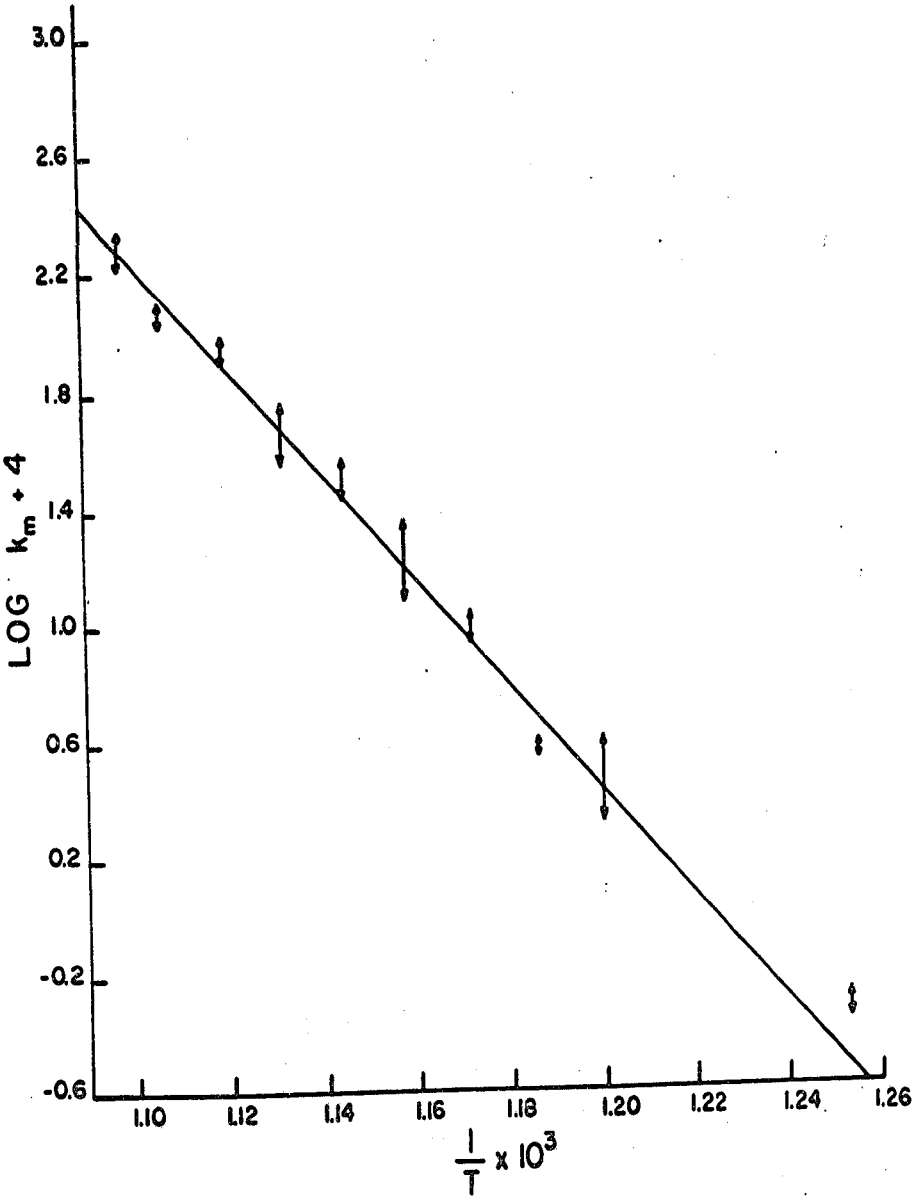

Figure 44. Arrhenius plot for the first-order rate constant k_m.

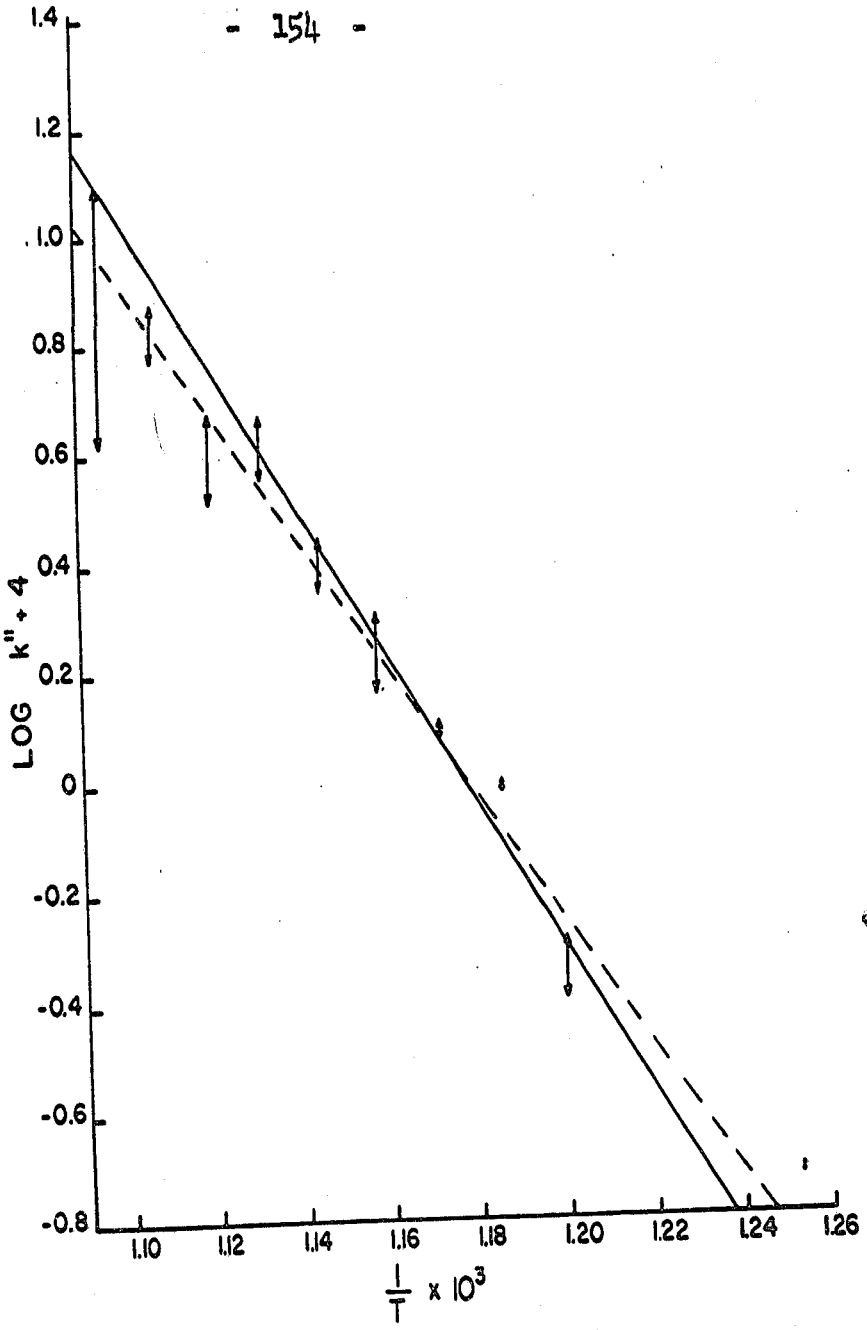

Figure 45. Arrhenius plot for the three-halves-order component (k'') of the inhibited pyrolysis of diethyl ether. The broken line was determined by the least-squares method. The solid line yields an activation energy of 62 kcal. $mole^{-1}$ as discussed in the text.

DISCUSSION

Mechanism of the Maximally Inhibited Reaction

The maximally inhibited reaction has been seen to consist of two components, a first-order reaction and a three-halves-order reaction, of which the former is presumably molecular and the latter free-radical. In the case of the dimethyl ether reaction (Part II B), the free-radical inhibited reaction was also three-halves order, and there was no molecular reaction.

The mechanism is presumably similar to that for the dimethyl ether decomposition. As in previous schemes for reactions inhibited by nitric oxide (see especially Wojciechowski and Laidler (38)) the chain-propagating steps are concluded to be the same as in the uninhibited decomposition, and these reactions were discussed in Part III A. The initiation of a bimolecular reaction between nitric oxide and ether, with the abstraction of a hydrogen atom:

$$NO + CH_3CH_2OC_2H_5 \rightarrow CH_2CH_2OC_2H_5 + HNO$$

and

$$NO + CH_3CH_2OC_2H_5 \rightarrow CH_3CHOC_2H_5 + HNO.$$

In order to obtain three-halves-order kinetics (cf. table 1 of Wojciechowski and Laidler (38)) termination must be between a β radical and NO, or a β radical and a radical βNO (formed

from NO and a β radical). The latter is more likely in the present case, since H atoms are not major chain-carriers, so that HNO will only be present at very low concentrations. The predominant radicals are the C_2H_5 radicals, so that C_2H_5NO will be present in larger amounts. As with dimethyl ether it is postulated that this radical will isomerise into the oxime; the main chain-ending step is therefore taken to be

$$C_2H_5 + CH_3CH = NOH \longrightarrow C_4H_{10} + NO.$$

The mechanism to which these considerations, and those of Part III A, lead is the following:

[1m] $C_2H_5OC_2H_5 \longrightarrow C_2H_5OH + C_2H_4$

[57] $NO + C_2H_5OC_2H_5 \longrightarrow CH_2CH_2OC_2H_5 + HNO$

[58] $NO + C_2H_5OC_2H_5 \longrightarrow CH_3CHOC_2H_5 + HNO$

[54] $CH_2CH_2OC_2H_5 \longrightarrow C_2H_4 + C_2H_5O$

[55] $CH_3CHOC_2H_5 \longrightarrow CH_3CHO + C_2H_5$

[53] $CH_2CH_2OC_2H_5 + C_2H_5OC_2H_5 \longrightarrow CH_3CHOC_2H_5 + C_2H_5OC_2H_5$

[50] $C_2H_5O \longrightarrow CH_2O + CH_3$

[48] $C_2H_5 + C_2H_5OC_2H_5 \longrightarrow C_2H_6 + CH_2CH_2OC_2H_5$

[49] $C_2H_5 + C_2H_5OC_2H_5 \longrightarrow C_2H_6 + CH_3CHOC_2H_5$

[59] $C_2H_5 \longrightarrow C_2H_4 + H$

[51] $CH_3 + C_2H_5OC_2H_5 \rightarrow CH_4 + CH_2CH_2OC_2H_5$

[52] $CH_3 + C_2H_5OC_2H_5 \rightarrow CH_4 + CH_3CHOC_2H_5$

[60] $H + C_2H_5OC_2H_5 \rightarrow H_2 + CH_2CH_2OC_2H_5$

[61] $H + C_2H_5OC_2H_5 \rightarrow H_2 + CH_3CHOC_2H_5$

[23a] $M + HNO \rightarrow M + H + NO$

$$C_2H_5 + NO \underset{[-62]}{\overset{[62]}{\rightleftharpoons}} C_2H_5NO$$

$$C_2H_5NO \underset{[-63]}{\overset{[63]}{\rightleftharpoons}} CH_3CH{=}NOH$$

[64] $C_2H_5 + CH_3CH{=}NOH \rightarrow C_4H_{10} + NO$

Reactions [54] to [61] correspond to the processes represented in Fig. 37 of Part III A. Reactions [59], [60] and [61] are included explicitly in the present scheme but were ignored in working out the steady-state equations for the uninhibited reaction; their inclusion is preferable here, since H atoms are involved in reaction [23a]. The H atom concentration will be so low that the reverse of reaction [23a] can be ignored.

Application of the steady-state treatment to this scheme of reactions leads to a series of equations which can be reduced to the following quadratic equation for the concentration of ethyl radicals:

$$k_{62}k_{63}k_{64}[C_2H_5]^2 - (k_{63}k_{64} + k_{-62}k_{52})(k_{57} + k_{58})[M][C_2H_5]$$

$$- (k_{57} + k_{58})k_{-62}k_{-63}[M] = 0 \qquad (12)$$

where M represents the diethyl ether molecule. The rate constant k_{-62} is much smaller than k_{63}, so that the equation reduces to

$$k_{62}k_{63}k_{64}[C_2H_5]^2 - (k_{57} + k_{58})k_{63}k_{64}[M][C_2H_5]$$

$$- (k_{57} + k_{58})k_{-62}k_{-63}[M] = 0 \qquad (13)$$

This equation is of the form

$$ax^2 - bx - c = 0 \qquad (14)$$

and its solution is approximately

$$x = \left(\frac{c}{a}\right)^{1/2} \qquad (15)$$

provided that

$$4ac \gg b^2,$$

or

$$4k_{62}k_{63}k_{64}k_{-62}k_{-63}(k_{57} + k_{58})[M] \gg (k_{57} + k_{58})^2 k_{63}^2 k_{64}^2 [M]^2$$

This inequality reduces to

$$4k_{62}^2 \gg (k_{57} + k_{58})k_{64}K[M]$$

where K, equal to $k_{62}k_{63}/k_{-62}k_{-63}$, is the equilibrium constant for the reaction $C_2H_5 \rightleftharpoons CH_3CH = NOH$. The rate and equilibrium constants in this inequality are not known with any certainty, but the following are reasonable estimates:

$$k_{62} = 10^{13} \text{ ml mole}^{-1} \text{ sec}^{-1}$$

$$k_{57} = k_{58} = 10^{14} e^{-45,000/RT} \text{ ml mole}^{-1} \text{sec}^{-1}$$

$$k_{64} = 10^{14} \text{ ml mole}^{-1} \text{ sec}^{-1}$$

$$K = 10^{-4} e^{59,000/RT} \text{ ml mole}^{-1}$$

Use of these values, with $[M] = 10^{-5}$ ml mole^{-1}, leads to the result that the left-hand-side of the inequality is several powers of ten larger than the right in the pressure range of the experiments.

In view of this the steady-state concentration of ethyl radicals is given accurately by the expression

$$[C_2H_5] = \left(\frac{(k_{57} + k_{58})k_{-62}k_{-63}}{k_{62}k_{63}k_{64}}\right)^{1/2} [C_2H_5OC_2H_5]^{1/2} \qquad (16)$$

$$= \left(\frac{k_{57} + k_{58}}{K\,k_{64}}\right)^{1/2} [C_2H_5OC_2H_5]^{1/2} \qquad (17)$$

Since the C_2H_5 radicals are predominant the over-all rate of disappearance of diethyl ether is given approximately by

$$v = k_{1m}[M][NO] + (k_{48} + k_{49})[M][C_2H_5] \qquad (18)$$

$$= k_{1m}[M] + 2(k_{57} + k_{58})[M][NO]$$

$$+ (k_{48} + k_{49}) \left(\frac{k_{57} + k_{58}}{K\, k_{64}}\right)^{1/2} [M]^{3/2} \qquad (19)$$

The first and third terms explain the behaviour in the region of maximal inhibition; the second term accounts for the acceleration of the reaction at high nitric oxide concentrations.

Activation Energies

The activation energy for the molecular reaction is 83.8 kcal per mole, and the frequency factor 2.75×10^{18} sec^{-1}. This rather high frequency factor (as compared with vibrational frequencies) is in line with the values for a large number of other unimolecular decompositions (105); presumably there is a loosening of several of the vibrations in the activated state. It must be admitted, in view of the method of numerical analysis used in obtaining the rate constants, that the activation energy is not known with high accuracy; there is no doubt, however, that the frequency factor is considerably higher than 10^{13} sec^{-1}, which is sometimes considered to be 'normal'.

The activation energy for the three-halves-order

chain component can be estimated; according to eq. (19) it is given by

$$E_{3/2} = E_{48} + \tfrac{1}{2}(E_{57} - \Delta E - E_{64}) \qquad (20)$$

where ΔE is the energy change in the reaction $C_2H_5 + NO \rightleftharpoons CH_3CH = NOH$. It is assumed that $E_{48} \approx E_{49}$ and $E_{57} \approx E_{58}$. Long and Skirrow (100) have obtained 9.75 kcal for E_{49} and Sagert and Laidler (42) arrived at a value of 59 kcal. for ΔE on the basis of a study of the butane decomposition inhibited by nitric oxide. Staveley and Hinshelwood (21) obtained an activation energy of 45 kcal for the diethyl ether decomposition accelerated by nitric oxide, and on the basis of equation (19) this value is taken to be E_{57}. Use of these values leads to

$$E_{3/2} = 62 \text{ kcal. per mole.}$$

The line drawn in Fig. 45 actually corresponds to this value, and is seen to pass reasonably well through the experimental points. Because of uncertainties in the method of analysing the experimental data there is considerable uncertainty in the experimental values, and the value of 62 kcal per mole is probably the best that can be derived. As seen above, it leads to a frequency factor of 5.5×10^{15} $cc^{1/2}$ $mole^{-1/2}$ sec^{-1}, which is typical of a three-halves-order frequency factor.

APPENDIX I

The basis for the values given in Table 1 for reactions (11a) and (17a) is as follows. Gill and Laidler's analysis (35) of the data for the recombination of methyl radicals and for the reverse reaction,

$$2\,CH_3 + M \underset{k_{-17a}}{\overset{k_{17a}}{\rightleftharpoons}} C_2H_6 + M,$$

led to the following rate constants at 200°C:

$$k_{17a} = 3 \times 10^{20}\ cc^2\ mole^{-2}\ sec^{-1}$$
$$= 1.67 \times 10^{17}\ e^{8000/RT}\ cc^2\ mole^{-2}\ sec^{-1}$$

$$k_{-17a} = 3 \times 10^{-16}\ cc\ mole^{-1}\ sec^{-1}$$
$$= 1.5 \times 10^{20}\ e^{-77,000/RT}\ cc\ mole^{-1}\ sec^{-1}$$

On the assumption that the temperature-dependence of these rate constants is given by the Hinshelwood formula, with $s = 9$ and $E_0 = 65$ kcal per mole as used by Gill and Laidler (35), the corresponding values at 800°K are:

$$k_{17a} = 3.5 \times 10^{10}\ cc^2\ mole^{-2}\ sec^{-1}$$
$$= 7.0 \times 10^{14}\ e^{13,500/RT}\ cc^2\ mole^{-2}\ sec^{-1}$$

$$k_{-17a} = 5 \times 10^{-2}\ cc\ mole^{-1}\ sec^{-1}$$
$$= 2.0 \times 10^{10}\ e^{-71,500/RT}\ cc\ mole^{-1}\ sec^{-1}$$

The parameters for k_{17a} are those given in Table 1.

For the dissociation of CH_3OCH_3 in its second-order region we have assumed the same frequency factor as for the dissociation of ethane, namely 2×10^{18} cc $mole^{-1}$ sec^{-1}. The low pressure activation energy (74.0 kcal.) was obtained by subtracting 8.5 RT from 87 kcal, which is supposed to be the high-pressure value (36). It is quite possible that the value of 81 kcal reported by Rice and Johnston (18) actually corresponds to the fallen-off region, in which case their activation energy is too low.

In view of the rather long extrapolation involved (from 200°C to 600°K) there may well be considerable error in the estimated values for reactions [11a] and [17a]. The present estimates seem, however, to be the best that can be made with the data available.

The parameters given in Table 1 for reaction [13] are also doubtful, as was noted in the main text.

APPENDIX II

Figure 22 summarizes our conclusions with regard to the thermochemistry of processes related to the species HNO and CH_3NO. The main evidence for these values is as follows. On the basis of their study of the ethane pyrolysis Laidler and Wojciechowski (40) concluded that the process $C_2H_6 + NO \rightleftharpoons C_2H_5 + HNO$ is endothermic by 50 kcal per mole and that the back reaction has no activation energy. The level of $2CH_3 + NO$ is higher than that of $C_2H_6 + NO$ by 85 kcal, the dissociation energy of the C-C bond in ethane.

The level of CH_3NO below that of $CH_3 + NO$ is not known with any certainty. Gray (66) has obtained a value of 57 kcal for $D(CH_3 - NO_2)$, and Gowenlock, Trotman and Batt (53) suggested that the value of $D(CH_3 - NO)$ should be approximately the same. Gowenlock (67) now, however, favors a lower value, of about 30 kcal, on the grounds that the $CH_3 - NO$ dissociation energy should be about 15 kcal weaker than that of H - NO. The dissociation of HNO, however, involves a predissociation (as may also that of CH_3NO), so that the evidence is not reliable. In Fig. 22 the value is about 50 kcal; the actual value has no bearing on the kinetics of the reaction. Rice, Yang and Eyring (48), in a recent discussion of reactions inhibited by nitric oxide, have concluded that the value may be as high as 69.7 kcal per mole.

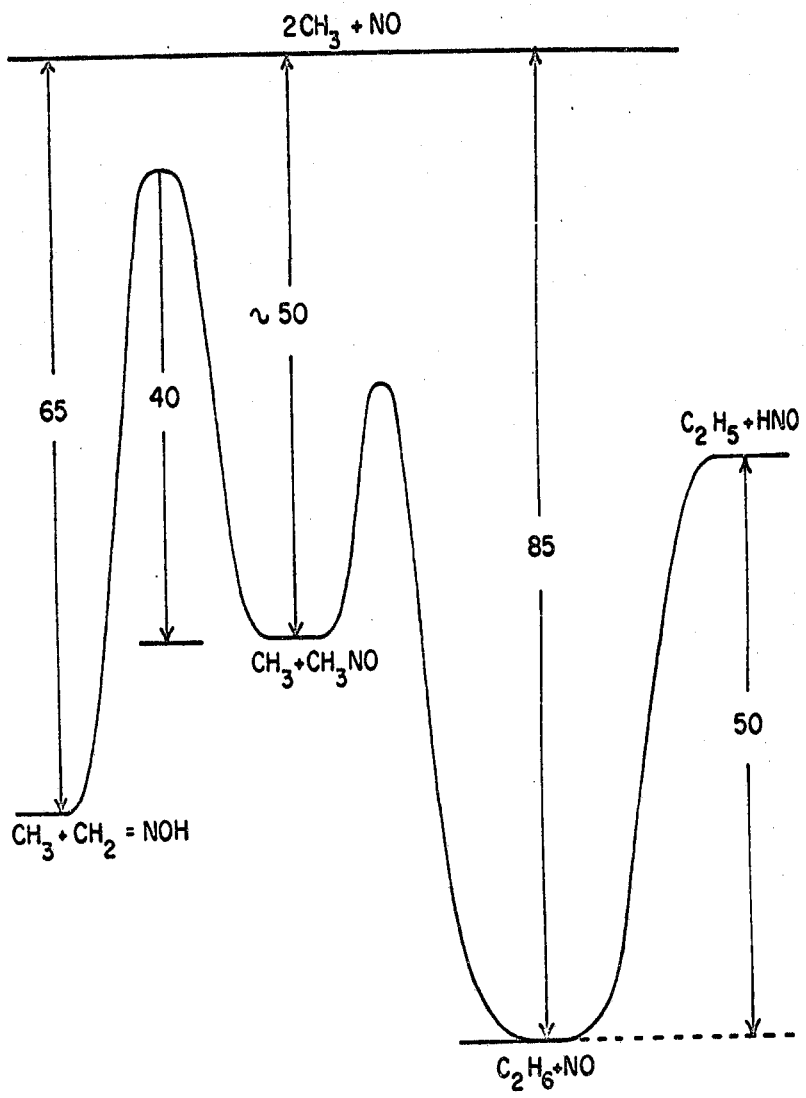

Figure 22. Schematic energy diagram for the various reactions involving nitric oxide; see Appendix II for discussion.

Since reaction between NO and C_2H_6 apparently gives C_2H_5 + HNO (40) and not CH_3 + CH_3NO it is postulated that there is a potential-energy barrier between C_2H_6 + NO and CH_3 + CH_3NO, as shown in the diagram.

Batt and Gowenlock (56) have shown that CH_3NO isomerises into formaldoxime, CH_2 = NOH, with an activation energy of about 40 kcal per mole. The results of the present work indicate that the level of CH_2 = NOH + CH_3 is 65 kcal below that of CH_3 + CH_3 + NO, and therefore significantly below that of CH_3 + CH_3NO. This is not unreasonable. Formaldoxime is expected to be a much more effective scavenger of radicals than is CH_3NO, and chain-ending is therefore postulated to be

$$CH_3 + CH_2{=}NOH \longrightarrow CH_2CH_2 - NOH \longrightarrow C_2H_6 + HO$$

The breakdown of CH_2NOH accounts for the disappearance of nitric oxide in this reaction, in contrast to the situation with certain hydrocarbon decompositions (e.g. ethene, ref. 40), where CH_2NOH is not formed in significant amount.

Since reaction between NO and C_2H_6 apparently gives C_2H_5 + HNO (40) and not CH_3 + CH_3NO it is postulated that there is a potential-energy barrier between C_2H_6 + NO and CH_3 + CH_3NO, as shown in the diagram.

Batt and Gowenlock (56) have shown that CH_3NO isomerises into formaldoxime, CH_2 = NOH, with an activation energy of about 40 kcal per mole. The results of the present work indicate that the level of CH_2 = NOH + CH_3 is 65 kcal below that of CH_3 + CH_3 + NO, and therefore significantly below that of CH_3 + CH_3NO. This is not unreasonable. Formaldoxime is expected to be a much more effective scavenger of radicals than is CH_3NO, and chain-ending is therefore postulated to be

$$CH_3 + CH_2{=}NOH \longrightarrow CH_2CH_2 - NOH \longrightarrow C_2H_6 + HO$$

The breakdown of CH_2NOH accounts for the disappearance of nitric oxide in this reaction, in contrast to the situation with certain hydrocarbon decompositions (e.g. ethane, ref. 40), where CH_2NOH is not formed in significant amount.

CLAIMS TO ORIGINAL RESEARCH

1. Potential-energy surfaces were constructed for the O_4 species considered as the three-body complex $O...O...O_2$. Consideration of these surfaces led to the conclusion that energy chains are not important in the thermal decomposition of ozone and in the photolytic decomposition by visible radiation.
2. The potential-energy surfaces for the O_4 species and the curves for the O_2 molecules provided a basis for suggesting a mechanism for the decomposition of ozone brought about by ultra-violet radiation. It was found that by invoking the Franck-Condon Principle the maximum in the population of vibrationally excited O_2 molecules at the v = 13 level could be explained.
3. The kinetics of the pyrolysis of dimethyl ether has been reinvestigated, and the data were generally in agreement with those of Benson and Jain (26). Measured rates however were always lower, and this was suggested as due to a different method of conditioning the surface of the reaction vessel.
4. A new mechanism for the uninhibited pyrolysis dimethyl ether was proposed involving second-order initiation and DDM termination. Calculation were made to determine the most probable termination reaction, and it was

concluded to be the recombination of methyl radicals in the presence of a third body.

5. An experimental study was made of the decomposition of dimethyl ether inhibited by nitric oxide, over a wider temperature and pressure range than heretofore. The order was found to be three-halves with respect to dimethyl ether in the maximally inhibited region.

6. A kinetic study was made of the dimethyl ether reaction accelerated by large quantities of nitric oxide. Rates were measured for the first time over a wide enough pressure and temperature range to obtain a fairly accurate value for the rate constant for the abstraction of a hydrogen atom from dimethyl ether by nitric oxide.

7. A detailed mechanism was proposed to describe the maximally inhibited decomposition of dimethyl ether. The mechanism also explained the reaction accelerated by large quantities of nitric oxide.

8. An estimate of 92 kcal mole^{-1} was made for $D(CH_3OCH_2\text{-}H)$ based on the activation energy for the reaction accelerated by large quantities of nitric oxide.

9. For the first time a detailed study was made of the pyrolysis of dimethyl ether inhibited by propylene. The reaction was found to obey three-halves-order kinetics. The limiting relative rates were slightly different from those observed for inhibition by nitric oxide.

10. A mechanism was proposed for inhibition of dimethyl ether by propylene and it successfully explained the observations.

11. The kinetics of the decomposition of dimethyl ether accelerated by hydrogen sulphide were investigated over a wide range of pressure and temperature. The pro- relative rate, which was found to depend on the proportion of H_2S relative to CH_3OCH_3, increased to a plateau and at higher concentration increased further. Data were obtained for both the plateau region and the region at very high percentages of hydrogen sulphide.

12. A detailed mechanism was proposed for the pyrolysis of dimethyl ether accelerated by hydrogen sulphide. For the first time the increase in relative rate at very high percentages of H_2S was explained.

13. On the basis of the results for the decomposition of dimethyl ether in the presence of hydrogen sulphide an estimate of 85.6 kcal $mole^{-1}$ was made for the dissociation energy of the split of the H_2S molecule into H and HS.

14. The uninhibited pyrolysis of diethyl ether was reinvestigated and the order in the pressure and temperature region studied was found to be between 1 and 3/2.

15. The data for the uninhibited decomposition of diethyl ether were analyzed in order to separate first-order and three-halves-order components of the reaction. Conclusions were made regarding the possible fates of the radicals CH_3CH_2O, $CH_2CH_2OC_2H_5$ and $CH_3CHOC_2H_5$.

16. A mechanism was proposed for the uninhibited pyrolysis of diethyl ether which successfully explained the kinetic and analytical data.

17. The thermal decomposition of diethyl ether inhibited by nitric oxide was studied over a wide range of pressure and temperature. The change from first-order kinetics at low pressures and high temperatures to three-halves-order at high pressures and low temperatures was clearly shown.

18. The data for the inhibited decomposition of diethyl ether were analyzed and the first and three-halves-order components separated. A value of the rate constant for the molecular split of diethyl ether into ethanol and ethylene was determined.

19. A detailed mechanism was proposed for the pyrolysis of diethyl ether inhibited by nitric oxide. The kinetic and analytical data were successfully explained.

20. The study of the inhibited decompositions of dimethyl and diethyl ether provided further evidence for the generality of the inhibition scheme postulated by

Wojciechowski and Laidler (37,38) but clearly showed that important differences arise depending on the nature of the predominant radicals in each system.

REFERENCES

1. H.J. Schumacher, J. Chem. Phys., 33, 938 (1960).
2. S.W. Benson, J. Chem. Phys., 33, 939 (1960).
3. W.D. McGrath and R.G.W. Norrish, Proc. Roy. Soc., A254, 317 (1960).
4. S.W. Benson, The Foundations of Chemical Kinetics, McGraw-Hill, New York, 1960. pp. 400-408.
5. E.K. Gill and K.J. Laidler, Can. J. Chem., 36, 79 (1958).
6. D.W.G. Heddle, J. Chem. Phys., 32, 1889 (1960).
7. J.T. Vanderslice, E.A. Mason and W.G. Maisch, J. Chem. Phys., 32, 515 (1960).
8. W.D. McGrath and R.G.W. Norrish, Proc. Roy. Soc., A242, 265 (1957).
9. J.A. Zaslowsky, H.B. Urbach, F. Leighton, R.J. Wnuk, and J.A. Wojtowicz, J. Am. Chem. Soc., 82, 2682 (1960).
10. S.W. Benson and A.E. Axworthy, J. Chem. Phys., 26, 1718 (1957).
11. E.K. Gill and K.J. Laidler, Trans. Faraday Soc., 55, 753 (1959).
12. E. Castellano and H.J. Schumacher, J. Chem. Phys., 36, 2238 (1962).
13. K.J. Laidler and B.W. Wojciechowski, Proc. Roy. Soc. A259, 257 (1960).
14. K.J. Laidler and B.W. Wojciechowski, Proc. Roy. Soc., A260, 91 (1961).

15. K.J. Laidler, N.H. Sagert and B.W. Wojciechowski, Proc. Roy. Soc., A270, 242 (1962).

16. N.H. Sagert and K.J. Laidler, Can. J. Chem., 41, 838 (1963).

17. P.J. Askey and C.N. Hinshelwood, Proc. Roy. Soc., A115, 215 (1927).

18. F.O. Rice and W.R.S. Johnston, J. Am. Chem. Soc., 56, 214 (1934).

19. R.N. Pease, J. Am. Chem. Soc., 59, 425 (1937).

20. L.A.K. Staveley and C.N. Hinshelwood, Nature, 137, 29 (1936).

21. L.A.K. Staveley and C.N. Hinshelwood, Proc. Roy. Soc., A154, 335 (1936).

22. L.A.K. Staveley and C.N. Hinshelwood, J. Chem. Soc., 812, 818 (1936).

23. F.P. Lossing, K.U. Ingold and A.W. Tichner, Discussions Faraday Soc., 14, 34 (1953).

24. F.O. Rice and K.F. Herzfeld, J. Am. Chem. Soc., 56, 284 (1934).

25. S.W. Benson, J. Chem. Phys., 25, 27 (1956).

26. S.W. Benson and D.V.S. Jain, J. Chem. Phys., 31, 1008 (1959).

27. K.H. Anderson and S.W. Benson, J. Chem. Phys., 36, 2320 (1962).

28. N. Inal and O. Toyama, Bull. Chem. Soc. Japan, 34, 328 (1961).

29. A.F. Trotman-Dickenson, J. Chem. Phys., 19, 261 (1951).

30. R.A. Marcus, B. de B. Darwent and E.W.R. Steacie, J. Chem. Phys., 16, 987 (1948).

31. R.L. Strong and K.O. Kutschke, Can. J. Chem., 37, 1456 (1959).

32. K.J. Laidler and B.W. Wojciechowski, Chemical Society Special Publication No. 16, 37 (1962).

33. J.H. Purnell and C.P. Quinn, Proc. Roy. Soc., A270, 267 (1962).

34. A.F. Trotman-Dickenson and E.W.R. Steacie, J. Chem. Phys., 19, 329 (1951).

35. E.K. Gill and K.J. Laidler, Proc. Roy. Soc., A250, 121 (1959).

36. B.C. Baughan, M.G. Evans and M. Polanyi, Trans. Faraday Soc., 37, 377 (1941).

37. B.W. Wojciechowski and K.J. Laidler, Can. J. Chem., 38, 1027 (1960).

38. K.J. Laidler and B.W. Wojciechowski, Trans. Faraday Soc., 59, 369 (1963).

39. K.J. Laidler and B.W. Wojciechowski, Proc. Roy. Soc., A259, 257 (1960).

40. K.J. Laidler and B.W. Wojciechowski, Proc. Roy. Soc., A260, 103 (1961).

41. K.J. Laidler, R.E. Sagert and B.W. Wojciechowski, Proc. Roy. Soc., A270, 254 (1962).

42. N.N. Sagert and K.J. Laidler, Can. J. Chem., 41, 848 (1963).

43. L.A.K. Staveley and C.N. Hinshelwood, Proc. Roy. Soc., A159, 192 (1937).

44. P.F. Gay and M.W. Travers, Nature, 138, 546 (1936).

45. H.W. Thompson and M. Heisner, Nature, 139, 1018 (1937).

46. V.E. Goldanskii, Uspekhi Khim., 15, 63 (1946). N.R.C. Technical translation TT-130.

47. F.O. Rice and O.L. Polly, J. Chem. Phys., 6, 273 (1938).

48. T. Ree, K. Yang and H. Eyring, Trans. Faraday Soc., 58, 2375 (1962).

49. N. Imai and C. Toyama, Bull. Chem. Soc. Japan, 35, 860 (1962).

50. R.G.W. Norrish and G.L. Pratt, Nature, 197, 143 (1963).

51. D.R. Blackmore and C.N. Hinshelwood, Proc. Roy. Soc., A268, 36 (1962).

52. D. Jost and L. Phillips, Proc. Chem. Soc., 73 (1960).

53. B.G. Gowenlock, J. Trotman and L. Batt, Chemical Society Special Publication No. 10, 75 (1957).

54. W.A. Bryce and K.U. Ingold, J. Chem. Phys., 23, 1968 (1955).

55. A.F. Trotman-Dickenson, Gas Kinetics, Butterworths Scientific Publications, London. 1955 p. 125.

56. L. Batt and B.G. Gowenlock, Trans. Faraday Soc., 56, 682 (1960).

57. M.A.A. Clyne and B.A. Thrush, Trans. Faraday Soc., 57, 1305 (1961).

58. F.H. Verhoeck, Trans. Faraday Soc., 31, 1533 (1935).

59. G.R. Freeman and C.J. Danby, Proc. Roy. Soc., A245, 68 (1958).

60. J.R. McNesby and A.S. Gordon, J. Chem. Phys., 31, 853 (1959).

61. A.S. Gordon, S.R. Smith and J.R. McNesby, J. Am. Chem. Soc., 81, 5059 (1959).

62. W.A. Bryce and D.J. Ruzicka, Can. J. Chem., 38, 835 (1960).

63. D.J. Ruzicka and W.A. Bryce, Can. J. Chem., 38, 827 (1960).

64. H. Saware, J. Chem. Phys., 17, 284 (1949).

65. A.F. Trotman-Dickenson and E.W.R. Steacie, J. Chem. Phys., 19, 329 (1951).

66. P. Gray, Trans. Faraday Soc., 51, 1367, 1409 (1955); 52, 344 (1956).

67. B.G. Gowenlock, Discussions Faraday Soc., 33, 287 (1962).

68. K.E.J. Barrett and W.A. Waters, Discussions Faraday Soc., 14, 221 (1953).

69. H.N. Birrell, H.F. Smith, A.F. Trotman-Dickenson and H. Wilkie, J. Chem. Soc., 2807 (1957).

70. J.A. Kerr and A.F. Trotman-Dickenson, J. Chem. Soc., 3322 (1957).

71. N. Imai and O. Toyama, Bull. Chem. Soc. Japan, 33, 1120 (1960).

72. N. Imai, Y. Yoshida and O. Toyama, Bull. Chem. Soc. Japan, 35, 752, 759 (1962).

73. N. Imai and O. Toyama, Bull. Chem. Soc. Japan, 33, 1408 (1960).

74. B. De B. Darwent and R. Roberts, Proc. Roy. Soc., A216, 344 (1953).

75. S.W. Benson and D.V.S. Jain, J. Chem. Phys., 31, 1008 (1959).

76. N. Imai and O. Toyama, Bull. Chem. Soc. Japan, 33, 652 (1960).

77. T.L. Cottrell, The Strengths of Chemical Bonds, Butterworths Scientific Publications, London. p. 188 (1958).

78. J.W.C. Johns and D.A. Ramsay, Can. J. Phys., 39, 210 (1961).

79. "Selected Values of Chemical Thermodynamic Properties", N.B.S. Circular 500 (1952).

80. D.A. Ansdell and F.M. Page, Trans. Faraday Soc., 58, 1084 (1962).

81. H. Meckle and N.T.B. McClean, Trans. Faraday Soc., 58, 895 (1962).

82. F. Palmer and F.P. Lossing, J. Am. Chem. Soc., 84, 4661 (1962).

83. C.N. Hinshelwood, Proc. Roy. Soc., A114, 84 (1927).

84. O.K. Rice and D.V. Sickman, J. Am. Chem. Soc., 56, 1144 (1934).

85. D.N. Hewitt and H.A. Vernon, Proc. Roy. Soc., A135, 307 (1932).

86. E.W.R. Steacie, W.H. Tatcher and S. Rosenberg, J. Chem. Phys., 4, 220 (1936).

87. E.W.R. Steacie and E. Solomon, J. Chem. Phys., 2, 503 (1934).

88. J.S.A. Forsyth, Trans. Faraday Soc., 37, 312 (1941).

89. C.J.M. Fletcher and G.K. Rollefson, J. Am. Chem. Soc., 58, 2135 (1936).

90. R.E. Rebbert and K.J. Laidler, J. Chem. Phys., 20, 574 (1952).

91. G.R. Freeman, D. Phil. Thesis, Oxford (1957).

92. G.R. Freeman, Proc. Roy. Soc., A245, 49 (1958).

93. G.R. Freeman, C.J. Danby and C.N. Hinshelwood, Proc. Roy. Soc., A245, 28 (1958).

94. C.J. Danby and G.R. Freeman, Proc. Roy. Soc., A245, 40 (1958).

95. J. Jach and C.N. Hinshelwood, Proc. Roy. Soc., A231, 145 (1955).

96. C.J.M. Fletcher and G.K. Rollefson, J. Am. Chem. Soc., 58, 2129 (1936).

97. S. Dymator and E.W.R. Steacie, J. Chem. Phys., 19, 326 (1951).

98. B.O. Gowenlock, J. Chem. Phys., 21, 941 (1953).

99. P. Goldfinger, M. Letort and M. Niclause, Volume Commémoratif Victor Henri: Contribution à l'Etude de la Structure Moléculaire, Desoer, Liège, 1948, p. 283.

100. J. Long and G. Skirrow, Trans. Faraday Soc., 58, 1403 (1962).

101. C.N. Hinshelwood, Z. Electrochem., 42, 445 (1936).

102. J.E. Hobbs, Proc. Roy. Soc., A167, 439 (1938).

103. J.R.E. Smith and C.N. Hinshelwood, Proc. Roy. Soc., A180, 237 (1942).

104. J.G. Davoud and C.N. Hinshelwood, Proc. Roy.Soc., A171, 52 (1939).

105. C. Steel and K.J. Laidler, J. Chem. Phys., 34, 1826 (1961).